

UC Berkeley

UC Berkeley Electronic Theses and Dissertations

Title

Advances in Generalized Valence Bond-Coupled Cluster Methods for Electronic Structure Theory

Permalink

<https://escholarship.org/uc/item/2j7526xc>

Author

Lawler, Keith Vanoy

Publication Date

2009

Peer reviewed|Thesis/dissertation

**Advances in Generalized Valence Bond-Coupled Cluster Methods for
Electronic Structure Theory**

by

Keith Vanoy Lawler Jr.

A dissertation submitted in partial satisfaction of the
requirements for the degree of
Doctor of Philosophy

in

Chemistry

in the

GRADUATE DIVISION

of the

UNIVERSITY OF CALIFORNIA, BERKELEY

Committee in charge:
Professor Martin Head-Gordon, Chair
Professor William H. Miller
Professor Joel S. Moore

Fall 2009

The dissertation of Keith Vanoy Lawler Jr., titled Advances in Generalized Valence Bond-Coupled Cluster Methods for Electronic Structure Theory, is approved:

Chair Date

Date

Date

University of California, Berkeley

Fall 2009

**Advances in Generalized Valence Bond-Coupled Cluster Methods for
Electronic Structure Theory**

Copyright 2009
by
Keith Vanoy Lawler Jr.

Abstract

Advances in Generalized Valence Bond-Coupled Cluster Methods for Electronic Structure Theory

by

Keith Vanoy Lawler Jr.
Doctor of Philosophy in Chemistry

University of California, Berkeley

Professor Martin Head-Gordon, Chair

The electron-electron correlation term in the electronic energy of a molecule is the most difficult term to compute, yet it is of both qualitative and quantitative importance for a diverse range of chemical applications of computational quantum chemistry. Generalized Valence Bond-Coupled Cluster (GVB-CC) methods are computationally efficient, size-consistent wavefunction based methods to capture the most important static (valence) contributions to the correlation energy. Despite these advantages early GVB-CC methods suffer four major short-comings: over-localization leading to symmetry breaking, poor behavior with spin-unrestriction, neglect of the dynamic (or residual) correlation energy, and multiple orbital minima. The work presented here is directed at rectifying these major short-comings of the GVB-CC methods.

The GVB-CC methods suffer from symmetry-breaking (SB) in systems with multiple resonance structures, which arises due to neglected correlations. We show how these problems can be significantly removed by using 2nd order perturbation theory (PT) for weak correlations coupling 3 different electron pairs, and (infinite order) CC theory for stronger correlations involving electrons in only 1 or 2 different pairs. The resulting Three-pair corrected Imperfect Pairing (TIP) method works quite well in removing SB from aromatic hydrocarbons, but it is shown that to robustly combine CC and PT it is necessary to modify several aspects of the basic method. A penalty function term needs to be introduced to regularize the PT amplitudes and ensure they remain small. When TIP is compared side-by-side with CC treatments of the 3-pair correlations, the results suggest that the penalty function is beneficial for any hybrid CC/PT method that includes orbital optimization. TIP greatly reduces SB and recovers a significantly higher fraction of the valence electron correlation energy than earlier double excitation based GVB-CC methods.

Spin-unrestriction is typically defined as a free variation of the molecular orbitals of different spins in order to lower the molecular energy. In GVB-CC methods, this approach

often leads to undesirable artifacts, so therefore we develop an alternate method for spin-unrestriction that transfers concepts from corresponding orbitals in Hartree-Fock theory to active space electron correlation methods. The Unrestriction-in-Active-Pairs (UAP) procedure forces an orbital to only mix with its corresponding virtual orbital to spin-unrestrict, thus limiting the number of degrees of freedom that the molecular orbitals can use to spin-unrestrict and thereby eliminating many of the undesirable artifacts of spin-unrestriction. It can be shown that in the unrestricted limit of ROHF fragments (the UAP dissociation orbitals) the CC equations are singular if only the strongly correlated electrons are considered. The CC equations can be regularized to alleviate this problem. UAP when combined with the GVB-CC model chemistries we have developed makes a powerful tool for predicting potential energy surfaces including appropriate orbitals on the molecular fragments at dissociation.

Finally, we consider the extension of the standard single-determinant Kohn-Sham (KS) method to the case of a multi-configuration auxiliary wave function, such as the GVB-CC methods. By applying the rigorous Kohn-Sham method to this case, we construct the proper interacting and auxiliary energy functionals. Following the Hohenberg-Kohn theorem for both energy functionals, we derive the corresponding multi-configuration Kohn-Sham equations, based on a local effective potential. At the end of the analysis we show that, at the ground state, the auxiliary wavefunction must collapse into a single-determinant wave function, equal to the regular KS wavefunction. We also discuss the stability of the wave function in multi-configuration density functional theory methods where the auxiliary system is partially interacting, and the residual correlation is evaluated as a functional of the density. We also discuss improvements to the definition of the residual correlation energy of the partially interacting system.

For everyone, everywhere who has ever had to debug source code.

Contents

List of Figures	v
List of Tables	xi
1 Introduction	1
1.1 The Electronic Problem	1
1.2 Ab initio Wavefunction Quantum Mechanics	3
1.2.1 Mean-Field Approximation	3
1.2.2 Orbital Rotations	5
1.2.3 The Need for Electron-Electron Correlation	7
1.3 Valence Active Space Correlation Methods	9
1.3.1 Truncated CI and Size-Consistency	9
1.3.2 CASSCF	11
1.3.3 GVB-PP	12
1.3.4 Localized Orbitals	13
1.4 Coupled Cluster Theory	15
1.4.1 Basics of Coupled Cluster Theory	15
1.4.2 Coupled Cluster Generalized Valence Bond Theory	17
1.5 Outline of this Work	20
1.5.1 Symmetry-breaking in GVB-CC methods	20
1.5.2 Penalty functions for combining coupled cluster and perturbation amplitudes in local correlation methods with optimized orbitals	21
1.5.3 The numerical condition of electron correlation theories when only active pairs of electrons are spin-unrestricted	21
1.5.4 Orbitals that are unrestricted in active pairs for GVB-CC methods	22
1.5.5 Analysis of multi-configurational Kohn-Sham methods: Theory and model application to bond-breaking.	22
2 Symmetry-breaking in GVB-CC methods	23
2.1 Introduction	23
2.2 Pilot calculations on benzene	27

2.3	Three-pair corrected imperfect pairing	32
2.3.1	General considerations	32
2.3.2	An Efficient Algorithm for the Energy	33
2.3.3	Analytical Nuclear Gradient	37
2.4	Numerical Tests and Examples	39
2.4.1	Benzene	39
2.4.2	Naphthalene	44
2.4.3	Phenalenyl cation and anion	45
2.5	Discussion and conclusions	46
3	Penalty functions for combining coupled cluster and perturbation amplitudes in local correlation methods with optimized orbitals	49
3.1	Introduction	49
3.2	Theory	53
3.2.1	Hybrid energy function	53
3.2.2	Choosing Penalty Function Parameters	55
3.3	Results	58
3.3.1	Correlation energy recovery with and without penalty functions	58
3.3.2	Equilibrium Bond-Lengths and Correlation Energies	61
3.3.3	Aromatic Hydrocarbons and Symmetry-Breaking	62
3.3.4	Linear Polyenes	67
3.3.5	Multiple Minima	68
3.4	Conclusions	69
4	The numerical condition of electron correlation theories when only active pairs of electrons are spin-unrestricted	72
4.1	Introduction	72
4.2	Results	73
4.3	Modified Equations Which are Well-Conditioned	77
4.4	Heuristic Understanding of the Problem	79
4.5	Conclusions	82
5	Orbitals that are unrestricted in active pairs for GVB-CC methods	83
5.1	Introduction	83
5.2	Theory	85
5.2.1	Unrestricted in Active Pairs (UAP) orbitals	85
5.2.2	Algorithm	87
5.2.3	Amplitude Regularization	88
5.3	Results	90
5.3.1	Performance and Timings	90
5.3.2	Minimal Active Space Homolytic Bond Dissociation	91

5.3.3	Full Active Space Bond Dissociation in Methane	93
5.3.4	Radical Properties	95
5.4	Conclusions	99
6	Analysis of multi-configurational Kohn-Sham methods: Theory and model application to bond-breaking.	101
6.1	Introduction	101
6.2	The Standard Kohn-Sham Method	103
6.3	Mapping the Interacting System onto an Auxiliary System via an Effective Local Potential	105
6.4	Mapping the Interacting Systems onto Partially Interacting Systems	108
6.5	Perfect Pairing as a Partially Interacting Reference	109
6.6	Discussion and Conclusions	113
7	Conclusions & Outlook	115
7.1	Summary	115
7.2	Future Research Directions	118
A	Supporting Information	119
A.1	Chapter 3: Penalty functions for combining coupled cluster and perturbation amplitudes in local correlation methods with optimized orbitals	119
A.1.1	Amplitude Equations	119
A.1.2	Supplementary Figures	122
A.2	Chapter 4: The numerical condition of electron correlation theories when only active pairs of electrons are spin-unrestricted	125
A.2.1	The Two Electron-Pair Case.	125
A.2.2	The Many-Pair Case.	126
A.3	Chapter 5: Orbitals that are unrestricted in active pairs for GVB-CC methods	128
A.3.1	Additional timings	128
A.3.2	The need for amplitude regularization in multi-pair cases	128
B	Basis Sets for Doing Electron Correlation with 3d Block Metals	131
B.1	Wachters-pQZ Basis	131
B.2	Wachters-p6Z Basis	134
	Bibliography	140

List of Figures

- 2.1 Potential energy curve for distortion of benzene along the coordinate described in Fig. 2.2, showing symmetry breaking with the PP and IP methods which neglect non-local correlations. Absolute energies (6-31G* basis) at D_{6h} geometry are: -230.702049 H for HF, -230.902841 H for PP, -231.014028 H for IP, and -231.089623 H for VOD. 26
- 2.2 The deformation angle Δ in benzene is defined as the magnitude of the deviation of the CXC (X being the geometric center) angles from 60° . Adjacent CXC angles will therefore be $(60+\Delta)$ and $(60-\Delta)^\circ$. Fig. 2.2a shows D_{6h} benzene with $\Delta=0$. Fig. 2.2b is an example of a D_{3h} benzene with $\Delta=10$. Carbon atom positions are fixed at 1.395249 Å from the geometric center and hydrogen atom positions are fixed at 2.482360 Å (from the MP2/6-31G* optimized D_{6h} geometry). 27
- 2.3 Potential energy curves for deformation of benzene using local correlation models which only retain correlations coupling up to 1, 2, 3 and 4 different electron pairs respectively, where the correlation energy is evaluated at the second-order perturbation theory (MP2) level. For reference, the absolute energies at the D_{6h} geometry for the 1-, 2-, 3-, and 4-pair models are: -230.834077 H, -230.965803 H, -231.020476 H, and -231.034350 H respectively. 30
- 2.4 Close-up view of the potential curve for small distortions of benzene away from D_{6h} symmetry for the 3-pair model shown above in Figure 2.3. 31
- 2.5 The average CPU cost per orbital iteration and the average cost of performing an analytical nuclear gradient of PP, IP, and TIP in seconds. The calculations were all performed with the 6-31G* basis and RIMP2-VDZ auxiliary basis. 38
- 2.6 Comparative potential energy curves for deformation of benzene using the TIP, IP, and VOD models. It is evident that TIP significantly improves upon the IP model that it is designed to correct, and approaches the VOD model that it is approximating. For reference, the absolute energies at the D_{6h} geometry for the models are: -231.01428 H for IP, -231.095001 H for TIP, and -231.089623 H for VOD. 40

2.7	Close-up view of the potential curve for very small distortions of benzene away from D_{6h} symmetry for the 3-pair MP2, TIP and VOD models shown above in Figs 2.4 and 2.6. While 3-pair MP2 slightly breaks symmetry along this distortion coordinate, TIP does not.	41
2.8	The 3 bonding and corresponding paired anti-bonding π orbitals (shown on the same line) for benzene as predicted by IP and TIP.	42
2.9	The localized occupied σ orbitals for benzene as predicted by TIP. Orbital A is a 6-fold degenerate inactive occupied s-type orbital on the carbons. Orbital B is a 6-fold degenerate C-H σ bonding orbital. Orbital C is a 2-fold degenerate C-C σ bonding orbital. Orbital D is a 4-fold degenerate C-C σ bonding orbital.	43
2.10	The optimized bond lengths of benzene predicted by Hartree-Fock, PP, IP, TIP, and VOD (using the 6-31G* basis). All bond lengths are in Angstroms.	43
2.11	A comparison of optimized naphthalene bond lengths for a Hartree-Fock, PP, IP, TIP and VOD. The (a) structures come from a guess of D_{2h} symmetry; the (b) structures come from a guess of C_{2v} symmetry. All bond lengths are in Angstroms. All bond lengths are colorC coded to indicate the symmetry equivalent bonds for a D_{2h} structure. *VOD was done in the 6-31G basis set with the rimp2-VDZ auxiliary basis set due to limitations in performing the optimization.	45
2.12	The occupied orbitals for naphthalene as predicted by TIP. Orbitals A-E are the unique π bonding orbitals for naphthalene Orbital F is an 11-fold degenerate C-C σ bonding orbital. Orbital G is an 8-fold degenerate C-H σ bonding orbital. Orbital H is a 10-fold degenerate inactive occupied s-type orbital on the carbons.	46
2.13	Optimized bond lengths for the phenalenyl cation for Hartree-Fock, PP, IP, and TIP. The PP, IP, and TIP (a) guess structures were the optimized Hartree-Fock structure. The TIP (b) guess structure was the optimized phenalenyl anion geometry. The energies for TIP (a) and TIP (b) are: -498.115876 H and -498.110478 H respectively. All bond lengths are in Angstroms, and bond-lengths that should be symmetry-related are color-coded to enable inspection of symmetry-breaking.	47
2.14	Optimized bond lengths for the phenalenyl anion for Hartree-Fock, PP, IP, and TIP. The guess structure for the PP, IP, and TIP optimizations was the Hartree-Fock structure. All bond lengths are in Angstroms. All bond lengths are color coded to indicate the symmetry equivalent bonds for a D_{3h} structure.	48

3.1	Electron correlations that couple one or two electron pairs together, where the correlations are described in a perfect pairing active space such that each valence occupied orbital has one correlating antibonding orbital. These two levels describe each electron pair, and thus perfect pairing (PP) contains only the intra-pair correlation that excites both electrons from bonding to anti-bonding level, as shown in (a). There are 4 types of electron correlation that couple 2 different electron pairs together. Two of these, shown in (b), involve no electron transfer and are included in the imperfect pairing (IP) model in addition to the PP correlations. Electron correlations that transfer either 1 or 2 electrons between pairs are shown in (c) and (d).	50
3.2	Electron correlations that couple three electron pairs together, where the correlations are described in a perfect pairing active space such that each valence occupied orbital has one correlating antibonding orbital. There are 4 distinct types of these correlations, shown schematically in the figure. The two left-most correlations transfer 1 electron from one pair to another, and the two right-most correlations transfer 2 electrons.	51
3.3	The orbitals for N ₂ for IP+DIP in the (6,6) active space at 6-31G. The top row is the occupied orbitals in increasing energy ordering from left to right. The bottom row are the virtual orbitals that correspond in the GVB-PP sense to the occupied orbital directly above it.	52
3.4	The orbitals for N ₂ for TIP in the (6,6) active space at 6-31G. The top row is the occupied orbitals in increasing energy ordering from left to right. The bottom row are the virtual orbitals that correspond in the GVB-PP sense to the occupied orbital directly above it.	53
3.5	A plot of the percent of the VOD correlation energy recovered by TIP for N ₂ at the MP2/6-31G* optimized geometry. Each curve represents a single choice of the amplitude scaling parameter, with the x-axis being the values of the penalty function scalar in Hartrees. The percent of the VOD correlation recovered by TIP with no penalty function at all is 115.71, and the percent recovered with no 2 nd -order perturbation theory is 96.56.	56
3.6	A plot of the percent of the VOD correlation energy recovered by TIP for D _{6h} N ₆ , at the MP2/6-31G* optimized geometry. Each curve represents a single choice of the amplitude scaling parameter, with the x-axis being the values of the penalty function scalar in Hartrees. The percent of the VOD correlation recovered by TIP with no penalty function at all is 98.95 and the percent recovered with no 2 nd -order perturbation theory is 78.68.	57

3.7	A plot of the percent of the VOD correlation energy recovered by TIP for benzene, C ₆ H ₆ , at the MP2/6-31G* optimized geometry. Each curve represents a single choice of the amplitude scaling parameter, with the x-axis being the values of the penalty function scalar in Hartrees. The percent of the VOD correlation recovered by TIP with no penalty function at all is 99.04, and the percent recovered with no 2 nd -order perturbation theory is 82.23.	58
3.8	A plot of the percent of the VOD correlation energy recovered by TIP for water, H ₂ O, at the MP2/6-31G* optimized geometry. Each curve represents a single choice of the amplitude scaling parameter, with the x-axis being the values of the penalty function scalar in Hartrees. The percent of the VOD correlation recovered by TIP with no penalty function at all is 98.48, and the percent recovered with no 2 nd -order perturbation theory is 97.88. . . .	59
3.9	A plot of the percent of the VOD correlation energy recovered by TIP for propane, C ₃ H ₈ , at the MP2/6-31G* optimized geometry. Each curve represents a single choice of the amplitude scaling parameter, with the x-axis being the values of the penalty function scalar in Hartrees. The percent of the VOD correlation recovered by TIP with no penalty function at all is 97.41, and the percent recovered with no 2 nd -order perturbation theory is 94.88.	60
3.10	Potential energy curve for the distortion of benzene along a D _{3h} to D _{6h} coordinate axis. The PP and IP models exhibit SB, whereas the HF, TIP, and VOD methods do not. Absolute energies at the D _{6h} are: -230.702049 H for HF, -230.902841 H for PP, -231.014028 H for IP, -231.075839 H for TIP, and -231.089623 H for VOD.	65
3.11	A chart of the optimized bond lengths for benzene as solved by TIP with the 6-31G* basis set. The TIP (a) bond lengths are without any penalty function. The TIP (b) bond lengths are with the re-formulation and penalty function. All bond lengths are in Å.	65
3.12	The TIP occupied and corresponding virtual orbitals for a) benzene and b) borazine.	67
3.13	The TIP lone pair orbitals for F ₂ computed with a) Pipek-Mezey [66] localized orbitals for the guess and b) the canonical orbitals for the guess. . . .	70
4.1	Unrestricted in active pairs orbitals at the dissociation limit for N ₂	74
4.2	Smallest Jacobian eigenvalue for various fragment dissociations, in the 6-31G basis for all cases except Mo ₂ which is in the CRENBS ECP [177].	76
4.3	The largest Lyapunov exponent as a function of bond length for a stability analysis of PP and IP exchange type amplitudes for 3 molecules using the IP energy ansatz with the UAP PP orbitals in a minimal active space [(4,4) for C ₂ H ₄ and C ₂ H ₃ F, (6,6) for N ₂] with the 6-31G* basis.	77

4.4	CCD parameters for H ₂ in STO-3G basis, horizontal axis θ , vertical axis R (Å).	80
4.5	Orbital labeling for H ₂ dissociation.	80
4.6	Orbital labeling for ethene dissociation.	81
5.1	The unrestriction angle PES for (2,2) H ₂ using PP (choosing most energy lowering amplitudes) with the STO-3G basis.	89
5.2	The C-C dissociation PES for ethene in the (4,4) active space in the 6-31G* basis.	92
5.3	The orbitals at 3.5 Å C-C separation in ethene using restricted, freely unrestric- ting, and UAP PP.	92
5.4	The absolute value of the nuclear gradient along the C-C bonding axis for ethene in the (4,4) active space in the 6-31G* basis.	93
5.5	The N-N dissociation PES for N ₂ in the (6,6) active space in the 6-31G* basis.	94
5.6	The spin-unrestriction point along the single hydrogen abstraction PES for CH ₄ in the (8,8) active space in the 6-31G* basis. The zero in energy is the UAP dissociation limit.	95
5.7	C-H bonding and anti-bonding orbitals from the CH ₃ + H reaction using a) freely unrestric- ting PP and b) UAP-PP. a) Includes an inactive virtual orbital to indicate re-arrangement of active space.	96
5.8	PP using different forms of spin-unrestriction potential energy surfaces along a distortion coordinate from their optimized structures in the cc-pVDZ basis.	98
6.1	Energy (in Hartrees) as a function of H-H separation in the hydrogen molecule by the restricted Hartree-Fock method, the perfect pairing (PP) method (PP for this case is identical to CASSCF with 2 electrons in 2 orbitals), the PP method with the LYP correction for dynamic correlation (uncompensated for double counting), and the exact answer. All calculations are performed in the aug-cc-pVTZ basis.	111
6.2	Energy (in Hartrees) as a function of H-H separation in the hydrogen molecule by the PP method with the compensated correction for residual dynamic correlation defined by Eq. 6.33 using several values of m, as defined in Eq. 6.31, as compared to the exact energy. All calculations are performed in the aug-cc-pVTZ basis.	112
A.1	A chart of the optimized bond lengths for naphthalene as solved by TIP with the 6-31G*. Structure (1) for each level of theory is a D_{2h} guess structure; structure (2) is from a C_{2v} guess. The TIP (a) bond lengths are without any penalty function. The TIP (b) bond lengths are with the re-formulation and penalty function. All bond lengths are in Å. *The VOD bond lengths are with the 6-31G basis set.	123

A.2	A chart of the optimized bond lengths for phenalenyl cation as solved by TIP with the 6-31G*. The TIP (a) bond lengths are without any penalty function. The TIP (b) bond lengths are with the re-formulation and penalty function. All bond lengths are in Å.	123
A.3	A chart of the optimized bond lengths for phenalenyl anion as solved by TIP with the 6-31G*. The TIP (a) bond lengths are without any penalty function. The TIP (b) bond lengths are with the re-formulation and penalty function. All bond lengths are in Å.	124
A.4	The unrestriction angle PES for (4,4) ethene at 1.33 Å C-C separation in ethene using PP (choosing the most energy lowering amplitudes) with the STO-3G basis.	129
A.5	The unrestriction angle PES for (4,4) ethene at 5.00 Å C-C separation in ethene using PP (choosing the most energy lowering amplitudes) with the STO-3G basis.	130

List of Tables

3.1	Correlation energies in Hartrees for a fixed geometry using the PP orbitals. ^a With the RI approximation in the 6-31G* basis (RIMP2-VDZ auxiliary basis). ^b Original formulation of TIP. ^c Re-Formulation of TIP. ^d Includes SIP amplitudes.	61
3.2	Correlation energies in Hartrees for a fixed geometry using the original formulation of TIP's orbitals in the 6-31G* basis (RIMP2-VDZ auxiliary basis). ^a With the RI approximation. ^b Original formulation of TIP. ^c Re-Formulation of TIP. ^d Includes SIP amplitudes.	62
3.3	Correlation and orbital relaxation energies in Hartrees for a fixed geometry using each method's own orbitals in the 6-31G* basis (RIMP2-VDZ auxiliary basis). ^a With the RI approximation. ^b Original formulation of TIP. ^c Re-Formulation of TIP. ^d Includes SIP amplitudes. [*] Converged to a different orbital solution, excluded from statistics.	63
3.4	Predicted equilibrium geometries in the 6-311g(3df,2p) basis (cc-pVTZ RI auxiliary basis) as compared to experiment. ^a Ref. [152], ^b Some structures asymmetric on the milliAngstrom scale, both bond lengths are listed. . . .	64
3.5	Predicted Structures for Li ₂ C ₄ H ₄ in the 6-31G*basis. All bond lengths are in Å. ^a Ref. [154]	66
3.6	Predicted C-C Bond Lengths in C ₄ H ₄ ²⁻ in the 6-31G* basis. All bond lengths are in Å.	66
3.7	Predicted N-S Bond Lengths in N ₂ S ₂ in the 6-31G* basis. All bond lengths are in Å. ^a Ref. [155]	66
3.8	Predicted D _{3h} structures for B ₃ N ₃ H ₆ in the 6-31G* basis. All bond lengths are in Å. ^a Original formulation of TIP. ^b Re-Formulation of TIP.	67
3.9	Predicted Bond Lengths of the first five conjugated polyenes in the 6-31G* basis. All bond lengths are in Å. ^a Ref. [37] ^b Ref. [156,157] ^c Ref. [158] ^d Ref. [159]	69
4.1	Linear coupling matrix for the PP and IP exchange amplitudes for ethene (H ₂ C=CH ₂) at a C-C bond length of 7.50 Å with unrestricted PP orbitals in the minimal active space in the 6-31G* basis.	81

5.1	A timing comparison of both spin-unrestricted implementations of PP for various sized radicals. All calculations are performed in the 6-31G* basis using exact (analytical) integrals with a convergence criterion of 10^{-5} for the orbitals and an integral threshold of 10^{-14} . The timings were done on an Apple Mac Pro with 3 GHz Quad-Core Intel Xeon processors.	90
5.2	Properties of some diatomic radicals in the cc-pVTZ basis (with the rimp2-cc-pVTZ auxiliary basis) using the UAP-PP method. The Mulliken charge and spin populations are given in the order of the molecular formula. The bond lengths are expressed in Angstroms.	96
5.3	Properties of some diatomic radicals in the cc-pVTZ basis (with the rimp2-cc-pVTZ auxiliary basis) using the UAP-2P method. The Mulliken charge and spin populations are given in the order of the molecular formula. The bond lengths are expressed in Angstroms.	97
5.4	Optimized geometries of pentadienyl and heptatrienyl radicals. The calculations were performed with the cc-pVDZ basis (with the rimp2-cc-pVDZ auxiliary basis) with the 3 spin-polarized correlation methods. The a) guess geometries are alternating single and double bonds with the radical electron on a terminal carbon. The b) guess geometries are structures of the appropriate C_{2v} geometry with the radical electron centered on the central carbon of the chain.	99
A.1	Linear coupling matrix for the PP and IP exchange amplitudes for fluoroethene ($\text{HFC}=\text{CH}_2$) at a C-C bond length of 7.50 Å with unrestricted PP orbitals in the minimal active space.	125
A.2	Linear coupling matrix for the PP and IP exchange amplitudes for nitrogen (N_2) at a N-N bond length of 7.50 Å with unrestricted PP orbitals in the minimal active space in the 6-31G* basis.	126
A.3	A timing comparison against all the developed spin implementations of PP. All calculations done in the aug-cc-pVDZ basis.	128
A.4	A timing comparison for different spin/charge states of diatomic molecules in UAP-PP. All calculations done in the aug-cc-pVDZ basis.	128

Acknowledgments

No scientific achievement is ever the work of one person alone, and I would like to acknowledge and thank all of the great people who have aided me along the way in preparing this thesis. First and foremost I would like to thank my advisor Martin Head-Gordon. His ability to mentor a graduate student and turn them into a scientist is really unparalleled. He is constantly a source of good ideas and challenging thoughts. And when I get over being grumpy about having to re-write all of my code for the eighth time this week to try some of his new ideas, it always amazes me how brilliant he is and how invaluable the education I have received from him truly is. I thank him for always being patient with me, and for teaching me so much. I would also like to thank Alex Sodt. He was a great mentor and teacher to me when I first joined the Head-Gordon group. No little bug or silly question was too trite for him to not help me with and to make sure that I learned from the experience. He taught me a lot of the foundations I really needed to know to do scientific computing, and above all else he provided a great friendship during my tenure at Berkeley. I also need to thank many members of the Head-Gordon group who provided much aid and advice throughout the years. I'd first like to thank Joe Subotnik for being a great friend who was always willing to listen no matter how inane my words were. Ryan Steele for being one of the most helpful guys in all of history. I'd like to specially thank my office mates Westin Kurlancheek and Eric Sundstrom for being there for me and always being amenable to blaring loud music to help us get through the work. I'd like to thank my long time collaborator, John Parkhill, for working with me and always being there to help. Greg Beran helped get me going when I first got to Berkeley, and he taught me all about the GVB-CC methods. I'd like to thank my two other collaborators, David Small and Yair Kurzweil, who provided good ideas and work on many projects.

On a personal level, I'd like to thank my family and friends for their constant support and encouragement throughout my entire attempts to complete a PhD at Berkeley. My parents have always been there for me and were willing to listen to my rants and tirades as I was working through everything. They challenged me from an early age to learn as much as possible and are the real reason I am here at Berkeley. I'd also like to send some special appreciation for my girlfriend Michelle. She has put up with me and my endless hunt for bugs and the oh-so faster algorithm. Her love and affection is what has helped propel me through many countless hours of work.

I would also like to thank the Department of Energy for the grant money which has supported this research. This work was supported by the Department of Energy through a grant under the program for Scientific Discovery through Advanced Computing (SciDAC). This work was supported by the Director, Office of Science, Office of Basic Energy Sciences, of the U.S. Department of Energy under Contract No. DE-AC02-05CH11231.

Chapter 1

Introduction

1.1 The Electronic Problem

Quantum mechanics is in essence the study of the behavior of the very small. The formal field of quantum mechanics arose in the early twentieth century [1–10] when many phenomena were being empirically observed [11–14] that defied the contemporary understanding of physics. Quantum mechanics arose from the realization that electrons and other matter behaved as both a particle and wave simultaneously [15]. From this, the mathematics of wave mechanics can be extended and combined with classical mechanics to understand the unique nature of the very small. In a time-independent manner, the entirety of a system of electrons and nuclei can be expressed by a wavefunction that is an eigenfunction of a Hamiltonian,

$$\hat{H}|\Psi\rangle = E|\Psi\rangle. \quad (1.1)$$

For atoms and molecules not in a field, the Hamiltonian is a combination of the kinetic and potential energy operators and a function of all the inter-particle distances.

The Born-Oppenheimer approximation [16] simplifies the time-independent Schrödinger equation into nuclear and electronic sets of variables. This separation of variables can be justified by an argument based on the motion and response of the different types of particles happening on different time scales. Electrons are lower in mass than nuclei and move and interact with each other very quickly, while the nuclei are slower and their motion can be viewed as a response to changes in the electronic state of the system. Nuclear motions occur on the pico-to-femto second time scale, whereas electronic motions occur on the femto-to-atto second time scale. The electronic degrees of freedom are therefore solved independently from those of the nuclei. This is done by creating a wavefunction containing only the electrons that is the eigenfunction of the electronic Hamiltonian (in atomic units):

$$\hat{H}_{elec}|\Psi_{elec}\rangle = E_{elec}|\Psi_{elec}\rangle$$

$$\hat{H}_{elec} = -\sum_i \frac{1}{2}\nabla_i^2 - \sum_i \sum_A \frac{Z_A}{r_{iA}} + \sum_i \sum_{j>i} \frac{1}{r_{ij}}. \quad (1.2)$$

The electronic Hamiltonian accounts for the kinetic energy of all electrons, i , the electronic-nuclear potential energy between all electrons i and all nuclei A , and the electronic-electronic potential energy between all electrons i and j . Solving this eigenfunction problem is the primary focus of the field of study known as electronic structure theory. Knowledge of the electronic wavefunction and electron density is necessary for computing the nuclear dynamics and related properties of the chemical system of interest within the Born-Oppenheimer approximation, and is often the starting point for going beyond it also.

The total N electron electronic wavefunction can be represented as a product of 1-particle wavefunctions. Spin orbitals are 1-particle wavefunctions that are parameterized by the position and the spin angular momentum of the electron, $\chi_i(r_1) = \psi_i(r_1)\alpha(\omega_1)$, or $\chi_i(r_1) = \psi_i(r_1)\beta(\omega_1)$. The spin angular momentum function of the spin orbital is parameterized by the variable, ω_1 . The two electronic spin functions are orthonormal:

$$\begin{aligned} \langle\alpha|\alpha\rangle &= 1 \\ \langle\beta|\beta\rangle &= 1 \\ \langle\alpha|\beta\rangle &= 0. \end{aligned} \quad (1.3)$$

The spatial functions are formed as linear combinations of atomic orbital, $\phi_\mu(r_1)$, basis functions that are optimized for specific atomic properties,

$$\psi_i(r_1) = \sum_\mu c_{\mu i}\phi_\mu(r_1). \quad (1.4)$$

The indices denoted by a lower case Greek letter, μ , represent a function in the atomic orbital (AO) basis, and indices denoted by a lower case Roman letter, i , represent a function in the molecular orbital (MO) basis.

Electrons are fermions and are anti-symmetric with respect to the interchange of two electrons and must obey the Pauli Exclusion Principle [17]. The repercussion of anti-symmetry on the electronic wavefunction is that

$$|\chi_1(r_1)\chi_2(r_2)\dots\rangle = -|\chi_1(r_2)\chi_2(r_1)\dots\rangle. \quad (1.5)$$

A direct product of spin orbitals is not a suitable wavefunction to describe more than one electron because of this property of anti-symmetry. To satisfy anti-symmetry for multi-electron systems, the wavefunction can be expressed as a Slater determinant [18,19] of spin orbitals for each of the N electrons,

$$|\Psi(r_1, r_2, \dots, r_N)\rangle = (N!)^{-\frac{1}{2}} \det\{\chi_i(r_1)\chi_2(r_2)\dots\chi_N(r_N)\}. \quad (1.6)$$

As we shall discuss below, such a form is not exact because it does not include electron correlation. A superposition of all determinants accounting for all possible orbital occupations can be exact and is called full configuration interaction (FCI).

1.2 Ab initio Wavefunction Quantum Mechanics

1.2.1 Mean-Field Approximation

The electronic Schrödinger equation is a difficult problem to solve exactly and much work has been done to approximate the electronic Schrödinger equation. The simplest approximation to understand the electronic problem is the mean-field approximation [20–24]. The mean-field approximation assumes that each electron only interacts with the other electrons by a mean-field created by their charge density.

In the mean-field, or Hartree-Fock (HF), approximation, the N electron wavefunction is represented by a single Slater determinant. The energy of the molecular system is the expectation value of the N electron Slater determinant with the electronic Hamiltonian.

$$\begin{aligned} E_{HF} &= \langle \Psi_{HF} | \hat{H} | \Psi_{HF} \rangle \\ E_{HF} &= \sum_i^{occ} \langle \chi_i | \hat{h} | \chi_i \rangle + \frac{1}{2} \sum_i^{occ} \sum_j^{occ} \left[\langle \chi_i \chi_j | \frac{1}{r_{ij}} | \chi_i \chi_j \rangle - \langle \chi_i \chi_j | \frac{1}{r_{ij}} | \chi_j \chi_i \rangle \right] \end{aligned} \quad (1.7)$$

The MO expansion coefficients from the AO basis, $c_{\mu i}$ from Eqn. 1.4, can be optimized using the variational theorem [25] to return the optimal HF wavefunction and energy. The HF energy is minimized under the constraints that the spin functions are orthonormal and that the individual orbitals remain orthonormal, $\langle \chi_i | \chi_j \rangle = \delta_{ij}$. The overlap of the spatial AO basis functions defines the AO overlap matrix,

$$S_{\mu\nu} = \langle \phi_\mu(r) | \phi_\nu(r) \rangle. \quad (1.8)$$

The overlap matrix can be transformed into the MO basis to form MO overlap matrix, S_{ij} . In HF theory, S_{ij} will be diagonal and will be identical to the identity matrix.

In the MO basis, the HF wavefunction will produce spin orbitals that are either occupied or unoccupied (virtual). For an N electron system in a linearly independent AO basis set of size K , HF produces an N occupied orbitals (denoted by i, j, k, \dots), and $2K - N$ virtual orbitals (denoted by a, b, c, \dots). The N occupied orbitals are the N lowest energy spin orbitals created in a HF calculation. Of course, K must be greater than $N/2$

to generate the appropriate number of occupied spin orbitals. Increasing the size of this AO basis set to be more complete improves the quality of the MOs and lowers the overall HF energy. If the basis set is perfectly flexible (ie. infinite-dimensional), this is known as the complete basis set (CBS). The energy for any method computed with an infinite basis set is known as the CBS limit for the method. Each method has its own convergence rate towards the CBS limit, and HF converges rapidly to this limit relative to other methods like perturbation theory and coupled cluster theory.

HF theory can be reduced to a set of one electron eigenvalue problems for the spin orbitals given their dependence on the other spin orbitals in the system:

$$\begin{aligned}
 \hat{f}(r_1)\chi_i(r_1) &= \varepsilon_i\chi_i(r_1) \\
 \hat{f}(r_1) &= \hat{h}(r_1) + \sum_{j \neq i} \hat{J}_j(r_1) - \sum_{j \neq i} \hat{K}_j(r_1) \\
 \hat{h}(r_1) &= -\sum_i \frac{1}{2} \nabla_i^2 - \sum_i \sum_A \frac{Z_A}{r_{iA}} \\
 \hat{J}_j(r_1)\chi_i(r_1) &= \left[\int dr_2 |\chi_j(r_2)|^2 \frac{1}{r_{ij}} \right] \chi_i(r_1) \\
 \hat{K}_j(r_1)\chi_i(r_1) &= \left[\int dr_2 \chi_j(r_2) \frac{1}{r_{ij}} \chi_i(r_2) \right] \chi_j(r_1)
 \end{aligned} \tag{1.9}$$

The eigenvalue expressions are evaluated for each spin orbital, the MO expansion coefficients are updated, and then the eigenvalue expressions are re-evaluated given the updated expansions for the MO spin orbitals. This process is repeated until the MOs and energy no longer vary. This process is known as a self-consistent field approach to optimizing orbitals and obtaining an energy for the chemical system. The resulting spin orbitals are used to form the HF Slater determinant, which is often used as a zeroth order reference for many higher order quantum chemistry methods.

In these methods, the Fock operator, \hat{f} , becomes the zeroth-order operator whose eigenvalues are sums of orbital energies, ε_i , for eigenvectors which are Slater determinants of spin orbitals. The Fock operator can be written as an expectation value matrix element which is diagonal in the canonical HF MO basis:

$$\begin{aligned}
 \varepsilon_{pq} &= \langle \chi_p(r_1) | \hat{f}(r_1) | \chi_q(r_1) \rangle \\
 \varepsilon_p &= \varepsilon_{pq} \delta_{pq}.
 \end{aligned} \tag{1.10}$$

The HF energy is not just the sum of the occupied spin orbital energies, $E_{HF} \neq \sum_{i=1}^{occ} \varepsilon_i$. The direct sum of spin orbital energies double counts the coulomb, \hat{J} , and exchange, \hat{K} ,

interactions as each eigenvalue includes the full value of these quantities. A factor of $\frac{1}{2}$ must be included on the coulomb and exchange interactions to equal the correct HF energy.

The Fock operator can be represented as matrix in the AO basis,

$$F_{\mu\nu} = \langle \phi_\mu(r_1) | \hat{f}(r_1) | \phi_\nu(r_1) \rangle. \quad (1.11)$$

Using this representation, the Roothaan [26] equations for solving the finite basis HF problem can be written:

$$\begin{aligned} \mathbf{FC} &= \mathbf{SC}\varepsilon \\ \sum_{\nu} F_{\mu\nu} c_{\nu i} &= \varepsilon_i \sum_{\nu} S_{\mu\nu} c_{\nu i} \end{aligned} \quad (1.12)$$

This is a matrix eigenvalue problem which is ideally suited for a computer to solve. The eigenvalue problem is for the MO expansion coefficient matrix, however the internal dependence of \mathbf{F} on \mathbf{C} is the reason the HF equations need to be solved self-consistently. If the spatial components of the spin orbitals of different spin are allowed to vary independently of each other, a similar set of equations known as the Pople-Nesbet equations [27] exist to solve the spin-unrestricted HF (UHF) problem. Allowing the spatial components of the spin orbitals of different spin to vary independently is known as spin-unrestriction.

1.2.2 Orbital Rotations

Spin orbitals can be optimized by the self-consistent field approach, repeated diagonalization, or by making an initial guess and rotating the orbitals into each other via a series of unitary orbital rotations. Unitary orbital rotations are a type of matrix transformation using unitary matrices. Unitary matrices are a special kind of matrix in which the matrix inverse is the adjoint of the matrix,

$$\mathbf{U}^\dagger \mathbf{U} = \mathbf{1}. \quad (1.13)$$

Unitary matrices also have the nice property of preserving the Hermitian inner product of any two vectors. A consequence of this property is that a unitary transformation of a matrix preserves the trace of the original matrix.

Unitary matrices can be constructed by taking the matrix exponential of any anti-Hermitian matrix:

$$\begin{aligned} \mathbf{U} &= e^\theta \\ \theta^\dagger &= -\theta. \end{aligned} \quad (1.14)$$

In the case of a real matrix, the anti-Hermitian property simplifies to the property of being anti-symmetric, and the adjoint simplifies to a matrix transpose.

Since all the eigenvalues of a unitary matrix lie on the unit circle, unitary transformations can be viewed as rotations by some angle between element p into element q , θ_{pq} . The anti-symmetric representation of this orbital rotation in a two-dimensional space is

$$\theta = \begin{bmatrix} 0 & \theta_{pq} \\ -\theta_{pq} & 0 \end{bmatrix}$$

Exponentiating this anti-symmetric matrix yields a Givens transformation,

$$\mathbf{G}(\theta_{\mathbf{pq}}) = e^\theta = \begin{bmatrix} \cos(\theta_{pq}) & \sin(\theta_{pq}) \\ -\sin(\theta_{pq}) & \cos(\theta_{pq}) \end{bmatrix}.$$

For more than two elements, the two-by-two rotation matrix element can be projected into an identity matrix of size N total elements by N total elements [28]. This matrix will resemble the identity matrix except for the $\mathbf{G}(p, p)$, $\mathbf{G}(p, q)$, $\mathbf{G}(q, p)$, and $\mathbf{G}(q, q)$ elements which will be those shown in the two-by-two case. The total unitary rotation matrix then can be constructed as a product of the projected two-by-two unitary rotation matrices,

$$\mathbf{U} = \prod_p^N \prod_q^N \mathbf{G}(\theta_{\mathbf{pq}}). \quad (1.15)$$

Unitary orbital rotations have utility in quantum chemistry because of their ability to simplify orbital optimization problems in quantum chemistry. MO expansion coefficients can be optimized by successive unitary transformations of some set of initial guess MO expansion coefficients,

$$\mathbf{C} = \mathbf{C}_0 \prod_i^{N_{iter}} \mathbf{U}_i. \quad (1.16)$$

This process is done iteratively for N_{iter} iterations after which the final spin orbitals should yield the optimal energy for the quantum chemistry method. The standard way to perform the iterative optimization of the set of MO expansion coefficients with respect to orbital rotations is to take orbital rotation steps until the orbital rotation gradient is zero or within tolerances,

$$\frac{\partial E}{\partial \theta_{pq}} = \sum_\mu \left[\frac{\partial E}{\partial C_{\mu p}} C_{\mu q} - \frac{\partial E}{\partial C_{\mu q}} C_{\mu p} \right] = 0. \quad (1.17)$$

The steepest descent algorithm for this minimization involves taking only gradient descent steps to generate a change in the orbital rotation angle, $\delta\theta_{pq} = -\frac{\partial E}{\partial \theta_{pq}}$. These steps

are re-constructed into a new orbital rotation matrix and the process is repeated. This method is slow and does not typically converge quadratically, rather its convergence is linear. Quadratic convergence is defined as the gradient and step size decreasing quadratically after each optimization iteration. The optimization process can be greatly enhanced by knowledge of the curvature of the potential energy surface, ie. a Hessian. A pure Newton method with knowledge of the full Hessian will optimize with quadratic convergence, but this approach is excessively expensive and complicated because exact evaluation of the Hessian is expensive and complicated. For most quasi-Newton or BFGS [29, 30] methods, only the diagonal of the orbital rotation Hessian is necessary and the convergence is intermediate between quadratic and linear. The diagonal of the orbital rotation Hessian expressed only in terms of MO expansion coefficients is

$$\begin{aligned} \frac{\partial^2 E}{\partial \theta_{pq}^2} &= \sum_{\mu} \sum_{\nu} \left[\frac{\partial^2 E}{\partial C_{\mu p} \partial C_{\nu p}} C_{\mu q} C_{\nu q} + \frac{\partial^2 E}{\partial C_{\mu q} \partial C_{\nu q}} C_{\mu p} C_{\nu p} - 2 \frac{\partial^2 E}{\partial C_{\mu p} \partial C_{\nu q}} C_{\mu q} C_{\nu p} \right] \\ &- \sum_{\mu} \left[\frac{\partial E}{\partial C_{\mu p}} C_{\mu p} + \frac{\partial E}{\partial C_{\mu q}} C_{\mu q} \right]. \end{aligned} \quad (1.18)$$

A BFGS method like Geometric Direct Minimization (GDM) [30] will optimize MO expansion coefficients with superlinear convergence depending on the quality of the diagonal of the orbital rotation Hessian. This procedure will work for any quantum chemistry method that relies on orbital optimization.

1.2.3 The Need for Electron-Electron Correlation

HF is qualitatively correct for many systems, but often it is quantitatively incorrect even for the systems for which it is qualitatively correct. HF theory only provides a mean-field description of the molecular system and does not account for any instantaneous electron-electron interactions. The missing energy arising from the neglected interactions is called the correlation energy and is expressed as the difference between the exact energy ground state energy and the HF energy in a given AO basis. The correlation energy is small in magnitude when compared to the mean-field energy obtained by an HF calculation. This correlation energy is important for many molecular systems. Some examples are dispersion bound complexes [31] and hydrogen abstraction processes [32, 33] that need dispersion and Van der Waals interactions to describe the energetics of the system. Another example is the oligo-acenes (the naphthalene, anthracene, tetracene, ... series) [34, 35] and any other molecular system where the wavefunction can only be described well by more than one Slater determinant, since the mean-field approximation only accounts for one possible configuration of the electrons within the basis functions that have been used in the calculation.

The mean-field approximation can be steadily improved upon to reach chemical accuracy for chemical systems. Instantaneous electron-electron correlations are modeled in wavefunction based methods as excitations from the HF occupied orbitals into the remaining virtual orbitals. One common approximation for the correlation energy is Rayleigh-Schrödinger perturbation theory [36]. The HF reference, $|\Psi_{ref}\rangle$, does not couple directly to singly excited Slater determinants, $|\Psi_i^a\rangle$, because the canonical MO representation of the Fock matrix is diagonal as is seen in Eqn. 1.10. In the order-by-order by expansion of Rayleigh-Schrödinger perturbation theory to the HF reference, the leading order is second-order perturbation theory. Second-order perturbation theory couples the HF reference Slater determinant to doubly excited Slater determinants, $|\Psi_{ij}^{ab}\rangle$, and is usually referred to as Møller-Plesset second-order perturbation theory (MP2). The energy expression for the MP2 correlation energy is

$$E_{MP2} = \frac{1}{4} \sum_{i,j}^{occ} \sum_{a,b}^{virt} \frac{|\langle \Psi_{ref} | \hat{H} | \Psi_{ij}^{ab} \rangle|^2}{\varepsilon_i + \varepsilon_j - \varepsilon_a - \varepsilon_b} = \frac{1}{4} \sum_{i,j}^{occ} \sum_{a,b}^{virt} \frac{|\langle ij || ab \rangle|^2}{\varepsilon_i + \varepsilon_j - \varepsilon_a - \varepsilon_b}. \quad (1.19)$$

The double bar integrals are the anti-symmetric four-center two-electron integrals:

$$\langle ij || ab \rangle = \langle \chi_i(r_1) \chi_j(r_2) | \frac{1}{r_{12}} | \chi_a(r_1) \chi_b(r_2) \rangle - \langle \chi_i(r_1) \chi_j(r_2) | \frac{1}{r_{12}} | \chi_b(r_1) \chi_a(r_2) \rangle. \quad (1.20)$$

MP2 is a useful method for improving the quantitative energetics compared to HF. MP2 works well in general for predicting equilibrium properties of molecules. MP2 does not perform well when HF theory provides a poor reference especially when the molecule is multi-configurational in nature. Open-shell radicals, diradical systems, conjugated systems like the oligo-acenes [34, 35] and polyenes [37] are all systems where the HF reference or a single Slater determinant is a poor reference. The strong (static) correlations in these types of cases need to be accounted for more directly.

Configuration interaction (CI) [38–41] theory is where the wavefunction is expanded as a linear combination of all possible determinants up to a certain selected level of electron excitations (ie. single excitations, double excitations, triple excitations, etc).

$$\begin{aligned} |\Psi_{CI}\rangle &= (1 + \hat{C}) |\Psi_{ref}\rangle \\ |\Psi_{CI}\rangle &= |\Psi_{ref}\rangle + \sum_i^{occ} \sum_a^{virt} c_i^a |\Psi_i^a\rangle + \sum_{i,j}^{occ} \sum_{a,b}^{virt} c_{ij}^{ab} |\Psi_{ij}^{ab}\rangle + \dots \\ |\Psi_i^a\rangle &= \hat{a}_a^\dagger \hat{a}_i |\Psi_{ref}\rangle \\ \hat{a}_i |i\rangle &= |0\rangle \\ \hat{a}_a^\dagger |0\rangle &= |a\rangle \end{aligned} \quad (1.21)$$

The ladder operators, \hat{a} , create and annihilate electrons in a formalism known as second quantization [42]. Second quantization is a useful algebraic tool for constructing matrix elements of the CI coupling matrix. The full configuration interaction (FCI) method constructs a full Hamiltonian matrix which accounts for the coupling between all possible N -electron Slater determinants. The CI Hamiltonian matrix is diagonalized and the lowest eigenvalue produces an eigenvector containing the optimized CI expansion coefficients for the ground state of the system within the given basis. The higher energy eigenvalues produce eigenvectors containing the CI expansion coefficients for the excited states of the molecular system. The main drawback to CI is its incredibly large cost. The cost grows factorially with the introduction of new electrons or orbitals to the system. FCI is only affordable for a very limited number of systems. Currently this limit is about 10 electrons in a medium sized basis as that leads to billions of configurations that need to be accounted for [43–48].

1.3 Valence Active Space Correlation Methods

1.3.1 Truncated CI and Size-Consistency

Due to the large cost of a FCI calculation, the number of configurations included in a CI calculation is often truncated [24, 39, 42]. This truncation is usually not done on a configuration by configuration basis, but rather by classes of configurations (ie. including only singly and doubly excited Slater determinants along with the reference). If the CI expansion is truncated, the energy is not size-consistent [42, 49]. Size-consistency is the property that a molecular supersystem of two non-interacting fragments A and B have the same energy as the sum of the energy of the fragments computed individually, $E^{A+B} = E^A + E^B$. In the limit of the fragments becoming non-interacting, the Hamiltonian is separable,

$$\hat{H} = \hat{H}_A + \hat{H}_B. \quad (1.22)$$

A multiplicatively separable wavefunction is one that can be factorized into a product wavefunction with each product localized on a fragment,

$$|\Psi_{A+B}\rangle = |\Psi_A\Psi_B\rangle. \quad (1.23)$$

For an approximation like the HF wavefunction where in the limit on non-interacting fragments, the wavefunction becomes multiplicatively separable, the energies of the supersystem and subsystems are

$$\begin{aligned} E^A &= \langle \Psi_A | \hat{H}_A | \Psi_A \rangle / \langle \Psi_A | \Psi_A \rangle \\ &= \langle \Psi_A | \hat{H}_A | \Psi_A \rangle \end{aligned}$$

$$\begin{aligned}
E^B &= \langle \Psi_B | \hat{H}_B | \Psi_B \rangle / \langle \Psi_B | \Psi_B \rangle \\
&= \langle \Psi_B | \hat{H}_B | \Psi_B \rangle \\
E^{A+B} &= \langle \Psi_A \Psi_B | \hat{H}_A + \hat{H}_B | \Psi_A \Psi_B \rangle / \langle \Psi_A \Psi_B | \Psi_A \Psi_B \rangle \\
&= \langle \Psi_A | \hat{H}_A | \Psi_A \rangle + \langle \Psi_B | \hat{H}_B | \Psi_B \rangle
\end{aligned} \tag{1.24}$$

All multiplicatively separable wavefunctions have size-consistent energy expressions. Because it is a complete wavefunction, the FCI can be expressed as a product wavefunction and is size consistent. The truncated CI wavefunction must be expressed as a linear expansion and is not generally multiplicatively separable. The truncated CI wavefunctions for the system of two non-interacting fragments, A and B , is

$$\begin{aligned}
|\Psi_{CI}\rangle &= (1 + \hat{C})|\Psi\rangle \\
|\Psi_{CI}^A\rangle &= (1 + \hat{C}_A)|\Psi_A\rangle \\
|\Psi_{CI}^B\rangle &= (1 + \hat{C}_B)|\Psi_B\rangle \\
|\Psi_{CI}^{A+B}\rangle &= (1 + \hat{C}_A + \hat{C}_B)|\Psi_{A+B}\rangle.
\end{aligned} \tag{1.25}$$

The expectation values of the CI wavefunction of the subsystems, A and B , with the Hamiltonian are

$$\begin{aligned}
E^A &= \langle \Psi_{CI}^A | \hat{H}_A | \Psi_{CI}^A \rangle / \langle \Psi_{CI}^A | \Psi_{CI}^A \rangle \\
E^B &= \langle \Psi_{CI}^B | \hat{H}_B | \Psi_{CI}^B \rangle / \langle \Psi_{CI}^B | \Psi_{CI}^B \rangle.
\end{aligned} \tag{1.26}$$

The expectation value of the truncated CI wavefunction of the supersystem with the Hamiltonian is

$$E^{A+B} = \langle \Psi_{CI}^{A+B} | \hat{H}_{A+B} | \Psi_{CI}^{A+B} \rangle / \langle \Psi_{CI}^{A+B} | \Psi_{CI}^{A+B} \rangle. \tag{1.27}$$

The numerator of Eqn 1.27 can be expressed as

$$\begin{aligned}
\langle \Psi_{CI}^{A+B} | \hat{H}_{A+B} | \Psi_{CI}^{A+B} \rangle &= \langle \Psi_A \Psi_B | \hat{H}_A + \hat{H}_B | \Psi_A \Psi_B \rangle \\
&+ \langle \Psi_A \Psi_B | (\hat{C}_A + \hat{C}_B) (\hat{H}_A - E_{HF}^A) (\hat{C}_A + \hat{C}_B) | \Psi_A \Psi_B \rangle \\
&+ \langle \Psi_A \Psi_B | (\hat{C}_A + \hat{C}_B) (\hat{H}_B - E_{HF}^B) (\hat{C}_A + \hat{C}_B) | \Psi_A \Psi_B \rangle.
\end{aligned} \tag{1.28}$$

Eqn. 1.28 simplifies to

$$\begin{aligned}
\langle \Psi_{CI}^{A+B} | \hat{H}_{A+B} | \Psi_{CI}^{A+B} \rangle &= E_{HF}^A + \langle \Psi_A | \hat{C}_A (\hat{H}_A - E_{HF}^A) \hat{C}_A | \Psi_A \rangle \\
&+ E_{HF}^B + \langle \Psi_B | \hat{C}_B (\hat{H}_B - E_{HF}^B) \hat{C}_B | \Psi_B \rangle \\
\langle \Psi_{CI}^{A+B} | \hat{H}_{A+B} | \Psi_{CI}^{A+B} \rangle &= \langle \Psi_{CI}^A | \hat{H}_A | \Psi_{CI}^A \rangle + \langle \Psi_{CI}^B | \hat{H}_B | \Psi_{CI}^B \rangle.
\end{aligned} \tag{1.29}$$

The numerator of the CI expectation value separates to an expression that appears to be size-consistent. The denominator of Eqn 1.27 can be expressed as

$$\begin{aligned} \langle \Psi_{CI}^{A+B} | \Psi_{CI}^{A+B} \rangle &= 1 + \langle \Psi^A | \hat{C}_A \hat{C}_A | \Psi^A \rangle + \langle \Psi^B | \hat{C}_B \hat{C}_B | \Psi^B \rangle \\ &= \langle \Psi_{CI}^A | \Psi_{CI}^A \rangle + \langle \Psi_{CI}^B | \Psi_{CI}^B \rangle - 1. \end{aligned} \quad (1.30)$$

The combination of the numerator in 1.29 and the denominator in 1.30 does not yield an expression that is equivalent to summing the two individual fragments energies in 1.26. The truncated CI wavefunction is not size-consistent because it must be expressed as a linear combination of determinants and not a product wavefunction.

1.3.2 CASSCF

The truncation of the set of configurations in the CI wavefunction by excitation level means that not all potentially important strong correlations are accounted for. An alternate truncation is to define an active space containing only a subset of the occupied and virtual spin orbitals for computing the correlation energy. An ideal active space includes only the valence orbitals. Valence orbitals are typically the highest energy occupied and lowest energy virtual orbitals. The physical interpretation for the types of orbitals included in the valence space are: bonding occupied orbitals, lone pair occupied orbitals, singly occupied orbitals, anti-bonding virtual orbitals, and virtual orbitals that correspond to the anti-bonding orbital of a lone pair occupied orbital. The cost of including additional electrons in the active space is exponential in cost for complete CI expansions of the wavefunction. The active space should include a sufficient but not excessive number of orbitals to describe the static correlations and form all the appropriate Slater determinants to describe the multi-reference/multi-configurational nature of the true wavefunction.

The MO expansion coefficients can be re-optimized along with the simultaneous determination of the the CI coefficients to improve the wavefunction. Complete Active Space Self-Consistent Field (CASSCF) [50–55] is a method for strong correlation which optimizes the MO expansion coefficients while accounting for all possible N -electron excitations within the active space. Unlike MP2 and the other CI theories discussed, CASSCF is a model chemistry that re-optimizes the MO expansion coefficients after they have been optimized in the HF level of theory. The re-optimization of the MO expansion coefficients emphasizes the other configurations as well as the reference configuration. The resulting wavefunction well describes the multi-configurational/multi-reference nature of molecular systems and provides an accurate correlation energy for the static correlations. CASSCF is a full CI method in the active space and therefore is size-consistent. However as a result, the cost of CASSCF increases exponentially with the number of active electrons. CASSCF also does not account for any residual, dynamic, correlation. The dynamic correlation is

necessary to describe obtain the true non-relativistic ground state energy of the system and to accurately predict phenomena such as reaction energies, reaction barrier heights, and Van der Waals interactions.

1.3.3 GVB-PP

CASSCF is exponential in computational cost to determine the CI coefficients and is iterative to simultaneously optimize the CI coefficients and the MO expansion coefficients. To apply valence active space correlation theories to larger molecular systems or larger active spaces, the overall cost of the calculation must be reduced. The strongest correlations are often local in nature, and a local approximation to the correlation can be used to improve the computational efficiency of CASSCF. Generalized Valence Bond-Perfect Pairing (GVB-PP) [56, 57] is a simple, highly local approximation to CASSCF in the active space which includes one active orbital per active electron (often called the pairing active space).

The GVB-PP wavefunction describes how electrons interact in a pairwise fashion. The spin orbitals in the active space can be assembled into two-electron pairs such that the two spin orbitals in the pair describe the same chemical feature, ie. a σ bond. In a spin-restricted calculation, these spatial functions of these paired spin orbitals are exactly the same. Each occupied pair is perfectly paired to a virtual pair of spin orbitals that are grouped together in a similar manner as the occupied spin orbital pairs. These occupied-virtual pairings are done in a one-to-one fashion with only one pair of occupied orbitals correlating with one pair of virtual orbitals. The occupied-virtual pairings are determined variationally to account for the strongest correlations. The strongest correlations will typically be with a bonding orbital pair, i , and its corresponding anti-bonding orbital pair, i^* . A consequence of this one-to-one type of occupied-virtual pairing is that the active space must have the same number of occupied orbitals as it does virtual orbitals.

Correlating a pair of occupied orbitals to a pair of virtual orbitals is equivalent to accounting for a single doubly excited CI configuration. A specific GVB-PP anti-symmetric geminal can be created for pair i to incorporate the correlation:

$$g_i^{PP}(r_1, r_2, \omega_1, \omega_2) = 2^{-\frac{1}{2}} \left[\phi_i(r_1)\phi_i(r_2) + c_{ii}^{i^*i^*} \phi_{i^*}(r_1)\phi_{i^*}(r_2) \right] (\alpha(\omega_1)\beta(\omega_2) - \alpha(\omega_2)\beta(\omega_1)). \quad (1.31)$$

The spatial portions of each of the occupied and virtual paired orbitals is shown here as different to represent the case of spin-unrestriction. The spatial one electron functions of different spin will be allowed to vary from one another to lower the overall energy in a spin-unrestricted formalism. If there is no truncation of correlations in the active space correlation method, as in CASSCF, then restricted orbitals can be employed to ensure a spin-eigenstate is obtained. If the correlation treatment is approximate, as in GVB-PP,

then spin-unrestricted orbitals are essential in order to obtain correct dissociation products, particularly for dissociating multiple bonds and generally for any system with multiple correlated electron pairs.

A total GVB-PP wavefunction can be expressed as an anti-symmetric Slater determinant, represented by the anti-symmetry operator \hat{A} , of the core orbitals outside the active space and the GVB-PP geminals,

$$|\Psi_{GVB-PP}\rangle = \hat{A}|\chi_1\chi_2\dots g_i^{PP}g_j^{PP}\dots\rangle. \quad (1.32)$$

Due to the nature of the occupied-virtual pairing, there are only a linear number of expansion coefficients, $c_{\bar{i}\bar{i}^*}^{i^*i}$, to optimize along with the MO expansion coefficients to obtain the GVB-PP wavefunction. This smaller number of variables greatly reduces the cost of the overall valence active space calculation for GVB-PP compared to CASSCF. GVB-PP can be used for larger molecular systems with larger active spaces than CASSCF. For example, GVB-PP can be used to analyze long arene chains with the full bonding active space as opposed to just the π bonding active space of benzene.

1.3.4 Localized Orbitals

Canonical HF MOs are very non-local and often span much of the whole molecular system, whereas the GVB-PP MOs localize in space due to the highly local nature of the correlation energy. The localized GVB-PP MOs resemble the MOs that would be predicted with some intuition about chemical bonding, ie. σ and π bonding orbitals that span only the space of a few atoms and core orbitals that localize on single atoms in the molecule. Linear combinations of the canonical HF MOs can be made to closely resemble the GVB-PP MOs. Localizing the canonical HF MOs before a GVB-PP orbital optimization improves the GVB-PP calculation by reducing the total number of iterations necessary to solve for the GVB-PP energy and wavefunction. Localization for active space methods is done independently in the subspaces of the inactive (core) occupied orbitals, the active occupied orbitals, the active virtual orbitals, and the inactive virtual orbitals.

Many methods exist to localize orbitals based on optimizing the orbitals to meet a certain criterion. The Boys localization [58] method minimizes the sum of spatial extent of the orbitals. For each orbital i in the subspace of orbitals being localized, the spatial extent integral is evaluated,

$$\langle\chi_i(r_1)\chi_i(r_2)|(r_1 - r_2)^2|\chi_i(r_1)\chi_i(r_2)\rangle. \quad (1.33)$$

These integrals are summed and the orbitals in the subspace are rotated with each other to minimize that sum. Boys localization can also be written as a maximization of the distance between orbital centroids,

$$\sum_{i,j} [\langle \chi_i(r_1) | r_1 | \chi_i(r_1) \rangle - \langle \chi_j(r_1) | r_1 | \chi_j(r_1) \rangle]^2. \quad (1.34)$$

This process can be done with just the dipole integrals and can be solved in third order time once those integrals are known. Boys localization is an iterative procedure repeated iteratively until the orbitals self-consistently extremize either representation of the localization kernel.

The Edmiston-Ruedenberg (ER) localization [59,60] method maximizes the self-interaction energy of the orbitals. For each orbital i in the subspace of orbitals being localized, the self-interaction energy integral is evaluated,

$$\langle \chi_i(r_1) \chi_i(r_2) | \frac{1}{|r_{12}|} | \chi_i(r_1) \chi_i(r_2) \rangle. \quad (1.35)$$

These integrals are summed for all the orbitals in the subspace being localized and rotated to maximize that sum. This localization procedure is also iterative and the formation of these integrals has equivalent computational cost to the formation of the coulomb integrals for HF. The ER procedure without the use of the resolution of the identity (RI) approximation [61–63] has equivalent overall computational cost to performing a HF computation. With RI, the ER procedure is reasonably efficient though still much costlier than the Boys method. These orbitals can be considered as the most classical and useful for creating a valence correlation picture as they minimize the overall exchange between all the orbitals by maximizing the self-interaction within an orbital [64,65].

The Pipek-Mezey (PM) localization [66] method is perhaps the best balance of speed and quality of orbitals. The PM localization scheme is based on population localization and seeks to minimize the number of atoms spanned by the charge density. In this procedure an atomic density projection operator is constructed for each atom A , \hat{P}_A , spanning all the atomic functions on atom A . The functional of the population can be created,

$$\mathbf{P} \{ \psi_i \dots \psi_N \} = \sum_i \sum_A \left[\langle i | \hat{P}_A | i \rangle \right]^2. \quad (1.36)$$

This population per atom is then maximized to localize the overall extent of each MO. PM localization is a third order method like Boys localization. PM localization works well for localized systems and typically converges faster than a Boys localization [67].

Once the occupied orbitals have been localized, how should the active space virtual orbitals that are the best guess to the pairing orbitals be found? The procedure of Sano [68] provides a good guess for the GVB-PP virtual orbitals. In the Sano procedure the active

occupied orbitals are gone through one-by-one and an exchange matrix is produced that evaluates the exchange of the occupied orbital i with that of the entire virtual space,

$$K_{ab}^{[ii]} = \langle ii|ab\rangle. \quad (1.37)$$

The eigenvalues of this matrix are found, and the largest eigenvalue's eigenvector is used to construct a guess virtual orbital. The largest eigenvalue is chosen because that virtual orbital has maximal exchange with the paired occupied orbital i . The virtual orbital with the maximal exchange with its paired occupied produces the lowest GVB-PP energy for that pair. The new modified virtual orbital is projected out of the virtual space and the procedure is then repeated for all other occupied orbitals in the active space. This new set of active space virtual orbitals is paired correctly for GVB-PP and does not need to be further localized. Only the remaining inactive virtual orbitals remain to be optionally localized to create a high quality initial guess for GVB-PP.

1.4 Coupled Cluster Theory

1.4.1 Basics of Coupled Cluster Theory

Coupled cluster (CC) theory [49, 69–77] is an alternative to CI for approximating the correlated wavefunction. Instead of a linear superposition of determinants, CC theory revolves around an exponential form of the wavefunction,

$$|\Psi_{CC}\rangle = e^{\hat{T}}|\Psi_{ref}\rangle. \quad (1.38)$$

The cluster operator, \hat{T} is a linear combination of excitation operators, like the CI operator \hat{C} , that can include single, double, triple, and higher excitations. If the cluster operator is not truncated it is the exact wavefunction, but it is often truncated to make the method computationally tractable for a variety of systems. The highest excitation operators included in the cluster operator define the level of the truncated CC theory.

$$\begin{aligned} \hat{H}e^{\hat{T}}|\Psi_{ref}\rangle &= Ee^{\hat{T}}|\Psi_{ref}\rangle \\ \hat{T} &= \hat{T}_1 + \hat{T}_2 + \dots \\ \hat{T}_1 &= \sum_i \sum_a t_i^a \hat{a}_a^\dagger \hat{a}_i \\ \hat{T}_2 &= \frac{1}{4} \sum_{i,j} \sum_{a,b} t_{ij}^{ab} \hat{a}_a^\dagger \hat{a}_b^\dagger \hat{a}_j \hat{a}_i. \end{aligned} \quad (1.39)$$

The equations for the energy and the amplitudes, t , can be determined by simply left projecting any level of excited determinant on the CC eigenvalue expression, with intermediate normalization assumed ($\langle \Psi_{ref} | \Psi_{CC} \rangle = 1$):

$$\begin{aligned}
\langle \Psi_{ref} | \hat{H} e^{\hat{T}} | \Psi_{ref} \rangle &= E \langle \Psi_{ref} | e^{\hat{T}} | \Psi_{ref} \rangle = E \\
\langle \Psi_{ij\dots}^{ab\dots} | \hat{H} e^{\hat{T}} | \Psi_{ref} \rangle &= E \langle \Psi_{ij\dots}^{ab\dots} | e^{\hat{T}} | \Psi_{ref} \rangle.
\end{aligned} \tag{1.40}$$

An equivalent form of the projection approach demonstrated in Eqn. 1.40 most commonly used to solve for the CC energy and amplitudes utilizes a left projection of the inverse of the exponential operator, $e^{-\hat{T}}$,

$$\begin{aligned}
\langle \Psi_{ref} | e^{-\hat{T}} \hat{H} e^{\hat{T}} | \Psi_{ref} \rangle &= E \langle \Psi_{ref} | e^{-\hat{T}} e^{\hat{T}} | \Psi_{ref} \rangle = E \langle \Psi_{ref} | \Psi_{ref} \rangle = E \\
\langle \Psi_i^a | e^{-\hat{T}} \hat{H} e^{\hat{T}} | \Psi_{ref} \rangle &= E \langle \Psi_i^a | e^{-\hat{T}} e^{\hat{T}} | \Psi_{ref} \rangle = E \langle \Psi_i^a | \Psi_{ref} \rangle = 0 \\
\langle \Psi_{ij}^{ab} | e^{-\hat{T}} \hat{H} e^{\hat{T}} | \Psi_{ref} \rangle &= E \langle \Psi_{ij}^{ab} | e^{-\hat{T}} e^{\hat{T}} | \Psi_{ref} \rangle = E \langle \Psi_{ij}^{ab} | \Psi_{ref} \rangle = 0 \\
t_i^a &: \omega_i^a = \langle \Psi_i^a | e^{-\hat{T}} \hat{H} e^{\hat{T}} | \Psi_{ref} \rangle = 0 \\
t_{ij}^{ab} &: \omega_{ij}^{ab} = \langle \Psi_{ij}^{ab} | e^{-\hat{T}} \hat{H} e^{\hat{T}} | \Psi_{ref} \rangle = 0.
\end{aligned} \tag{1.41}$$

This form uses the similarity transformed Hamiltonian, $e^{-\hat{T}} \hat{H} e^{\hat{T}}$, which is not Hermitian but has an identical eigenvalue spectrum to the original Hamiltonian if the cluster operator is not truncated and is very similar if the cluster operator is truncated [49]. The similarity transformed Hamiltonian can be evaluated as a sum of nested commutators of \hat{H} and \hat{T} in order to solve equations in 1.41.

The projective approach to solving the CC equations is non-variational as the left projection is not equivalent to an expectation value expression of the CC equations as the inverse of the exponential cluster operator is not equivalent to the adjoint of the exponential cluster operator, $e^{-\hat{T}} \neq e^{\hat{T}^\dagger}$. The CC energy evaluated in this fashion will not be an upper bound to the true ground state energy unless the cluster operator is not truncated. The CC amplitudes are formally exact if the cluster operator is not truncated.

To examine the size-consistency of the CC energy, the same model used in Section 1.3.1 needs to be applied to the CC wavefunction and energy. Using the exponential cluster operator, the wavefunction of the supersystem of $A + B$ is

$$\begin{aligned}
|\Psi_{CC}\rangle &= e^{\hat{T}_A + \hat{T}_B} |\Psi_{A+B}\rangle \\
|\Psi_{CC}\rangle &= e^{\hat{T}_A} e^{\hat{T}_B} |\Psi_{A+B}\rangle \\
|\Psi_{CC}\rangle &= |e^{\hat{T}_A} \Psi_A e^{\hat{T}_B} \Psi_B\rangle.
\end{aligned} \tag{1.42}$$

The CC wavefunction for the non-interacting fragments can be expressed as a multiplicatively separable product wavefunction. The energy can be evaluated similarly to Eqn. 1.24. Regardless of the level of truncation, the CC energy is size-consistent because the

CC wavefunction can always be expressed as a product wavefunction.

Coupled cluster doubles (CCD) is the smallest truncation that makes any correction to the energy obtained using the HF wavefunction as the reference wavefunction for CC theory. By contrast with MP2, the CCD amplitudes, t_{ij}^{ab} , include contributions up to infinite-order not just first-order, and they produce better overall energies and properties. The energy expression for CCD using the HF wavefunction as a reference is

$$E_{CCD} = E_{HF} + \frac{1}{4} \sum_{i,j}^{occ} \sum_{a,b}^{virt} t_{ij}^{ab} \langle ij || ab \rangle. \quad (1.43)$$

Solving the full CCD amplitude equations scales with the 6th power of molecular size computationally. For large basis sets, the scaling is more precisely the size of the occupied space squared, o^2 , by the size of the virtual space to the 4th power, v^4 , yielding the true 6th order scaling of the method, o^2v^4 . Increasing the molecular system size only raises the cost of a CCD calculation 6th order polynomial time, not factorial time like CI.

1.4.2 Coupled Cluster Generalized Valence Bond Theory

Because of the highly desirable properties of size-consistency and containing infinite-order perturbation contributions, GVB wavefunctions can be re-cast from the geminal form shown in Eqn. 1.32 into an exponential CC wavefunction [78, 79]. This re-formulation is called generalized valence bond-coupled cluster (GVB-CC) theory. The one CI doubles excitation operator per geminal can be replaced with an exponential CCD operator that only includes only the diagonal amplitudes correlating pairs in the active space,

$$\begin{aligned} \hat{T}_{PP} &= \sum_i^{N_{pairs}} t_{i\bar{i}}^{i^* \bar{i}^*} \hat{a}_{i^*}^\dagger \hat{a}_{\bar{i}^*}^\dagger \hat{a}_{\bar{i}} \hat{a}_i \\ E_{PP} &= E_{ref} + \sum_i^{N_{pairs}} t_{i\bar{i}}^{i^* \bar{i}^*} \langle i\bar{i} || i^* \bar{i}^* \rangle. \end{aligned} \quad (1.44)$$

The perfect pairing (PP) method optimizes both the small number of retained CCD amplitudes and the MO expansion coefficients. To do this, CC theory can be made to be pseudo-variational by using Lagrange's method of undetermined multipliers by using a de-excitation operator in the left projections of Eqn. 1.41. For a full treatment of CCD, the pseudo-variational Lagrangian looks like:

$$\hat{\Lambda}_2 = \frac{1}{4} \sum_{i,j}^{occ} \sum_{a,b}^{virt} \lambda_{ij}^{ab} \hat{a}_i^\dagger \hat{a}_j^\dagger \hat{a}_b \hat{a}_a$$

$$\begin{aligned}
L_{CCD} &= \langle \Psi_{ref} | (1 + \hat{\Lambda}_2) e^{-\hat{T}_2} \hat{H} e^{\hat{T}_2} | \Psi_{Ref} \rangle \\
L_{CCD} &= E_{ref} + \frac{1}{4} \sum_{i,j}^{occ} \sum_{a,b}^{virt} t_{ij}^{ab} \langle ij || ab \rangle + \frac{1}{4} \sum_{i,j}^{occ} \sum_{a,b}^{virt} \lambda_{ij}^{ab} \omega_{ij}^{ab}.
\end{aligned} \tag{1.45}$$

The specific PP Lagrangian can be found by substituting the PP cluster operator, \hat{T}_{PP} , and its analogous PP de-excitation operator, $\hat{\Lambda}_{PP}$, into the final expression in Eqn. 1.45. The amplitudes and Lagrange multipliers are simultaneously optimized via the conditions:

$$\begin{aligned}
\frac{\partial L_{CCD}}{\partial t_{ij}^{ab}} &= 0 \\
\frac{\partial L_{CCD}}{\partial \lambda_{ij}^{ab}} &= 0.
\end{aligned} \tag{1.46}$$

The CCD residual, ω_{ij}^{ab} , can be expanded in terms of four-center two-electron integrals, Fock matrix elements, and amplitudes into the expression in Eqn. 1.45. Collecting similar terms in this full algebraic expansion yields effective one-particle and two-particle density matrices,

$$\begin{aligned}
\gamma_{ii} f_{ii} &= [-t_{ij}^{ab} \lambda_{ij}^{ab} + \dots] f_{ii} \\
\Gamma_{ijab} \langle ij || ab \rangle &= [t_{ij}^{ab} + \lambda_{ij}^{ab} + \dots] \langle ij || ab \rangle.
\end{aligned} \tag{1.47}$$

Since t and λ are stationary as shown in Eqn. 1.46, these density matrices can be used to construct gradients and Hessians as demonstrated in Section 1.2.2. The GVB-CC PP equations can be optimized for both amplitudes, Lagrange multipliers and MO expansion coefficients similar to the way they are optimized in Section 1.3.3.

The GVB-CC methods as shown can be expanded to including additional determinants beyond those of PP. The expansion is done by improving the cluster operator \hat{T} by including additional terms beyond PP. Adding more substitutions to a GVB-CC cluster operator requires only polynomial additional computational effort, not factorial extra effort. The valence optimized doubles (VOD) [80, 81] method is a GVB-CC model that contains all active space double substitutions via \hat{T}_2 . VOD has 6^{th} order computational cost like solving the full set of CCD amplitude equations. Since VOD is done in the PP active space, the number of correlated virtual and occupied orbitals is equivalent yielding a scaling of σ_{act}^6 . Unlike CCD, VOD optimizes the MO expansion coefficients making the whole process iteratively 6^{th} order. The computational cost of VOD is an improvement over the computational cost of CASSCF, but it is much slower than a PP calculation. The PP amplitudes can be expressed as a sequence of quadratic equations that can be solved in linear time, so PP is limited only by the cost of forming the necessary four-center two-electron MO

integrals and the Fock matrix.

Another approximate GVB-CC method that is a truncation of the full doubles operator is imperfect pairing (IP) [82,83]. In addition to the PP correlations, IP extracts the leading inter-pair correlations that couple up to only two pairs. The cluster operator for IP is

$$\hat{T}_{IP} = \hat{T}_{PP} + \sum_{i,j \neq i}^{N_{pairs}} \left[t_{ij}^{i^*j^*} \hat{a}_i^\dagger \hat{a}_{i^*}^\dagger \hat{a}_j \hat{a}_i + t_{ij}^{j^*i^*} \hat{a}_j^\dagger \hat{a}_{j^*}^\dagger \hat{a}_i \hat{a}_j \right]. \quad (1.48)$$

The IP amplitudes and Lagrange multipliers can be obtained in 3^{rd} order time, o_{act}^3 , using only quadratic memory. PP and IP are both iterative and limited in cost by the formation of the four-center two-electron MO integrals. IP produces better energies than PP, but still suffers from some of the problems like symmetry-breaking [84]. Additionally it is not exact for two pairs of electrons relative to CASSCF. Addition of all such terms define the perfect quadruples (PQ) method [85].

The GVB-CC methods developed to date solve the static correlation well for most systems, but they suffer from a few key outstanding problems. The first problem is that methods with a truncated set of doubles amplitudes like PP and IP prefer electronic structures localized only over a single bond as opposed to electronic structures de-localized over larger sections of a molecule. This is not problem for molecules like linear alkanes, but it is a problem in aromatic systems like benzene. The well understood electronic symmetry of these kinds of molecules is lost to emphasize highly localized bonds [84]. The PP and IP correlation energies from D_{3h} structures with the π bonds localized to resemble three distinct double bonds are lower than the correlation energy produced in a D_{6h} structure with the π bonds de-localized over the entire ring.

The second outstanding problem is with spin-unrestriction [86,87]. As mentioned in section 1.3.3, methods that do not include all possible correlations with the active space must utilize spin-unrestriction to obtain the correct dissociation products and energy. Artifacts arise in trying to use spin-unrestriction with an active space method. As a bond that is being correlated dissociates, its energetic contribution to the correlation energy goes to zero with spin-unrestricted orbitals. With orbitals allowed to freely spin-unrestrict, in this limit the orbitals producing zero correlation energy are rotated out of the active space and orbitals that were inactive before are rotated into the active space to lower the energy. The deformations of the active space are irreparable at the level of freely spin-unrestricting PP [86,87].

Another problem is that GVB methods solve for static correlations and lack a good description of the residual dynamic correlation. All static correlation methods suffer from this problem. CASPT2 [88–93] is usually employed to correct for the missing dynamic cor-

relations in CASSCF. CASPT2 employs Møller-Plesset second-order perturbation theory using the optimized CASSCF wavefunction as a reference. CASPT2 correlates inactive orbitals with themselves and the orbitals in the active space. CASPT2 is very accurate, but very computationally expensive. Second-order Møller-Plesset perturbation theory has also been combined with GVB-PP methods [94–98]. In order to use a perturbation theory correction to GVB-CC PP, the second-order perturbation theory needs to be adapted to work with the similarity transformation Hamiltonian [99–102]. The PP(2) method uses the appropriate form of second-order perturbation theory with the GVB-CC implementation of PP [103]. The perturbation theory corrections to PP are algebraically simpler than what is necessary for CASPT2 and are less computationally expensive. The perturbative correction in PP(2) scales the same as doing a single MP2 calculation. The cost of a perturbative correction to a CASSCF calculation is relatively inexpensive compared to the full cost of obtaining the CASSCF energy and wavefunction. However, the perturbative correction in PP(2) can often be more expensive than the optimization of the PP energy and wavefunction. All of these perturbative corrections produce results that typically agree much better with FCI than the parent static correlation method. The drawbacks to all of these methods is that the cost of the perturbative correction can be quite expensive compared to a single iteration of the parent method, the perturbative corrections are only applied at the end of the static correlation calculation and are not self-consistent, and the quality of the correction depends on the quality of the solution produced by the static correlation calculation.

Density functional theory (DFT) has also been used to obtain the residual correlation energies after a static correlation method [104–117]. Using DFT over second-order perturbation theory has the advantage of improved computational efficiency, and it can be solved for self-consistently with the static correlation. The existing DFT functionals for correlation energy are not well-suited for use in getting the residual correlation energy when combined with static correlation methods and potentially double count the correlations already accounted for in the static correlation method.

Another practical problem is that of multiple orbital solutions to the energy minimization problem. This is a problem that is even experienced with CASSCF. The best solution is to test several initial guesses with an optimization algorithm that does not readily hop between different solutions [30] to isolate the various low energy solutions.

1.5 Outline of this Work

1.5.1 Symmetry-breaking in GVB-CC methods

A localized orbital reference is the key to the speed and accuracy of the Generalized Valence Bond methods. This can be problematic when the nature of the orbitals is actually

de-localized, for example in aromatic hydrocarbons. This over-localization is often quite dramatic and leads to undesirable symmetry breaking artifacts. These artifacts are dramatic enough that methods like Perfect Pairing will predict two different 3-fold symmetric bond lengths for benzene as opposed to one 6-fold symmetric bond length [84]. In chapter 2, the ability to correct the coupled cluster based GVB methods like perfect and imperfect pairing [82, 83, 86] by making a mixed Lagrangian of infinite-order coupled cluster theory and second-order perturbation theory (PT) is explored. We justify that the PT only needs to couple up to three correlating pairs, and then we discuss the algorithmic implementation of the energy and nuclear gradient for the resulting mixed Lagrangian method that we have dubbed Three-Pair Corrected Imperfect Pairing (TIP). Finally, the results of the TIP method on large aromatic hydrocarbons are presented. This chapter has been published as an article in the Journal of Chemical Physics [118].

1.5.2 Penalty functions for combining coupled cluster and perturbation amplitudes in local correlation methods with optimized orbitals

All correlation methods that completely span the space of correlations they account for (i.e. CCD) gain rotational invariance of their orbitals. CCD has occupied-occupied and virtual-virtual rotational invariance, meaning that any rotation of an occupied orbital with another occupied orbital or the rotation of any virtual orbital with another virtual orbital will not affect the energy produced by the calculation. Since the GVB-CC methods specifically truncate the space of all possible correlations, this typical rotational invariance exhibited by CC theory when truncated only by excitation level is lost. Particularly in the case of the mixed Lagrangian TIP method [118], this loss of invariance proves to be quite catastrophic. In TIP, the correlations are separated into spaces of weak and strong correlations and this lost rotational invariance leads to the orbitals re-ordering and the sub-spaces of strong and weak correlations losing their appropriate meaning and leading to energies that are fictitiously too low. In chapter 3, we demonstrate the ability to apply a penalty function to the TIP correlations and prevent these rotations which artificially lower the energy. The parameterizing of this penalty function and the results of applying the improved TIP method to several chemical systems are presented. This chapter has been published as an article in Molecular Physics [119].

1.5.3 The numerical condition of electron correlation theories when only active pairs of electrons are spin-unrestricted

Many electronic structure theories simplify the complicated nature of separating electron pairs by allowing the wavefunction to break spin symmetry instead of accounting for all possible correlations that would be necessary to fully and accurately describe this

process with spin-restricted orbitals. The spin-unrestricted wavefunction at dissociation should match the energy of the non-interacting fragments at dissociation, however artifacts arise when doing spin-unrestriction with valence space correlation methods [86, 87]. In re-defining a basis for spin-unrestriction, we found that the CC amplitude equations became ill-conditioned to the point of being singular. In chapter 4, the ill-conditioning is examined and its origins are examined. A simple fix to this singularity in the form of a regularization via a penalty function on the coupled cluster amplitudes is offered. This chapter has been published as an article in the Journal of Chemical Physics [120].

1.5.4 Orbitals that are unrestricted in active pairs for GVB-CC methods

Spin-unrestriction is vital to dissociating electron pairs when the wavefunction is only approximate and has a truncated description of the actual electron correlations. Valence active space space correlation methods tend to have artifacts with spin-unrestriction. In chapter 5, the Unrestricted-in-Active-Pairs (UAP) approximation is explored. UAP is designed to smoothly spin-unrestrict one pair at a time by allowing an occupied orbital pair in the active space to mix only with its perfectly paired virtual orbital pair in order to spin-unrestrict. This spin-unrestriction is controlled via a single degree of freedom for each correlating pair reducing the number of degrees of freedom needed in spin-unrestriction from an additional number of total orbitals squared to just a single variable for each correlating pair. The algorithm and implementation of UAP is analyzed. Results on the smooth dissociation of many types of chemically bonded systems and the predictive capabilities for UAP on open-shell systems are presented. This chapter has been submitted for publication as an article in the Journal of Physical Chemistry A.

1.5.5 Analysis of multi-configurational Kohn-Sham methods: Theory and model application to bond-breaking.

GVB-CC methods only account for static (strong) correlations. In chapter 6, we show that Density functional theory (DFT) [121] can be combined with multi-configuration/multi-reference wavefunction theory without any loss of exactness. This combination can be used to account for the missing dynamic (residual) correlation energy that is typically lacking in multi-configurational wavefunction methods. We explore combining DFT, and more specifically the correlation function of Lee, Yang, and Parr [122] with PP. An approximate form of the correlated PP density with a correction for double-counting of the correlation energy for use in the DFT correlation energy is presented with results for this formulation on a simple bond breaking example. This chapter has been published as an article in Molecular Physics [123].

Chapter 2

Symmetry-breaking in GVB-CC methods

2.1 Introduction

Kohn-Sham density functional theory methods [124, 125] are the most computationally efficient electronic structure theories for molecules [126], because with present-day exchange and correlation functionals, they have only the computational requirements of one-particle methods. However due to limitations of the functionals, they are not satisfactory for treating many molecules that exhibit strong correlations (for example, the phenalenyl dimer [127]). Since such systems exhibit more than one important orbital configuration, efficient single-reference wavefunction approaches like second-order perturbation theory are also inadequate.

Instead, strong correlations between electrons are often treated by wavefunction-based methods that are either literally or conceptually of the complete active space (CAS) type [50, 53, 54]. Real CAS methods correspond to solving the time-independent Schrödinger equation in an orbital active space that spans valence bonding and anti-bonding orbitals, as exemplified by the perfect pairing (PP) active space which provides one correlating orbital for each valence occupied orbital. The orbitals are optimized to minimize the energy, defining the CAS self-consistent field (CASSCF). The computational cost associated with CASSCF is approximately exponential in the number of active electrons, as it is a Schrödinger equation. Thus, while correlating all valence electrons is in principle the goal, it is impossible in practice for all but the smallest molecules. Practical CASSCF calculations always involve a very difficult molecule-dependent definition of a truncated active space, often by trial and error.

Instead of truncating the active space, a desirable alternative is to approximate the

CASSCF model so that all valence electrons could be retained as active. This is sometimes done in CI language by restricting the excitations within the active space [51], but this is generally not size-consistent. There are also promising results from the numerical density matrix renormalization group (DMRG) [128,129], which stores many-body matrix elements rather than explicit eigenvectors. However, this is not yet a theoretical model chemistry, and is so far most applicable to one-dimensional systems.

In this work, we consider an active space coupled cluster (CC) approach (where the wavefunction, $\Psi = \exp(\hat{T})\Phi$, is formed by the action of a non-linear correlation factor on a mean field reference Φ). The cluster operator, \hat{T} , is truncated at a given level such as double excitations, defining the valence optimized doubles (VOD) model [80,81]. Within a PP active space this corresponds (for the closed shell singlet case) to the following cluster operator:

$$\hat{T}^{VOD} = \sum_i^v \sum_{k^*l^*}^v t_{i\bar{i}}^{k^*\bar{l}^*} a_{k^*}^\dagger a_{l^*}^\dagger a_{\bar{i}} a_i + \sum_{i>j}^v \sum_{k^*l^*}^v t_{ij}^{k^*l^*} \hat{E}_{ik^*} \hat{E}_{jl^*} \quad (2.1)$$

where we have introduced the unitary group generators, \hat{E}_{ij} . The orbitals are optimized together with the amplitudes, defining the active space. The computational cost of the VOD model is M^6 with molecule size, which is still too limiting for applications to large molecules.

It is possible to further truncate the double substitution operator based on spatial locality considerations, along the lines of the local correlation models that have been pursued in wavefunction methods that do not employ active spaces. The strongest correlations are between electrons in the two orbitals that define a pair (i.e. intra-pair) since they are closest together, and thus a model that includes only these excitations may be defined [78,86]

$$\hat{T}^{PP} = \sum_{i^*}^{v/2} t_{i\bar{i}}^{i^*\bar{i}^*} \hat{a}_{i^*}^\dagger \hat{a}_{\bar{i}^*}^\dagger \hat{a}_{\bar{i}} \hat{a}_i \quad (2.2)$$

This is commonly known as the perfect pairing model, and it reproduces CASSCF for a single pair in the PP active space, while also being size-consistent. It is the CC version of the more widely known variational generalized valence bond PP (GVB-PP) method [56,57]. PP has the chemical advantage of leading naturally to active orbitals that when fully optimized are often localized into bonds or lone pairs, and accordingly may be interpreted to understand the nature of the strongest correlations. The CC version is identical to GVB-PP for a single pair, but is not guaranteed variational for larger systems (though we have not seen breakdowns in practice).

In the PP model, electrons in different pairs are uncorrelated. We have suggested extensions to the CC PP model that include the leading inter-pair correlations – defining

the imperfect pairing (IP) model [79, 83]:

$$\hat{T}^{IP} = \hat{T}^{PP} + \sum_{i \neq j}^{v/2} \left(t_{ij}^{i^*j^*} \hat{E}_{ii^*} \hat{E}_{jj^*} + t_{ij}^{j^*i^*} \hat{E}_{ij^*} \hat{E}_{ji^*} \right) \quad (2.3)$$

The IP model is, in a sense [79], an extensive analog of the GVB-RCI approach [130]. IP recovers a significantly higher fraction of the valence correlation energy than PP, and additionally performs better for systems with multiple strongly correlated electron pairs, such as double and triple bonds. The IP-type excitations are known from test calculations to be the next largest amplitudes behind those of PP type when localized orbitals are employed [84].

The PP and IP models have been efficiently implemented [82, 131], including orbital optimization and nuclear gradients, and have been used in a variety of chemical applications to diradicaloid molecules [132–135]. Second-order perturbation corrections to both the GVB [136] and CC [103] forms of PP theory have been suggested. Within the valence space, it is also possible to consider the further extension that includes all correlations coupling two electron pairs [84], although this appears challenging to implement efficiently.

While these methods are chemically very appealing, it has been known for possibly as long as 30 years that GVB-PP exhibits undesirable symmetry-breaking (SB) artifacts. The CC-based PP method is no different. Benzene is a simple and striking example of these problems, because, as shown in Fig. 2.1 (see Fig. 2.2 for the definition of the distortion coordinate), the PP model favors alternating short and long bonds giving D_{3h} symmetry rather than the correct D_{6h} symmetry. Not only is the potential curve qualitatively wrong, but at the D_{6h} geometry, the wavefunction breaks symmetry, as indicated by a slight charge alternation. There are two such solutions, corresponding to the curves to the left and right of D_{6h} in Figure 2.1, and they intersect at a sharp cusp. This effect arises because the PP optimized orbitals for the 6 π electrons localize into 3 partial double bonds of a single resonance structure (and at the symmetric geometry there are 2 equivalent resonance structures).

This is a very troublesome issue for chemical applications, which can potentially afflict many molecules whose electronic structure consists of superpositions of resonance structures. One might hope that inclusion of some non-local correlations coupling electrons in different pairs in the more advanced IP model might solve this problem. However IP was also shown to break symmetry for benzene, though to a lesser extent (see Fig. 2.1). Full geometry optimization with the same basis yields alternating bondlengths of 1.37 Å and 1.46 Å for PP, while at the IP level the bond lengths are 1.38 Å and 1.45 Å. This is a substantial artifact, and therefore solutions to the SB problem have been proposed, such as resonating GVB-PP [137], or the related “breathing orbital” valence bond method [138].

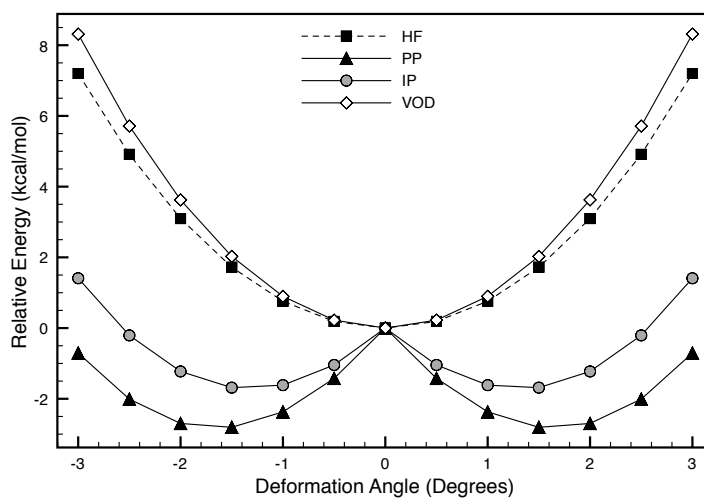


Figure 2.1: Potential energy curve for distortion of benzene along the coordinate described in Fig. 2.2, showing symmetry breaking with the PP and IP methods which neglect non-local correlations. Absolute energies (6-31G* basis) at D_{6h} geometry are: -230.702049 H for HF, -230.902841 H for PP, -231.014028 H for IP, and -231.089623 H for VOD.

These approaches, however, fail to be well-defined chemical models, because they rely on identifying the multiple resonance structures, which is a molecule-by-molecule (and even geometry-by-geometry) problem.

The SB issue in benzene is also a manifestation of a more general problem with the practical performance of local correlation models [139]. Along the distortion coordinate that deforms benzene from D_{6h} symmetry to D_{3h} symmetry, the extent of localization of electron correlation effects changes. Correlation effects are most delocalized at the symmetric geometry, and become more localized as the electronic structure tilts away from aromatic and towards localized alternating single and double bonds. Thus the fractional recovery of the correlation energy by a local correlation model changes along the reaction coordinate [84], and this changing error causes the relative energy to be lower at symmetry-broken geometries. This situation will, unfortunately, be common on many reaction coordinates. Reactants and products, as stable chemical species, will typically display greater localization of electronic structure, while geometries corresponding to intermediate saddle points may display more delocalized bonding. Local correlation models such as PP and IP will perform relatively better on the localized structures, and will therefore potentially exhibit relative errors due to local correlation that are not present in a complete treatment of the valence pair correlation operator (VOD) (or even in the mean field Hartree-Fock model which neglects all electron correlations, as shown in Fig. 2.1). Conversely, other local

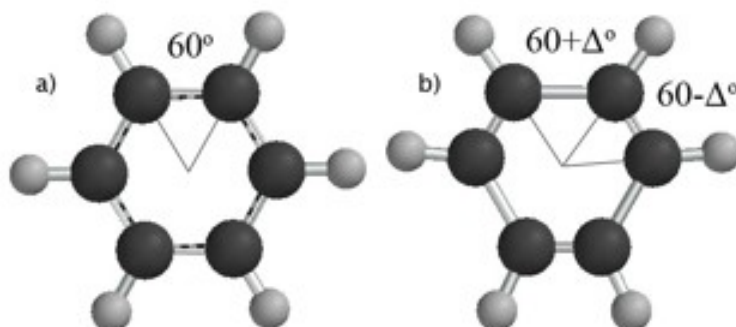


Figure 2.2: The deformation angle Δ in benzene is defined as the magnitude of the deviation of the CXC (X being the geometric center) angles from 60° . Adjacent CXC angles will therefore be $(60+\Delta)$ and $(60-\Delta)^\circ$. Fig. 2.2a shows D_{6h} benzene with $\Delta=0$. Fig. 2.2b is an example of a D_{3h} benzene with $\Delta=10$. Carbon atom positions are fixed at 1.395249 \AA from the geometric center and hydrogen atom positions are fixed at 2.482360 \AA (from the MP2/6-31G* optimized D_{6h} geometry).

correlation methods also exhibit SB in benzene for the same reason [140].

The first goal of this paper is to systematically explore the origin of SB in GVB methods from a local electron correlation perspective. The second goal is given some understanding of this origin, to propose a solution which is not molecule-specific, and which retains the computational advantages of PP and IP, as well as the conceptual advantage of localized orbitals. The outline of the rest of the paper is as follows. First, in Sec. 2.2, we describe pilot calculations using second-order perturbation theory in an active space to explore the effect of inter-pair correlations and to what extent they need to be described in order to ameliorate SB. Based on these pilot results, we formulate a three-pair correction to imperfect pairing (TIP) in Sec. 2.3, and describe how amplitude, orbital and geometry optimization can be efficiently implemented for this new model. In Sec. 2.4 we look at applications of the proposed TIP method to SB in aromatic hydrocarbons starting with benzene, continuing to naphthalene, and then the cation and anion of phenalenyl. We present our conclusions in Sec. 2.5.

2.2 Pilot calculations on benzene

It is a fact, as was shown in Figure 2.1, that the PP and IP models break symmetry for benzene, while a fully delocalized treatment of pair correlations, such as VOD in the same active space, does not. We can therefore be sure that the origin of SB is the incomplete treatment of inter-pair correlations. The question we wish to address is how extensive does

the treatment of inter-pair correlations have to be in order to eliminate this problem? Let us clarify at the outset the context in which we shall answer this question:

Active space: We shall always make all valence electrons active, as this is the active space which can always be unambiguously defined (in contrast to the π active space). SB artifacts will be more pronounced in larger active spaces since inter-pair correlation effects will generally be larger. We have performed tests in the (6,6) π active space that strongly support this obvious fact.

Orbital representation: Different orbital representations will give different results. For example, if redundant, non-orthogonal functions are used to span the active occupied and active virtual π spaces, symmetry breaking can be overcome at the level of non-orthogonal perfect pairing [141]. It is an open question whether or not that is still true in a full valence space. Here we shall work in the non-redundant orthogonal orbital framework of the PP, IP and VOD models.

Excitation level: We restrict ourselves to orbital-optimized coupled cluster approximations to CASSCF that are truncated at double excitations, as defines the VOD model. Local correlation models are therefore local approximations to VOD. More accurate approximations to CASSCF would proceed to take some account of triple and higher excitations, but these are premature when fully viable doubles-only models are only just emerging.

Local correlation modeling: One can usefully distinguish “fixed domain” models which retain a given number of pair correlations over an entire potential surface, versus “variable domain” models where the number of retained pair correlations vary as a function of geometry based on a various criteria. To ensure smooth potential surfaces, and no parameters or cutoffs to define domains, we work with fixed domains, based on electron pairs.

With the perfect pairing active space, we can define fixed-domain local models that are exact for 1, 2, 3 pairs respectively. The 1-pair model is of course simply perfect pairing (see Eq. 2.2): the PP model is exact for a single pair and size-consistent. The 2-pair model has been defined previously as “doubly ionic pairing” since transfers of up to 2 electrons between pairs are possible [84]. It includes additional inter-pair correlations beyond the IP operator, Eq. 2.3, which transfer either 1 or 2 electrons between 2 electron pairs. This model was implemented without orbital optimization previously, and could not fully correct SB in benzene in the (6,6) space using fixed PP orbitals. It is an open question as to what happens in the full valence space with orbital optimization. The 3-pair model has not been explored hitherto. It corresponds to the subset of all possible valence pair correlations that involve only 3 distinct pairs (and thus summations over 3-pair indexes). While a plethora of other models that are possible (e.g. exact for single pairs and partially correct for 2 pairs such as IP, or partially correct for 3 pairs and exact for 2 pairs etc), we shall confine ourselves to this simple 3-rung hierarchy in describing the extent of the inter-pair correlations treatment.

There is of course a fourth and final rung. The inclusion of correlations coupling up

to 4 electron pairs is complete at the level of double excitations, and simply corresponds to Eq. 2.1. If we are forced to go to this level to eliminate SB, then no local correlation treatment is possible within the framework we have chosen.

A development version of Q-Chem 3.0 [142] was modified to enable orbital optimization with each of these models and to evaluate the model described later on in this work. Distinct intra-pair and inter-pair correlations can be described by limiting the number of indices in Eq. 2.1 to the number of inter-pair correlations desired, i.e. for 1-pair, there would only be one index and the expression would simplify to Eq. 2.2. Partly for simplicity and partly with an eye towards constructing a tractable extension to existing GVB methods, we limited the treatment of all the different inter-pair correlations to a second-order treatment for these pilot calculations. The Lagrangian that emerges for the electron correlation becomes simply the second-order Hylleras functional:

$$L = E_0 + L^{(2)} = \langle \Phi_0 | \hat{H} | (1 + 2\hat{T}_2) \Phi_0 \rangle + \langle \hat{T}_2 \Phi_0 | \hat{F} | \hat{T}_2 \Phi_0 \rangle_C \quad (2.4)$$

Here \hat{F} is the mean field Fock operator associated with the reference Φ_0 , \hat{H} is the full Hamiltonian, and \hat{T}_2 is the operator describing the double excitations to first order in perturbation theory (see, e.g. Eq. 2.1). The subscript C indicates only connected terms are included. This Lagrangian is to be minimized with respect to those doubles amplitudes, t_d , contained in the \hat{T}_2 operator for the desired level of inter-pair correlation, and with respect to orbital variations θ_s :

$$\frac{\partial L}{\partial t_d} = \frac{\partial L}{\partial \theta_s} = 0 \quad (2.5)$$

Here we omit the well-known expressions for the second-order amplitudes and the orbital gradient expressions that are required for optimization of the orbitals – they may be obtained using the standard methods of analytical gradient theory [143]. The implementation of this second-order model selectively solves for amplitudes that are necessary for the different levels of inter-pair correlations and leaves the others as zero. The amplitudes can be defined in two ways. The first is the standard non-canonical MP2 approach where the amplitudes are coupled to each other via off-diagonal Fock elements and iteratively solved. Alternatively, motivated by double perturbation theory as described by Kapuy [144–146] the off-diagonal elements can be ignored to leading order giving a non-iterative expression for the amplitudes as an integral divided by differences of diagonal Fock elements (K-MP2). We have recently used K-MP2 in other contexts [147, 148], and for efficiency we shall use it here also.

Fig. 2.3 presents data for the N-pair models acquired at the MP2 level of theory. The complete 4-pair model is a valence optimized MP2, which is invariant to orbital transformations within any of the 4 orbital subspaces (inactive occupied, active occupied, active

virtual, and inactive virtual). As expected, it does not break symmetry. Indeed comparing Fig. 2.1 and Fig. 2.3 indicates that the MP2 approximation is sufficiently close to the full coupled cluster treatment to be useful.

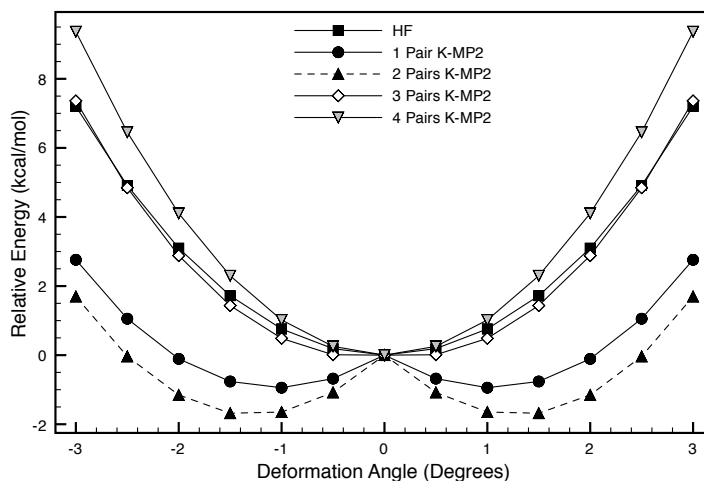


Figure 2.3: Potential energy curves for deformation of benzene using local correlation models which only retain correlations coupling up to 1, 2, 3 and 4 different electron pairs respectively, where the correlation energy is evaluated at the second-order perturbation theory (MP2) level. For reference, the absolute energies at the D_{6h} geometry for the 1-, 2-, 3-, and 4-pair models are: -230.834077 H, -230.965803 H, -231.020476 H, and -231.034350 H respectively.

The 1-pair model breaks symmetry as expected, with the lowest energy corresponding to around 1.0° of deformation. This number agrees reasonably well with the full coupled cluster PP as shown in Figure 2.1, which exhibits a minimum at around 1.6° deformation. The 2-pair model breaks symmetry, and, perhaps surprisingly, the degree of SB is larger, with a preferred geometry of around 1.5° deformation. We suspect the extent of SB in the 2-pair model would be less than the 1-pair model in a coupled cluster implementation, based on the fixed orbital (6,6) results we reported previously [84].

If the 3-pair model is used in the computation, then the SB effects are greatly reduced, and the molecule comes very close to not breaking symmetry. As shown in Figures 2.3 and 2.4, the 3-pair model breaks symmetry only slightly (~ 0.05 kcal/mol) with its optimal configuration being at 0.2° deformation. The improvement relative to the 2-pair model is very striking, and indicates that in benzene (with 30 active electrons, in 30 active orbitals), there is only a very small differential energetic effect due to omitted 4-pair correlations. This is the most important result of this section – it indicates that even in a π -delocalized system like benzene, electron correlations still retain sufficient locality that it may be pos-

sible to neglect the 4-pair couplings and nonetheless have sufficient accuracy for chemical applications. This is the approach that we shall use in the remainder of this paper, so that we may stay within a local correlation framework.

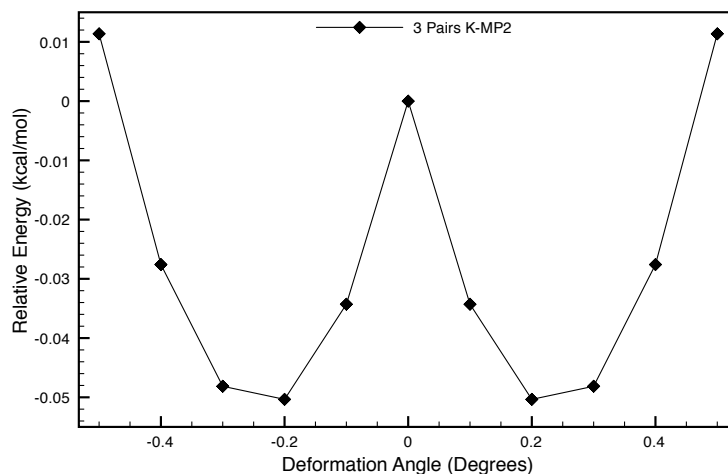


Figure 2.4: Close-up view of the potential curve for small distortions of benzene away from D_{6h} symmetry for the 3-pair model shown above in Figure 2.3.

Finally it is useful to briefly examine the percentages of correlation energy that are recovered by each model. At the D_{6h} geometry, the percentages are 39.7% (1-pair), 79.3% (2-pairs), 95.8% (3-pairs), relative to the 100% recovery defined by the 4-pair model. The performance of the 1-pair model for benzene is significantly worse than for normal saturated molecules where it may typically recover around 60% of the correlation energy. Likewise, the IP model, which is a subset of the 2-pair model, usually recovers around 90% of the correlation energy. And, at 1° deformation, the percentages of correlation energy recovered shift to 40.6% (1-pair), 80.6% (2-pairs), and 96.1% (3-pairs). This serves to emphasize that the changes in extent of locality of electron correlation as a function of deformation are subtle rather than dramatic. The underlying framework of σ bonds (12 pairs) is well localized for all deformations considered here, and it is only the 3 π pairs that change significantly. Therefore the inter-pair correlations involving σ and π electrons, as well as π electrons in different pairs are the principal terms that change along the deformation coordinate. Our results indicate that the main inter-pair couplings are accounted for in a fairly satisfactory absolute and relative sense at the 3-pair level.

2.3 Three-pair corrected imperfect pairing

2.3.1 General considerations

Within the fixed domain inter-pair coupling hierarchy employed in this paper it appears from the results above that one must take account of correlations between at least 3 distinct electron pairs to approach satisfactory reproduction of the full non-local result for benzene. We could attempt to translate that result into a coupled cluster method by simply retaining all correlations that couple no more than 3 different pairs. The computational gains with this method would be relatively modest however, since it would be likely to reduce the overall cost by just one power of system size (from 6th order to 5th order), and also have quite a significant prefactor. However, it remains true, as demonstrated in previous work [84] that by far the strongest correlations are the intra-pair (perfect pairing) type, followed by the non-charge-transfer inter-pair correlations (the imperfect pairing type). We are therefore tempted to group correlations into strong and weak, and treat the (small number of) strong imperfect pairing correlations by infinite order coupled cluster theory, and the (vastly larger number of) weak correlations by second-order perturbation theory. This will define an approach we shall call three-pair corrected imperfect pairing (TIP).

As in the previous section, we neglect off-diagonal terms in the MP2 amplitude equations [144–146], so that the K-MP2 amplitudes can be obtained directly without iteration. We then define a hybrid TIP Lagrangian:

$$L^{corr} = E_0 + L(IP)^{(\infty)} + L(3 - IP)^{(2)} \quad (2.6)$$

The first term is the mean-field reference energy. The second term is the IP Lagrangian, which is of the form:

$$\begin{aligned} L_{IP}^{(\infty)} = & \sum_i^{N_{pairs}} t_{ii}^{i^* \bar{i}^*} (ii^* | \bar{i} \bar{i}^*) + \lambda_{ii}^{i^* \bar{i}^*} w_{ii}^{i^* \bar{i}^*} + \sum_{i \neq j}^{N_{pairs}} t_{ij}^{i^* j^*} [2(ii^* | \bar{j} \bar{j}^*) - (ij^* | \bar{j} \bar{i}^*)] \\ & + \lambda_{ij}^{i^* j^*} w_{ij}^{i^* j^*} + t_{ij}^{i^* j^*} [2(ij^* | \bar{j} \bar{i}^*) - (ii^* | \bar{j} \bar{j}^*)] + \lambda_{ij}^{j^* i^*} w_{ij}^{j^* i^*} \end{aligned} \quad (2.7)$$

The K-MP2 term (3rd term) of Eq. 2.6 contains several separate classes of excitations of the form $(ij) \rightarrow (i^*k^*)$, $(ii) \rightarrow (j^*k^*)$ and $(ij) \rightarrow (k^*k^*)$, with the PP+IP subset (which is treated non-perturbatively) deleted.

Upon further investigation of Eq. 2.6, we found that SB in benzene and other aromatics was not reduced as greatly as we had expected based on the pilot calculations reported in Sec. 2.2. To achieve a model slightly closer to full treatment of the 3-pair couplings, we then decided to correct the strong correlations (IP-type) with the one-electron coupling to

the weak amplitudes, based on the assumption that the weak amplitudes are adequately described by perturbation theory. This leads to the following modifications to the IP amplitude equations:

$$\begin{aligned}
 \omega_{ii}^{i^*i^*} (TIP) &= \omega_{ii}^{i^*i^*} (IP) + \sum_{k^* \neq i^*}^v [f_{i^*k^*} t_{ii}^{i^*k^*} + f_{i^*k^*} t_{ii}^{k^*i^*}] - \sum_{c \neq i}^v [f_{ic} t_{ic}^{i^*i^*} + f_{ic} t_{ci}^{i^*i^*}] \\
 \omega_{ij}^{i^*j^*} (TIP) &= \omega_{ij}^{i^*j^*} (IP) + \sum_{k^* \neq i^*, j^*}^v [f_{j^*k^*} t_{ij}^{i^*k^*} + f_{i^*k^*} t_{ij}^{k^*j^*}] - \sum_{c \neq i, j}^v [f_{jc} t_{ic}^{i^*j^*} + f_{ic} t_{cj}^{i^*j^*}] \\
 \omega_{ij}^{j^*i^*} (TIP) &= \omega_{ij}^{j^*i^*} (IP) + \sum_{k^* \neq i^*, j^*}^v [f_{i^*k^*} t_{ij}^{j^*k^*} + f_{j^*k^*} t_{ij}^{k^*i^*}] - \sum_{c \neq i, j}^v [f_{jc} t_{ic}^{j^*i^*} + f_{ic} t_{cj}^{j^*i^*}]
 \end{aligned} \tag{2.8}$$

The most important effect of these coupling terms on the TIP model is to usually somewhat reduce the magnitude of the IP amplitudes. This is likely to be beneficial in reducing SB artifacts. The coupling terms also cause some additional complications in the expressions and resulting algorithms for optimization of the orbitals, and then finally the geometry, as discussed in the subsections below.

While this defines the TIP model for the purposes of this paper, it is useful to note that these last two design decisions (use of K-MP2 and inclusion of one-electron coupling of the weak amplitudes to the strong amplitudes) could be modified. We believe they are the simplest useful choices. For example, it would be interesting (though substantially more complicated) to explore the additional effects of two-electron coupling of the weak amplitudes to the strong ones, and the effect of all one-electron couplings (i.e. MP2 rather than K-MP2) on the results. Additionally, other slightly empirical variants of TIP can be constructed by dividing the IP and MP2 amplitudes into different spin components [149, 150], and scaling them.

2.3.2 An Efficient Algorithm for the Energy

Energy evaluation for TIP requires making the Lagrangian stationary with respect to both the correlation amplitudes and the orbitals; the latter evaluated assuming optimized amplitudes. The corresponding algorithms for IP have been discussed extensively [82, 131]. TIP is a correction to IP, and the TIP algorithm described here is structured as an addition to the previously described IP algorithm. The implementation of the additional terms must be handled carefully since a cubic number of amplitudes are involved relative to the vastly smaller quadratic number in IP itself. The existing IP algorithm uses Resolution of the Identity (RI) [61–63], with the bottleneck being the fourth order steps needed to make the molecular integrals. Our TIP algorithm is also RI-based, and is designed to not introduce any steps greater than fourth order or to exceed a memory usage for the new pieces greater than three times the number of auxiliary basis functions squared.

For notation, K, L will denote RI basis functions, $\mu, \nu, \lambda, \sigma$ will denote atomic orbital (AO) basis functions, i, j, k will represent active occupied molecular orbitals (MO's), i^*, j^*, k^* , a, b will represent active virtual MOs, and p, q, r, s will represent general MO indices, while the index m will represent any core or active occupied MO. We have chosen to implement TIP in a restricted closed-shell formalism initially, and therefore the algebra presented below is in the restricted formalism. Generalization to unrestricted orbitals is possible, and is a desirable future development.

The MP2 energy portion of the Lagrangian, (i.e. the third term of Eq. 2.6), can be expressed as

$$L_{3-IP}^{(2)} = \sum_{ijab}^{3-IP} [t_{ij}^{ab} (ia | jb) + \lambda_{ij}^{ab} \omega_{ij}^{ab}] \quad (2.9)$$

where:

$$\begin{aligned} \omega_{ij}^{ab} &= 2 (ia | jb) - (ib | ja) - t_{ij}^{ab} \Delta_{ij}^{ab} \\ \Delta_{ij}^{ab} &= f_{ii} + f_{jj} - f_{aa} - f_{bb} \end{aligned} \quad (2.10)$$

The summation indices in Eq. 2.9 are limited to include only those amplitudes that involve up to 3 unique indices (e.g. a virtual index, a , is defined by the corresponding GVB occupied index,) excluding the PP and IP amplitudes, which are treated in the second term of Eq. 2.6. This is symbolized by using 3-IP as the summation range, both here and in subsequent equations where the same consideration applies. Derivatives of the total Lagrangian, Eq. 2.6, with respect to the \mathbf{t} amplitudes and the corresponding Lagrange multipliers, λ , yield the equations defining those unknowns. Derivatives of the total Lagrangian with respect to orbitals, given optimized \mathbf{t} and λ amplitudes, then defines the orbital gradient.

Before generating the \mathbf{t} and λ amplitudes a few RI precursors must be computed. During the very first iteration of an orbital optimization cycle, the RI three-center integrals and the associated RI expansion matrix for the AO functions pairs, C , is formed

$$C_{\mu\nu}^K = \sum_L^{AUX} (\mu\nu | L) (L | K)^{-1} \quad (2.11)$$

They only need to be computed once at a given geometry. At the beginning of each orbital iteration the three-center integrals are transformed into the current MO basis, and then the cubic number of required (3-pair) MO integrals are constructed and saved to disk, and the amplitudes and initial Lagrange multipliers are computed

$$(ia | jb) = \sum_K^{AUX} (ia | K) C_{jb}^K = \sum_L^{AUX} \sum_K^{AUX} (ia | K) (K | L)^{-1} (L | jb). \quad (2.12)$$

Once these original quantities and the previously described IP and PP amplitude couplings are determined, the couplings of the PP and IP Lagrange multipliers to the MP2 Lagrange multipliers are determined. For example a weak amplitude multiplier, $\lambda_{ii}^{i^*j^*}$, is given by:

$$\lambda_{ii}^{i^*j^*} = t_{ii}^{i^*j^*} + \frac{\left[\sum_i^v \lambda_{ii}^{i^*i^*} f_{j^*i^*} - \sum_i^v \sum_{j \neq i}^v \left[\lambda_{ij}^{i^*j^*} f_{ji} + \lambda_{ji}^{i^*j^*} f_{ji} \right] \right]}{\Delta_{ii}^{i^*j^*}} \quad (2.13)$$

The second term arises from the couplings illustrated in Eq. 2.8. From the computed weak \mathbf{t} and λ amplitudes, a correction to the correlated 1-PDM from the IP expressions is generated

$$\begin{aligned} P_{ij}(TIP) &= P_{ij}(IP) - \sum_{kab}^{3-IP} t_{ik}^{ab} \lambda_{jk}^{ab} \\ P_{ab}(TIP) &= P_{ab}(IP) + \sum_{ijc}^{3-IP} t_{ij}^{ac} \lambda_{ij}^{bc} \end{aligned} \quad (2.14)$$

These amplitudes also give rise to a 3-center two-particle density matrix:

$$\Gamma_{ia}^K = \sum_{jb}^{3-IP} \frac{(t_{ij}^{ab} + 2\lambda_{ij}^{ab} - \lambda_{ij}^{ba})}{2} C_{jb}^K \quad (2.15)$$

With these two elements defined, the MO coefficient derivatives of the Lagrangian for the MP2 amplitudes and their corresponding back contributions can be simply determined as the sum of a base contribution

$$\frac{\partial L_{3-IP}^{(2)}}{\partial C_{\mu}^{m(occ)}} = \sum_j^v \sum_k^v P_{ij} [4(\mu m | ij) - 2(\mu i | jm)] + P_{i^*j^*} [4(\mu m | i^*j^*) - 2(\mu i^* | j^*m)] \quad (2.16)$$

for any general occupied MO index, plus specific additional terms for the active occupied MO's:

$$\frac{\partial L_{3-IP}^{(2)}}{\partial C_{\mu}^i} = \frac{\partial L_{3-IP}^{(2)}}{\partial C_{\mu}^{i(occ)}} + \sum_a^v \sum_K^{AUX} 4\Gamma_{ia}^K (K | \mu a) + \sum_j^v (P_{ij} + P_{ji}) f_{\mu j} \quad (2.17)$$

The derivative expression with respect to active virtual MO's is of the form:

$$\frac{\partial L_{3-IP}^{(2)}}{\partial C_{\mu}^{i^*}} = \sum_j^v \sum_K^{AUX} 4\Gamma_{ji^*}^K (K | j\mu) + \sum_{j^*}^v (P_{i^*j^*} + P_{j^*i^*}) f_{\mu j^*} \quad (2.18)$$

and the derivative with respect to inactive virtual orbitals is always zero.

These derivatives are combined with the existing IP MO coefficient derivatives to form the full molecular orbital coefficient derivative of the Lagrangian, which is then transformed into an anti-symmetric orbital rotation gradient

$$\frac{\partial E}{\partial \theta_{pq}} = \sum_{\mu}^{AO} \frac{\partial L}{\partial C_{\mu}^p} C_{\mu}^q - \frac{\partial L}{\partial C_{\mu}^q} C_{\mu}^p \quad (2.19)$$

Here the values and an approximation to the diagonal rotation matrix Hessian are passed into an orbital optimization algorithm (in our case, geometric direct minimization [30]) to minimize the energy with respect to orbital rotations.

The algorithm is an extension of our previous IP implementation, and can be summarized in terms of the following steps, where o, N, X, and NB2 represent the size of the occupied space, number of basis functions, number of auxiliary basis functions, and the number of basis function pairs formed.

(0) *SCF Procedure and guess orbitals*, a Hartree-Fock calculation is performed and then the core and active occupied subspaces are localized. The procedure of Sano [68] is then applied to get a corresponding localized valence virtual space. The default orbital localization in our implementation is that of Pipek and Mezey [66].

(1) *Form the RI 3-center integrals and C matrix*, take care of all the RI overhead costs for the integrals in the AO basis before any orbital optimization iterations. The computational cost is NB2 X for the 3-center integrals and NB2 X² for the C matrix.

(2) *Transform the RI integrals to the MO basis*. On each orbital iteration, the RI 3-center integrals and C matrix are half and fully transformed into the MO basis. The cost for performing the half transformation is oNB2 X, and the cost of the full transformation is o²NX.

(3) *Form the 2-electron integrals, the amplitudes, and the couplings to the IP amplitudes*. The 4-center 2-electron integrals are evaluated, the amplitudes, and the couplings are evaluated and saved to disk for later use. The cost to form the 4-center integrals is o³X. The costs for solving for the amplitudes and the couplings are each o³.

(4) *Perform the standard IP routines for amplitudes and energy*. All of the costs of these routines and necessary steps have been described previously [131].

(5) *Solve for the MP2 Lagrange multipliers, the 1-PDM and the Gamma Matrix*. These are computed in a similar loop structure to that found in the amplitude solver. Cubic I/O is required to reading the amplitudes from disk (after this step the amplitudes can be thrown away). The cost associated with finding the Lagrange multipliers and the 1-PDMs is o³. The cost for getting the two-particle density matrix is o³X.

(6) *Solve for the MO coefficient derivatives of the MP2 part*. There are three pieces that need to be solved as shown in Eqs. 2.17 and 2.18. The cost for the Gamma matrix

part is $\mathcal{O}(N^2)$ and the 1-PDM Fock element part has a cost of $\mathcal{O}(N)$. The general occupied elements derivative terms are simply solved by transforming the correlated 1-PDM into the AO basis, and then constructing only the four-centered two electron integral portion of a Fock element. These matrix elements are then half transformed and built into the gradient. The RI implementation of IP already includes the generation of the four-center two electron integrals, so the only cost associated with this is an $\mathcal{O}(N)$ and an $\mathcal{O}(N^2)$ step to generate the 1-PDM in the AO basis.

(7) *Solve for the MO coefficient derivatives of the IP part.* This step is executed here so that the four-center two-electron integral parts of the coefficient derivatives are efficiently evaluated with only one call to the existing integral evaluation routines.

(8) *Apply Geometric Direct Minimization and take additional steps.* The orbital rotations are evaluated and applied in a standard fashion and the process from 1-7 is repeated until the orbitals have converged to within a specified threshold.

Finally it is worth commenting that the additional 1 and 2 PDM terms associated with the 3-pair correction are adapted from our recently developed RI-MP2 analytical nuclear gradient [151]. The key modifications made to those routines is to exploit the fact that the TIP model has only a cubic number of amplitudes so that the computational costs can be reduced from 5th order to no larger than 4th order in the system size, as was already mentioned above. Figure 2.5 is a demonstration of this; it shows the average cpu cost of all the steps. The average time includes an average of all the one-time computations like the localization in step 0 and the formation of the necessary AO-RI quantities in step 1. TIP benefits the most from this type of evaluation since it typically takes more orbital iterations than PP or IP to find a solution from the Pipek-Mezey and Sano guess, so the decently expensive steps (like step 1) get washed out over many orbital iterations. The timings shown illustrate how TIP is IP with only one extra 4th order step for each orbital iterations and one extra 4th order step at the very beginning by having the TIP cpu times being slightly less than twice as long as the IP cpu times. The TIP timings are also monotonically increasing towards the limit of being around twice as large IP timings, which should be the case. In the small molecules the 3rd order steps should dominate, but as the molecules get larger the 4th order steps take over and should make TIP scale pretty much exactly as twice that of IP with the initial extra costs being washed out over the number of cycles needed by TIP.

2.3.3 Analytical Nuclear Gradient

The nuclear gradient for TIP is implemented in a similar fashion to the way the TIP energy correction was described above. The existing IP routines are minimally modified, and the extra TIP routines are added in alongside the existing IP ones. The MP2 part of the TIP nuclear gradient was also designed to exploit components of our analytical RI-MP2 nuclear gradient [151]. Most of the components needed to evaluate a nuclear gradient

# Basis Functions	# Aux Basis Functions	# Correlated Pairs	Avg. CPU time/00 Iter.			Avg. CPU time: Gradient		
			PP	IP	TIP	PP	IP	TIP
19	82	4	0.08	0.12	0.15	0.34	0.35	0.42
102	402	15	2.1	3.7	5.1	14.4	17.6	17.8
166	640	24	9.2	14.5	25.9	67.4	67.5	76.5
260	982	37	35.8	56.7	109.0	352.7	368.8	414.9
272	1072	40	39.2	60.3	117.8	401.1	423.1	406.2

Figure 2.5: The average CPU cost per orbital iteration and the average cost of performing an analytical nuclear gradient of PP, IP, and TIP in seconds. The calculations were all performed with the 6-31G* basis and RIMP2-VDZ auxiliary basis.

of this form were generated in the process of finding the energy. The expression for the restricted closed-shell TIP analytical gradient is given as

$$\begin{aligned}
E^{(x)} = & E_{IP}^{(x)} + 4 \sum_{\mu}^{AO} \sum_{\nu}^{AO} \sum_K^{AUX} (\mu\nu|K)^{(x)} \Gamma_{\mu\nu}^K - 2 \sum_K^{AUX} \sum_L^{AUX} (K|L)^{(x)} \Gamma^{KL} \\
& + \sum_p^{MO} \sum_q^{MO} P_{pq}^{TIP} f_{pq}^{(x)} + W_{pq}^{TIP} S_{pq}^{(x)}
\end{aligned} \tag{2.20}$$

The one electron term of the expression is already a necessary component of the IP gradient, and is buried within the first term on the right hand side, which contains the full 1-PDM for both the reference wavefunction and the IP and MP2 correlation corrections.

The energy weighted 1-PDM is evaluated just as it is for IP itself, as the symmetrized version of the MO coefficient derivative

$$W_{pq} = \frac{1}{2} \sum_{\mu}^{AO} \frac{\partial L}{\partial C_{\mu}^p} C_{\mu}^q + \frac{\partial L}{\partial C_{\mu}^q} C_{\mu}^p \tag{2.21}$$

This simple form for W is a consequence of using optimized orbitals, so that no response equations need to be solved, unlike MP2 theory using Hartree-Fock orbitals. The full energy weighted 1-PDM is formed and symmetrized within step 7 of the algorithm, at trivial N^2 cost.

All of these simplifications mean that only the two RI-based 2-particle density terms of the TIP nuclear gradient need to be dealt with in some fashion that is not already included

in an IP gradient algorithm. Both of these terms involve transforming the RI 2PDM in Eq. 2.15 into another basis,

$$\Gamma_{\mu\nu}^K = \sum_i^v \sum_a^v \Gamma_{ia}^K C_\mu^i C_\nu^a \quad (2.22)$$

$$\Gamma^{KL} = \sum_i^v \sum_a^v \Gamma_{ia}^K C_{ia}^L, \quad (2.23)$$

followed by contraction with the appropriate 2 and 3-center atomic orbital basis 2-electron integral derivatives. Again the evaluation of those terms follows the procedure described recently for the same terms in the RIMP2 gradient. The algorithm is quite simply then an addition of the two 2-PDM TIP gradient terms at the very end of an IP gradient calculation. The additional cost for a nuclear gradient beyond evaluation of the energy itself is generally quite small (<15% for the calculations on naphthalene described later, for example). This can be seen in Fig. 2.5, where the costs for a gradient for TIP and IP are almost the same, save for one fortunate run where the TIP came out faster than IP.

2.4 Numerical Tests and Examples

A series of tests on conjugated aromatic molecules that exhibit SB when treated by perfect-pairing (PP) or imperfect-pairing (IP) are described below. All of the calculations were performed in the 6-31G* basis set in conjunction with the rimp2-VDZ auxiliary basis set in a full valence perfect-pairing active space. This basis is sufficient to illustrate the challenge of obtaining a balanced description of local versus non-local correlations within these active space methods.

2.4.1 Benzene

The first test of the TIP model is the benzene SB problem, shown in Fig. 2.6, where TIP is compared against a full CC treatment of all active space amplitudes (i.e. the 4-pair CC model, which is simply VOD), and the original IP model (already shown in Fig. 2.1). These results are encouraging. The distortion of benzene yields a smooth potential energy curve with a single minimum at D_{6h} (see Fig 2.7 for a blow-up of the small angle region). There is only a small overall difference between the full VOD curve using a fourth order number of CC amplitudes and the TIP curve which uses a quadratic number of CC amplitudes and a cubic number of MP2 amplitudes. The largest deviation in the calculated distortion energies between TIP and VOD is about 1.5 kcal/mol at the largest distortion, which represents more than a 5-fold reduction over the corresponding IP error. It is interesting to compare this deviation against the corresponding 1 kcal/mol difference between the pilot calculations at the K-MP2 level for 3 and 4 pairs shown in Fig. 2.3, which was a

direct test of the effect of the missing correlations that couple 4 pairs when all are treated at the same level of theory. The difference is of similar magnitude to the VOD-TIP difference, but is of opposite sign. This suggests that errors due to neglect of 4-pair correlations are of similar magnitude to errors due to approximating the weak amplitudes by second-order perturbation theory.

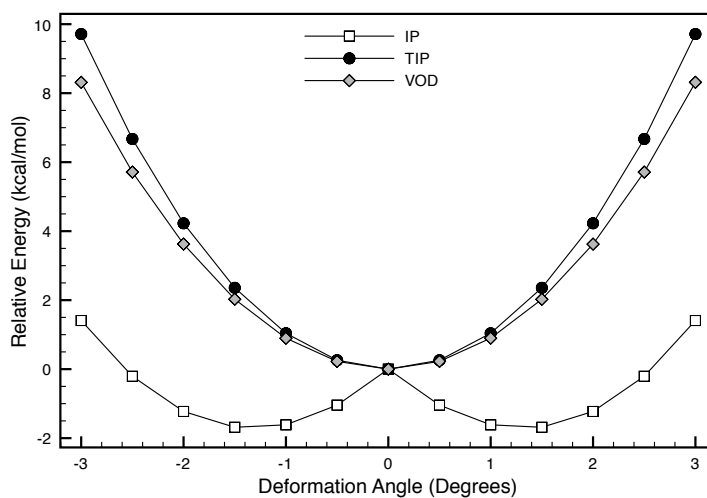


Figure 2.6: Comparative potential energy curves for deformation of benzene using the TIP, IP, and VOD models. It is evident that TIP significantly improves upon the IP model that it is designed to correct, and approaches the VOD model that it is approximating. For reference, the absolute energies at the D_{6h} geometry for the models are: -231.01428 H for IP, -231.095001 H for TIP, and -231.089623 H for VOD.

Another way to compare the error associated with the local 3-pair model against the errors associated with the perturbative treatment of the non-IP correlations is by examining the absolute energies at the D_{6h} geometry. The TIP energy exceeds the VOD energy by 3.37 kcal/mol. On the other hand, referring back to the caption of Fig. 2.3, the 3-pair MP2 model recovers about 8.7 kcal/mol less correlation energy than the full 4-pair result. This result is broadly consistent with the relative energies discussed above, and again suggests that the remaining local correlation error is of similar magnitude (in fact somewhat smaller) than the error associated with replacing cluster amplitudes by perturbation theory amplitudes, and has opposite sign.

To dig deeper into the origin of the results obtained in Figs 2.6 and 2.7, we now consider the form of the active orbitals obtained from the TIP calculations, relative to those from IP calculations. In each case the active orbitals are uniquely determined, in contrast to VOD

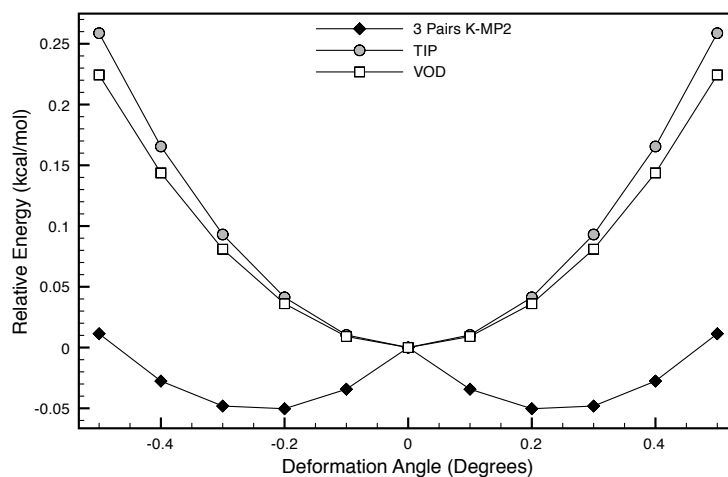


Figure 2.7: Close-up view of the potential curve for very small distortions of benzene away from D_{6h} symmetry for the 3-pair MP2, TIP and VOD models shown above in Figs 2.4 and 2.6. While 3-pair MP2 slightly breaks symmetry along this distortion coordinate, TIP does not.

or CASSCF calculations where only the active space spanned by the orbitals is determined. We first consider the π and π^* orbitals in Fig. 2.8 (both IP and TIP yield orbitals with σ/π symmetry). IP yields 3 active occupied π orbitals that essentially localize into a given bond, corresponding to the 3 double bonds of a given Kekule structure. The fact that the optimized π orbitals take this form is clearly the driving force for SB within the IP model: localized π orbitals in a strongly local correlation model preferentially correlate one of the 2 Kekule structures.

By contrast the TIP orbitals shown on the right-hand side of Fig. 2.8 optimize to be delocalized. Indeed both the occupied and virtual levels are quite reminiscent of canonical orbitals. The fact that the optimized π orbitals change form so strongly from IP to TIP is consistent with the striking improvement in performance of TIP over IP with respect to SB shown in Fig. 2.6 and 2.7. The change to delocalized π orbitals within a local correlation theory for benzene is a clear success of the TIP model, because now the 2 Kekule structures can be correlated on an essentially equal footing. This is one of the most physically interesting results of this paper.

One of the most important aspects of perfect-pairing models is the fact that the optimized orbitals localize strongly, and thus are physically interpretable as bonds, lone-pairs, anti-bonds, etc. The π space of benzene demands delocalized orbitals in order to eliminate SB by a balanced treatment of the two Kekule structures. However, the underlying

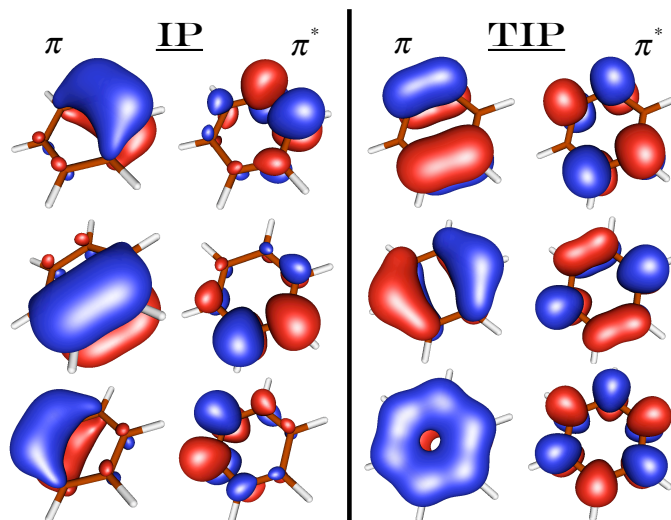


Figure 2.8: The 3 bonding and corresponding paired anti-bonding π orbitals (shown on the same line) for benzene as predicted by IP and TIP.

σ framework can still be localized, because it corresponds to a single Lewis structure. To what extent is this the case in practice for the TIP model? The answers are shown in Fig. 2.9, where the unique σ active orbitals are shown. They are still strongly localized into C-C and C-H bonds, although we note that there are in fact two types of C-C σ bonds – 2 of the first case (c) and 4 of the second case (d). While very similar in general form, they are nonetheless visually distinguishable. The implication of this is that a very small degree of electronic SB still persists in the TIP model. The general picture that comes from the TIP model is still a tremendously appealing improvement over the IP model – instead of all orbitals localizing as in IP, TIP orbital optimization leads naturally to a delocalized π system which correlates the two Kekule structures on an equal footing and a localized σ system.

The next step is to perform full geometry optimization with no imposition of symmetry to see the extent to which TIP removes the SB associated with IP and PP, when all degrees of freedom are permitted to relax. The results are shown in Figure 2.10. VOD and Hartree-Fock both correctly predict D_{6h} geometries, as they involve no local correlation modeling. PP and IP both incorrectly predict an optimal D_{3h} structure with large bond-alternation, of 0.09 Å and 0.08 Å respectively. TIP, on the other hand, actually predicts a D_{2h} structure, with a difference of 0.002 Å between the 2 unique bond-lengths. This is a 30-fold to 40-fold reduction in the extent of SB, relative to IP and PP.

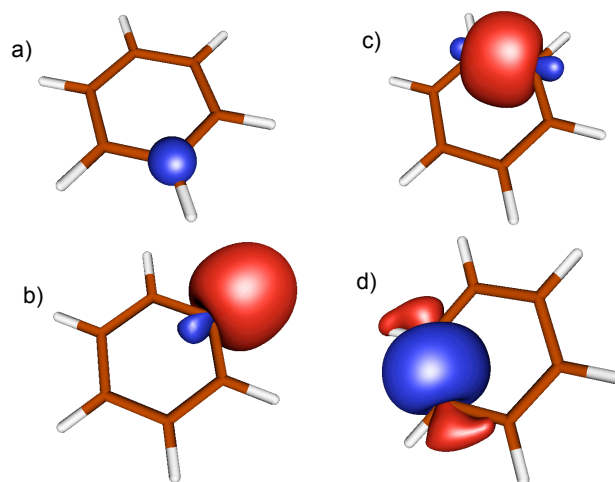


Figure 2.9: The localized occupied σ orbitals for benzene as predicted by TIP. Orbital A is a 6-fold degenerate inactive occupied s-type orbital on the carbons. Orbital B is a 6-fold degenerate C-H σ bonding orbital. Orbital C is a 2-fold degenerate C-C σ bonding orbital. Orbital D is a 4-fold degenerate C-C σ bonding orbital.

Bond	Method				
	HF	PP	IP	TIP	VOD
C1-C2	1.3862	1.3664	1.3796	1.4194	1.4123
C2-C3	1.3862	1.4551	1.4535	1.4218	1.4123
C3-C4	1.3862	1.3664	1.3796	1.4218	1.4123
C4-C5	1.3862	1.4551	1.4535	1.4194	1.4123
C5-C6	1.3862	1.3664	1.3796	1.4218	1.4123
C6-C1	1.3862	1.4551	1.4535	1.4218	1.4123

Figure 2.10: The optimized bond lengths of benzene predicted by Hartree-Fock, PP, IP, TIP, and VOD (using the 6-31G* basis). All bond lengths are in Angstroms.

The fact that the optimized TIP geometry has D_{2h} symmetry with 4 bond-lengths of one type and 2 of another is absolutely consistent with the form of the optimized orbitals shown in Figs. 2.8 and 2.9. The active occupied π orbitals correlating two bonds on opposite sides of the ring (middle orbitals in Fig. 2.8) leads to ever-so-slightly shorter bond-lengths than the 4 other bonds that are primarily described by the active π orbitals at the bottom of Fig. 2.8. This is also consistent with the form of the C-C sigma orbitals (4 of one type and

2 of another) in Fig 2.9 already noted earlier.

The TIP optimized bond-lengths are approximately 0.01 Å longer than the VOD bond-lengths that they are in principle approximating. While the very small residual SB is a consequence of only including correlations that couple up to 3 pairs in TIP (i.e. local correlation), the systematic error in the TIP geometry relative to VOD is a consequence of the low-order perturbation treatment of the 3-pair correlation amplitudes. As we inferred earlier, the latter seems to be the larger error.

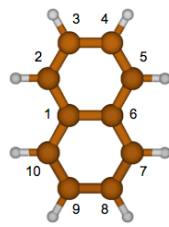
2.4.2 Naphthalene

We now turn to the question of how transferable the TIP results for benzene are to larger aromatic molecules with a more extended network of conjugated π bonding. At what stage will the optimized TIP π orbitals start to localize? What consequences will this have for addressing problems of SB? And are the pathologies of perfect and imperfect pairing for benzene similar, larger or smaller for such systems? In this section, we consider naphthalene, which has 48 valence electrons, and therefore 24 active electron pairs. It has 10 π electrons.

The results of geometry optimizations on naphthalene are collected in Figure 2.11. Both HF and VOD predict qualitatively correct results, giving a D_{2h} structure, which is a resonance hybrid with contributions from several important Lewis dot structures. By contrast, PP and IP optimizations incorrectly lead to 2 bond isomers (depending on the guess), labeled as (a) and (b) in Figure 2.11. These isomers correspond to 2 distinct Lewis structures, one having D_{2h} symmetry and the other having C_{2v} symmetry. This is a more drastic consequence of SB than in benzene, where the two possible alternating bond structures (left and right wells of Fig. 2.1 for instance) were equivalent. The bond-length alternation is pronounced, with differences of about 0.10 Å.

To explore the extent to which TIP corrects the SB associated with PP and IP, TIP optimizations were started from both D_{2h} and C_{2v} guess structures. As is evident from Fig. 2.11, both guesses converge to the same D_{2h} structure with TIP, indicating that the SB problem in naphthalene is resolved with the TIP approach. We view this as another very encouraging validation of the TIP method. Comparison of the structure against the VOD geometry (which was optimized in the smaller 6-31G basis due to the large memory, disk and CPU requirements of the VOD method) indicates reasonable agreement. The main discrepancy is the central (C1-C6) bond, which is slightly longer in TIP than in the VOD method.

A selection of the TIP optimized occupied orbitals are shown in Fig. 2.12. It is evident that σ - π separation is properly retained. The 5 active π orbitals are partially delocalized,



Bond	Method							
	HF	PP (a)	PP (b)	IP (a)	IP (b)	TIP (a)	TIP (b)	VOD*
C1-C2	1.4206	1.4623	1.3771	1.4661	1.3898	1.4475	1.4475	1.4452
C2-C3	1.3583	1.3623	1.4360	1.3718	1.4384	1.4124	1.4124	1.3913
C3-C4	1.4166	1.4610	1.3745	1.4633	1.3865	1.4319	1.4319	1.4399
C4-C5	1.3583	1.3623	1.4360	1.3718	1.4384	1.4124	1.4124	1.3913
C5-C6	1.4206	1.4623	1.3771	1.4661	1.3898	1.4475	1.4475	1.4452
C6-C7	1.4206	1.4623	1.4831	1.4661	1.4883	1.4475	1.4475	1.4452
C7-C8	1.3583	1.3623	1.3538	1.3718	1.3615	1.4124	1.4124	1.3913
C8-C9	1.4166	1.4610	1.4840	1.4633	1.4874	1.4319	1.4319	1.4399
C9-C10	1.3583	1.3623	1.3538	1.3718	1.3615	1.4124	1.4124	1.3913
C10-C1	1.4206	1.4623	1.4831	1.4661	1.4883	1.4475	1.4475	1.4452
C6-C1	1.4092	1.3871	1.4597	1.3996	1.4608	1.4528	1.4528	1.4371

Figure 2.11: A comparison of optimized naphthalene bond lengths for a Hartree-Fock, PP, IP, TIP and VOD. The (a) structures come from a guess of D_{2h} symmetry; the (b) structures come from a guess of C_{2v} symmetry. All bond lengths are in Angstroms. All bond lengths are colorC coded to indicate the symmetry equivalent bonds for a D_{2h} structure. *VOD was done in the 6-31G basis set with the rimp2-VDZ auxiliary basis set due to limitations in performing the optimization.

with one orbital, A, exhibiting nearly complete delocalization. The strongly localized form of the σ orbitals demonstrates that with a more extended π system, TIP still has the desirable property of generating a balanced mix of localized and delocalized orbitals. It is also encouraging that this orbital solution is unique across the potential energy surface such that the two different guess geometries converge to the same final optimized TIP geometry without any constraints on the point group.

2.4.3 Phenalenyl cation and anion

To explore a larger molecule, we decided to examine the system comprised of three fused benzene rings, $C_{13}H_9$. The neutral species is the phenalenyl radical, but its cation and anion are closed shell systems, and we therefore chose to test the performance of PP, IP and TIP on them. The optimized geometries obtained are summarized in Figures 2.13 and 2.14. Both cation and anion should exhibit a D_{3h} geometry consistent with 12 and 14 delocalized π electrons, as seen for instance in the HF results. By contrast, PP and IP show significant SB, with bond alternation of up to 0.06 Å. In addition, another isomer, not shown in the figures, was located for PP and IP, with bond-alternation around the periphery (i.e. C_{3v} symmetry).

For the TIP method, the data for the cation in Fig. 2.13 and the anion in Fig. 2.14 are the least successful and most successful presented thus far. For the cation, two isomeric structures were obtained, although both exhibit significantly less SB than PP and IP. Nevertheless, this is an illustration of the limitations of the TIP model to remove SB

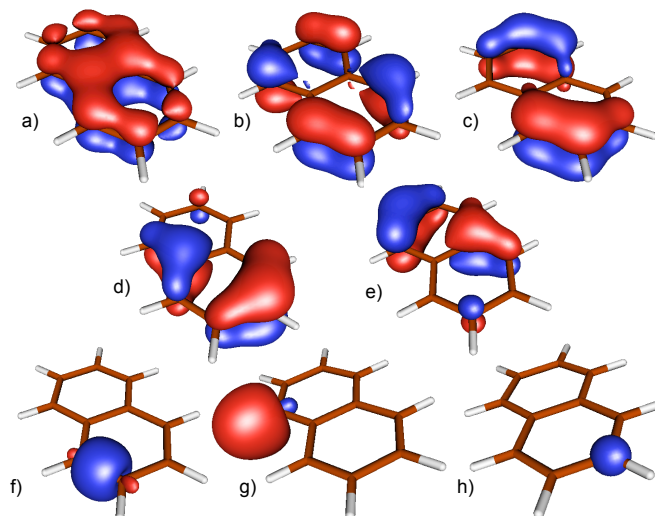
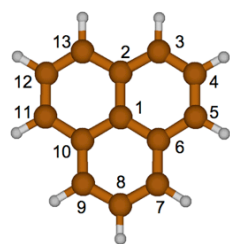


Figure 2.12: The occupied orbitals for naphthalene as predicted by TIP. Orbitals A-E are the unique π bonding orbitals for naphthalene. Orbital F is an 11-fold degenerate C-C σ bonding orbital. Orbital G is an 8-fold degenerate C-H σ bonding orbital. Orbital H is a 10-fold degenerate inactive occupied s-type orbital on the carbons.

effects. Since it is still a local correlation model, it still has the potential to exhibit SB. By contrast, the case of the anion shows complete removal of SB effects, as the optimized structure converges to D_{3h} symmetry. Evidently, removal (ionization) of a π electron to yield the cation poses a more difficult challenge for the TIP local correlation model than attachment of an electron to yield the anion. This leaves an interesting open question of how a future open-shell TIP implementation would perform for the neutral phenalenyl radical. It appears likely to be of intermediate difficulty.

2.5 Discussion and conclusions

Generalized valence bond coupled cluster methods such as perfect and imperfect pairing inherit to a large degree the known symmetry-breaking (SB) problems of conventional generalized valence bond methods. In benzene, the preference for localized relative to delocalized electronic structure leads to SB in which the equilibrium geometry is D_{3h} symmetry rather than D_{6h} , and the electronic structure at D_{6h} is symmetry broken, suggesting that one Kekule structure is preferentially correlated. In naphthalene and phenalenyl cation one can locate distinct isomers corresponding to preferentially correlating the localized orbitals associated with different resonance structures. These examples are limitations that prevent



Bond	Method				
	HF	PP	IP	TIP (a)	TIP (b)
C1-C2	1.4108	1.3899	1.3948	1.4502	1.4159
C2-C3	1.4089	1.4498	1.4600	1.4234	1.4408
C3-C4	1.3837	1.3745	1.3792	1.4166	1.4131
C4-C5	1.3838	1.4381	1.4503	1.4068	1.4092
C5-C6	1.4090	1.3834	1.3875	1.4486	1.4398
C6-C7	1.4089	1.4569	1.4675	1.4389	1.4382
C7-C8	1.3836	1.3802	1.3856	1.4077	1.4114
C8-C9	1.3836	1.4164	1.4239	1.4184	1.4114
C9-C10	1.4088	1.4207	1.4289	1.4302	1.4382
C10-C11	1.4087	1.3969	1.3996	1.4517	1.4398
C11-C12	1.3837	1.4267	1.4400	1.4068	1.4092
C12-C13	1.3838	1.3797	1.3833	1.4093	1.4131
C13-C2	1.4089	1.4497	1.4061	1.4447	1.4408
C6-C1	1.4108	1.4448	1.4557	1.4357	1.4427
C10-C1	1.4107	1.4498	1.4588	1.4379	1.4427

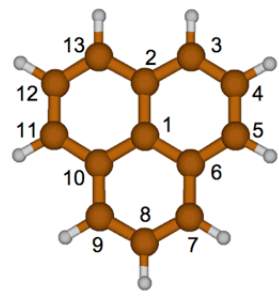
Figure 2.13: Optimized bond lengths for the phenalenyl cation for Hartree-Fock, PP, IP, and TIP. The PP, IP, and TIP (a) guess structures were the optimized Hartree-Fock structure. The TIP (b) guess structure was the optimized phenalenyl anion geometry. The energies for TIP (a) and TIP (b) are: -498.115876 H and -498.110478 H respectively. All bond lengths are in Angstroms, and bond-lengths that should be symmetry-related are color-coded to enable inspection of symmetry-breaking.

general usage of these methods for chemical applications.

The origin of SB is that fact that correlations involving multiple electron pairs are omitted in these computationally efficient methods. The PP method correlates only electrons within a pair, while IP augments this with the leading correlations between 2 pairs. By contrast, the calculations presented in this paper show that to obtain a reasonably balanced description of valence electron correlation effects in benzene along a D_{6h} to D_{3h} distortion coordinate, one must minimally include all pair correlation effects that couple electrons in up to 3 different electron pairs.

A tractable method for doing so is to treat the strongest (IP-type) correlations fully at the coupled cluster level while weaker but far more numerous correlations coupling up to 3 pairs at once are treated only by 2nd order perturbation theory. This three-pair corrected IP (TIP) method reduces the magnitude of the local correlation error by a factor typically between 10 and 20, relative to IP itself, and accordingly should significantly reduce the magnitude of SB effects.

This was seen in several numerical examples. TIP yields a potential curve for distortion of benzene with a single D_{6h} minimum, and the fully optimized TIP structure shows D_{2h}



Bond	Method			
	HF	PP	IP	TIP
C1-C2	1.4345	1.4754	1.4895	1.4654
C2-C3	1.4142	1.4317	1.4448	1.4438
C3-C4	1.3804	1.4080	1.4167	1.4088
C4-C5	1.3804	1.3804	1.3845	1.4088
C5-C6	1.4142	1.4557	1.4691	1.4438
C6-C7	1.4142	1.3912	1.3931	1.4438
C7-C8	1.3804	1.4336	1.4457	1.4088
C8-C9	1.3804	1.3701	1.3751	1.4088
C9-C10	1.4142	1.4548	1.4629	1.4438
C10-C11	1.4142	1.4451	1.4615	1.4438
C11-C12	1.3804	1.3760	1.3772	1.4088
C12-C13	1.3804	1.4187	1.4389	1.4088
C13-C2	1.4142	1.4060	1.4033	1.4438
C6-C1	1.4345	1.4726	1.4833	1.4654
C10-C1	1.4345	1.4101	1.4102	1.4654

Figure 2.14: Optimized bond lengths for the phenalenyl anion for Hartree-Fock, PP, IP, and TIP. The guess structure for the PP, IP, and TIP optimizations was the Hartree-Fock structure. All bond lengths are in Angstroms. All bond lengths are color coded to indicate the symmetry equivalent bonds for a D_{3h} structure.

symmetry with deviations of less than 0.002 Å from D_{6h} . With TIP, the two spurious isomers obtained for naphthalene at the IP level collapse to a single structure. For the phenalenyl cation, TIP still exhibits noticeable SB, though its magnitude is significantly diminished relative to IP (or PP). For the phenalenyl anion, SB is removed entirely.

A particularly interesting aspect of the TIP optimized orbitals in these aromatic systems is that the σ orbitals localize strongly into bonds, while the π orbitals exhibit significant delocalization, in contrast to PP or IP. This means that the TIP local correlation approach can give a better balanced description of correlation effects arising from each resonance structure than in PP or IP where a single resonance structure is preferentially correlated, leading to SB. Overall, TIP seems to give a very significant reduction in the SB problems associated with existing generalized valence bond coupled cluster methods, while maintaining their desirable physical features (of orbitals that localize when possible – such as for a molecule with a single Lewis structure) and computational efficiency. We intend to present TIP results across a broader range of molecules including open-shell systems in the future.

Chapter 3

Penalty functions for combining coupled cluster and perturbation amplitudes in local correlation methods with optimized orbitals

3.1 Introduction

Symmetry Breaking (SB) in generalized valence bond (GVB) methods has been known since the inception of the perfect pairing (GVB-PP) [56,57] method thirty years ago. The extension of the GVB-PP model to include other correlations via coupled-cluster generalized valence bond (CC-GVB) approaches [78,79] also exhibits problems with SB [83,84,86]. In other respects these more sophisticated CC-GVB methods are very promising because they recover the leading correlations omitted in the basic PP model, which are clearly important in systems with coupled strongly correlated pairs, as exemplified by multiple bonds [83,84,86]. The intrapair PP correlations are shown in part (a) of Fig. 3.1, together with the additional interpair correlations that are included in the imperfect pairing (IP) model, the 2-electron transfers between pairs that were previously shown to be next most important [84], and finally the 1-electron charge transfer correlations.

Solutions to SB have been presented, such as the resonating GVB method [137] and the 'breathing-orbital' method [138]. Models such as these rely on the identification of multiple resonance structures for each molecule being studied, which is unsatisfactory in general. Other solutions include resorting to a fully delocalized Complete Active Space Self-Consistent Field (CASSCF) [50, 51, 53, 54] approach, or approximations such as the density matrix renormalization group [128, 129], or the valence orbital-optimized coupled cluster doubles (VOD) approach [80, 81]. These methods are, however, high in computa-

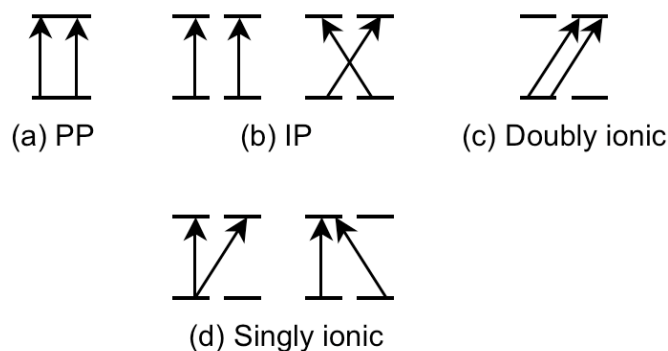


Figure 3.1: Electron correlations that couple one or two electron pairs together, where the correlations are described in a perfect pairing active space such that each valence occupied orbital has one correlating antibonding orbital. These two levels describe each electron pair, and thus perfect pairing (PP) contains only the intra-pair correlation that excites both electrons from bonding to anti-bonding level, as shown in (a). There are 4 types of electron correlation that couple 2 different electron pairs together. Two of these, shown in (b), involve no electron transfer and are included in the imperfect pairing (IP) model in addition to the PP correlations. Electron correlations that transfer either 1 or 2 electrons between pairs are shown in (c) and (d).

tional cost at present.

Recently, we explored the origin of the SB observed in aromatic hydrocarbons, such as benzene and naphthalene, and suggested a model [118] that reduced it by at least a factor of 10. Of course, SB could be completely eliminated if all missing correlations that involve double excitations in the active space were included, since we then recover the VOD method. We discovered, however, that SB could be dramatically reduced if only correlations coupling up to 3 different electron pairs were included, while the far more numerous (and smaller) terms coupling up to 4 different pairs were completely neglected. To make the cost of including the 3-pair terms as low as possible, we then explored treating their contribution to the correlation energy by second order perturbation theory, rather than full coupled cluster theory. Since their magnitude should be small relative to the largest amplitudes (of the types shown in parts (a), (b) of Fig. 3.1), this approximation should introduce very little error.

The resulting method, Three-Pair Corrected Imperfect Pairing (TIP), separates the valence electron correlations in a PP active space into strong, weak and negligible terms. Negligible terms (defined as coupling 4 different electron pairs) were completely neglected. The strongly correlating terms were treated with coupled cluster theory (intrapair and the imperfect pairing interpair correlations shown in Fig. 3.1). The weakly correlating terms coupling electrons in 2 pairs ((c) and (d) of Fig. 3.1) and those coupling 3 different electron pairs, shown in Fig. 3.2 were treated at a simplified second-order perturbation theory level. The effect of the weak amplitudes on the strong amplitudes was included by 1-electron couplings. The resulting hybrid energy function was then minimized with respect to both amplitude and orbital variations. TIP increases the computational cost of IP itself by only a factor of about 2, independent of system size, and is therefore a promising potential replacement for the study of large systems where more accurate alternatives are unfeasible.



Figure 3.2: Electron correlations that couple three electron pairs together, where the correlations are described in a perfect pairing active space such that each valence occupied orbital has one correlating antibonding orbital. There are 4 distinct types of these correlations, shown schematically in the figure. The two left-most correlations transfer 1 electron from one pair to another, and the two right-most correlations transfer 2 electrons.

However, when we subsequently began to use TIP to examine other systems, orbital optimization pathologies resulting from the combination of an infinite-order and a second-order treatment of different correlations can be observed. For instance, Fig. 3.3 shows

the exact solution for N_2 if it is treated only at an orbital optimized doubles level for the 6-31G* basis set in a (6,6) active space (i.e. 6 active electrons in 6 orbitals), describing the σ and π bonding orbitals. The virtual orbitals show the expected anti-bonding character of the occupied orbitals they correspond to in the GVB-PP sense. However, Fig. 3.4 shows the orbitals for the same system as produced by TIP. The occupied orbitals have switched their ordering so that their correlating virtual orbitals (shown below) are unexpected (for instance the correlating orbital for σ is of π^* character).

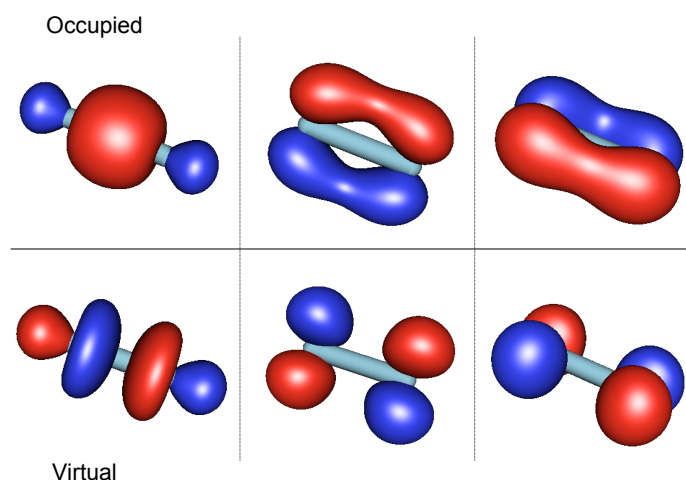


Figure 3.3: The orbitals for N_2 for IP+DIP in the (6,6) active space at 6-31G. The top row is the occupied orbitals in increasing energy ordering from left to right. The bottom row are the virtual orbitals that correspond in the GVB-PP sense to the occupied orbital directly above it.

Such a re-arrangement leads to an artificial lowering of the energy by transferring some "strong" correlations from being treated by CC theory to being treated by PT, which turns out to significantly overestimate their contribution to the correlation energy. The energy produced by TIP is -109.10528 Eh, but the energy produced with a full coupled-cluster treatment of all the three pair correlations for those orbitals is only -109.07512 Eh. Thus re-ordering the occupied orbitals (which should leave the correlation energy invariant) creates a chemically significant error of 0.030 Eh (0.8 eV). It is a failure of the proposed TIP model, as now most of the largest correlations are treated at the low level (PT) while the high level of theory (CC) is being used to treat weak correlations. This is the opposite of our original purpose.

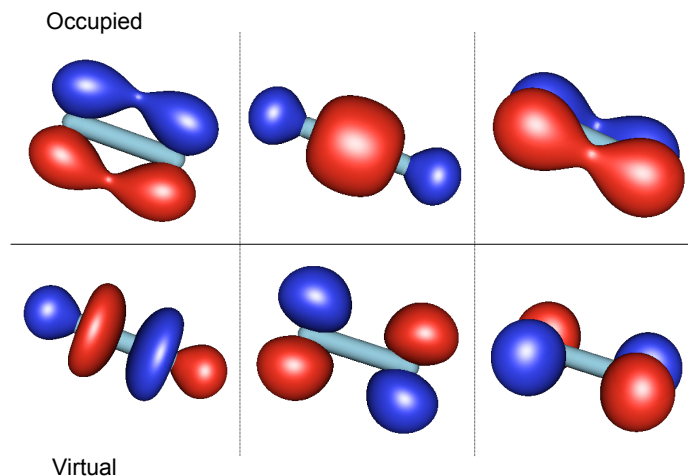


Figure 3.4: The orbitals for N₂ for TIP in the (6,6) active space at 6-31G. The top row is the occupied orbitals in increasing energy ordering from left to right. The bottom row are the virtual orbitals that correspond in the GVB-PP sense to the occupied orbital directly above it.

The goal of this paper is to modify the TIP model to eliminate pathologies such as the ones discussed above associated with arbitrary orbital rotations or second-order perturbation theory over-estimating the magnitude of a correlation. This will be accomplished using a penalty function that ensures that "strong" correlations are not treated by PT. The result is not molecule specific, and retains all of the desirable properties of the original TIP method. In Sec. 3.2, we will discuss the modifications to the TIP theory. In Sec. 3.3, we will present tests of the improved TIP across a wide spectrum of molecular cases, and in Sec. 3.4 we will present our conclusions.

3.2 Theory

3.2.1 Hybrid energy function

The design goals for the modified TIP local correlation model may be summarized as follows. 1) Maintain the physical advantage of GVB-CC methods: namely orbitals that localize when this is physically possible. 2) Remove the tendency of GVB-CC methods to over-localize orbitals by breaking symmetry, as in compounds with multiple resonance structures 3) Maintain the computational cost advantage of scaling at least 2 powers of system size less than the valence orbital optimized CCD (VOD) method we are approximating

by using perturbation theory [144–147] for weak correlations. 4) Remove the possibility of artificial energy lowering when PT amplitudes describe strong correlations because they yield overestimates of their energy contributions (as in the nitrogen example discussed above).

Allowing orbitals to localize requires that we break the orbital invariance of full VOD in the same active space by neglecting some terms. As a result our goal is *not* the recovery of 100% of the VOD correlation energy, because we would then not obtain localized orbitals in general. We want slightly less than 100%, yet still enough that orbitals in systems with multiple resonance structures will properly delocalize, as necessary to ameliorate symmetry-breaking. We discovered in our pilot study on aromatic hydrocarbons [118] that inclusion of correlations coupling only up to 3 distinct pairs would accomplish this goal, and we shall attempt to preserve this framework.

To ensure that orbital rotations do not interchange orbitals to make PT describe strong correlations, we shall employ penalty functions. The energy contribution of an amplitude t_j which is treated by perturbation theory is given by a modification of the standard Hylleraas expression where the zero order energy difference, $D_{j0} = E_j^{(0)} - E_0^{(0)}$ is penalized by λ_j :

$$E(t_j) = t_j[D_{j0} + \lambda_j]t_j + 2V_{j0} \quad (3.1)$$

Typically in regularization methods, λ_j is just taken as a small constant. This permits solution for the amplitude, $t_j = [D_{j0} + \lambda_j]^{-1}V_{j0}$ even when D_{j0} approaches zero.

In our application, we want to ensure that the partition between employing CC theory for large amplitudes and PT for small amplitudes is stable under orbital optimization. Therefore we shall use a non-standard penalty function that vanishes when the PT amplitude is small in comparison to a partitioning threshold, t_c , and grows rapidly to be very large as the PT amplitude exceeds t_c . A suitable form is therefore:

$$\lambda_j = \gamma[\exp((t_j/t_c)^2) - 1] \quad (3.2)$$

γ is an additional parameter to control how large the effect of the penalty function is on the PT amplitude. Since the penalty function depends on the amplitude it is penalizing, the PT amplitudes need to be solved for iteratively. The amplitudes only need to be solved for one at a time, which involves computational cost that is third order with respect to active space size (which is not limiting in any sense). Newton steps are used to converge the amplitudes.

We have made two other changes to the pilot method reported previously. The first is a clear improvement that is sometimes physically important. That is to treat pair correlations that move two electrons from one pair into the correlating orbital of the other

pair at the CC level. The equations are shown in the appendix, and it turns out that these doubly ionic paired (DIP) terms can be treated by CC theory without increasing the computational cost significantly beyond the IP method [82, 131]. As shown in an earlier investigation [84], these amplitudes are typically the largest of the ones we were treating by PT, and a correct CC treatment will therefore yield a more robust method. When used on its own, we refer to this model as the IP+DIP method. IP+DIP correctly accounts for the PP terms, the IP terms and the DIP terms, shown in the diagram in Fig. 3.1.

The second change is entirely remove the remaining (smaller) amplitudes that couple together two electrons in 2 pairs (by transferring 1 electron between them, as shown in part (d) of Fig. 3.1), which were previously treated by PT. This is equivalent to applying a value of $t_c \rightarrow 0$ for these singly ionic paired (SIP) amplitudes, and seems to be necessary in order to fully prevent orbital rotations yielding artifacts. For example, two slightly inequivalent bond lengths in water are obtained unless such large values of the penalty parameters are applied that virtually no correlation energy is recovered by PT. It would be more desirable to treat these terms by CC theory (as discussed above for the two-electron transfers coupling 2 pairs), but it appears this cannot be accomplished without a substantial increase in the computational cost and complexity of the resulting theory. It may be worthwhile to implement this extension in the future, but the results shown later generally support the adequacy of neglecting them entirely.

The final TIP Lagrangian takes the form $L_{IP+DIP}^{(\infty)} + L_{3P}^{(2)}$, with the definitions of these Lagrangians and their subsequent amplitudes found in the Appendix. We utilize the same algorithm based on the efficient resolution of the identity [61–63] MP2 gradient implementation [151] as in our previous work, with significant improvements in formation of the two-particle density matrix contributions from the cluster amplitudes which speed up the nuclear gradient evaluation by a factor of six. The modified TIP method has been implemented in a modified version of Q-Chem 3.0 [142]. Additionally, for test purposes, a machine-generated program has been produced which solves the cluster equations for *all* amplitudes in the TIP model has developed by John Parkhill – this will have much higher intrinsic fifth order scaling, but will permit direct assessment of the errors in the production algorithm.

3.2.2 Choosing Penalty Function Parameters

The introduction of a parameterized penalty function into TIP necessitates an evaluation of those parameters with respect to the ideal performance of the method. The first criterion is that TIP should recover less than or equal to the same correlation energy as VOD. N₂ is a good challenge for this, since the original pilot TIP method results in a recovery of 155.71% of the VOD correlation energy in the 6-31G* basis set. Our CC-treatment of the IP+DIP terms alone recovers 96.56% of the VOD correlation energy. Removing the

SIP terms from the PT correction reduces the correlation energy to about 116% of the correct result, before applying the penalty to the three-pair PT terms. Fig. 3.5 shows the family of curves for several possible parameter combinations for N_2 . As the penalty parameters increase, the nature of the TIP orbital solution changes. At smaller values of the critical amplitude parameter, $t_c < 0.01$, and larger values of the penalty function scalar, (> 0.04 Eh), the curves all settle on one solution whose energy gradually decreases as the strength of the penalty function is increased, towards the limit of 96.56%. Penalty function parameters that lower the N_2 correlation energy below 100% are too large to maintain the SB reducing property of TIP, therefore N_2 percent correlation energy will need to (slightly) exceed that of VOD.

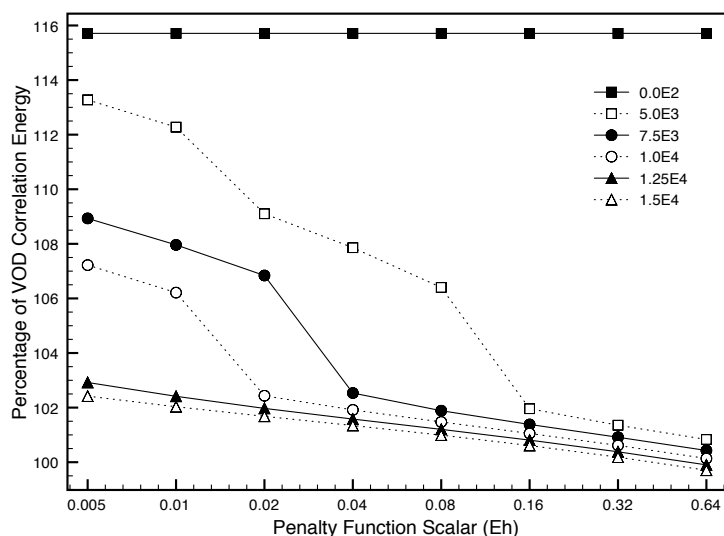


Figure 3.5: A plot of the percent of the VOD correlation energy recovered by TIP for N_2 at the MP2/6-31G* optimized geometry. Each curve represents a single choice of the amplitude scaling parameter, with the x-axis being the values of the penalty function scalar in Hartrees. The percent of the VOD correlation energy recovered by TIP with no penalty function at all is 115.71, and the percent recovered with no 2^{nd} -order perturbation theory is 96.56.

Fig. 3.6 presents the case of the N_6 molecule in a D_{6h} ring, which is the saddle point in the dissociation into three N_2 molecules. It also exhibits solution instability for weaker choices of the penalty function. Not until stronger values of the two parameters are used does TIP result in one orbital solution that monotonically decreases in percent correlation energy with increased strength of parameters. Fig. 3.7 shows the isoelectronic case of D_{6h} benzene. The TIP solution becomes stable for weaker values of the penalty function in this case. For both N_6 and benzene, the un-penalized TIP correlation energy never exceeds

100% of the VOD correlation energy, and all reasonable choices for parameters result in over 95% recovery of the VOD correlation energy.

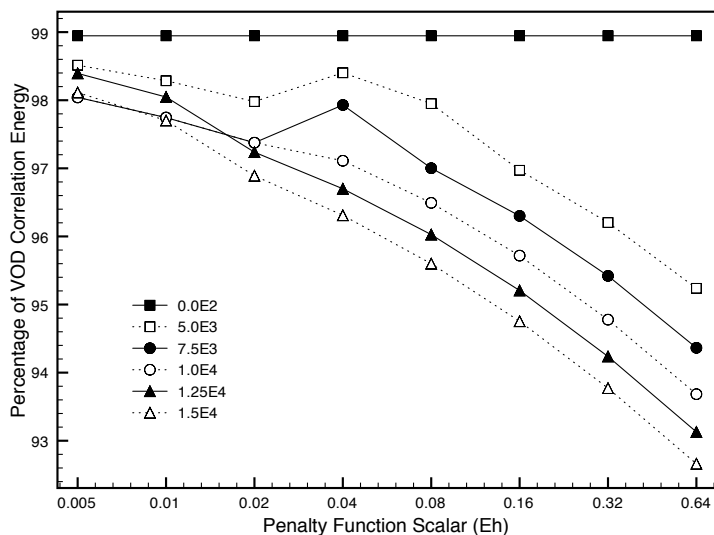


Figure 3.6: A plot of the percent of the VOD correlation energy recovered by TIP for D_{6h} N_6 , at the MP2/6-31G* optimized geometry. Each curve represents a single choice of the amplitude scaling parameter, with the x-axis being the values of the penalty function scalar in Hartrees. The percent of the VOD correlation recovered by TIP with no penalty function at all is 98.95 and the percent recovered with no 2nd-order perturbation theory is 78.68.

The final two examples are water in Fig. 3.8 and propane in Fig. 3.9. Both of these molecules retain the nature of their TIP solution regardless of the choice of parameters, and even the strongest penalty functions tests reduce the recovered correlation energy by only 0.04%. On the basis of these results (the weakest possible penalty function that gives stable solutions for N_2 , N_6 and benzene), we think that a critical amplitude of $t_c = 0.009$ and a prefactor of 0.16 Eh are reasonable choices that will robustly partition strong correlations to CC theory and weak correlations to PT, while recovering as large a PT correction as possible. These values will be used for all subsequent calculations reported in the Results section below.

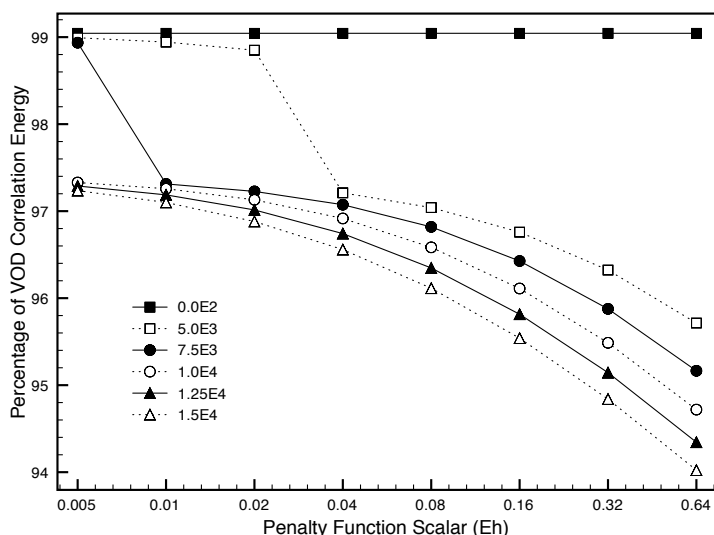


Figure 3.7: A plot of the percent of the VOD correlation energy recovered by TIP for benzene, C_6H_6 , at the MP2/6-31G* optimized geometry. Each curve represents a single choice of the amplitude scaling parameter, with the x-axis being the values of the penalty function scalar in Hartrees. The percent of the VOD correlation energy recovered by TIP with no penalty function at all is 99.04, and the percent recovered with no 2^{nd} -order perturbation theory is 82.23.

3.3 Results

3.3.1 Correlation energy recovery with and without penalty functions

The first and most basic test of the modified TIP method is to assess how effectively valence electron correlation energy is recovered relative to more exact treatments. For this purpose we employ the coupled cluster test code discussed earlier that can solve the equations including all 3 pair correlations (i.e. all terms included in the pilot TIP method), or delete the SIP terms to permit a CC treatment of all terms included present version. Note that this code (and the VOD code which includes all valence space pair correlations) uses exact 2-electron integrals while the TIP codes use the resolution of the identity (RI) approximation. The RI approximation introduces around 50-60 μ Hartrees of error per atom to the correlation energy for MP2, so for these molecules there is an RI error around 100 μ Hartrees, which will be small compared to the errors we are going to assess. The perfect pairing active space includes all valence electron pairs.

Table 3.1 shows the correlation energy in Hartrees for a set of small 2 heavy-atom

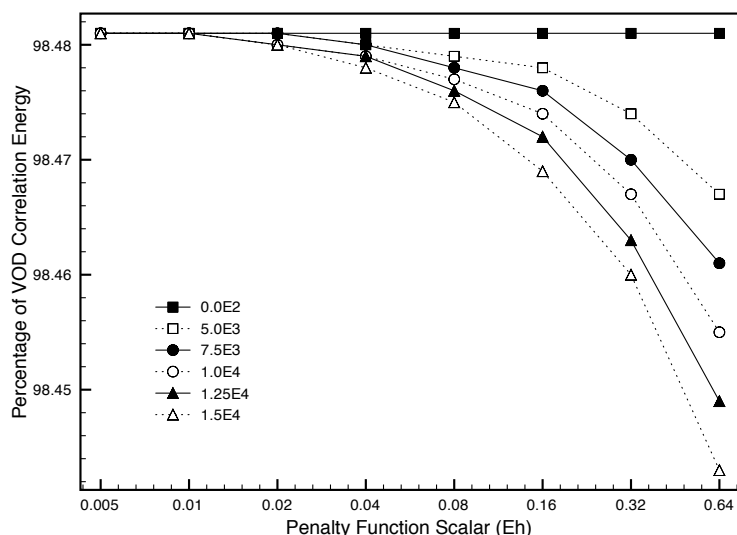


Figure 3.8: A plot of the percent of the VOD correlation energy recovered by TIP for water, H_2O , at the MP2/6-31G* optimized geometry. Each curve represents a single choice of the amplitude scaling parameter, with the x-axis being the values of the penalty function scalar in Hartrees. The percent of the VOD correlation energy recovered by TIP with no penalty function at all is 98.48, and the percent recovered with no 2^{nd} -order perturbation theory is 97.88.

molecules at a fixed geometry using fixed PP orbitals for all correlation methods. These systems contain between 4 and 7 electron pairs. TIP, for the most part, recovers almost the same correlation energy as its full coupled-cluster counterpart. For some cases, like N_2 and F_2 , TIP recovers slightly more correlation than its full coupled-cluster counterpart, but that correlation energy does not exceed that of the full three pair model. For most of the molecules TIP recovers less correlation energy than the full valence space CCD method, which is not surprising given the percent correlation energies seen in the previous section. Even without a penalty, TIP without the SIP amplitudes only gathered around 98% of the VOD correlation energy. The removal of the SIP amplitudes from TIP clearly has a small effect on its energy recovery, lowering the overall correlation energy that is recovered. Indeed the differences between the new and pilot forms of TIP track quite well the differences between the corresponding CCD energies when the SIP amplitudes are removed. The effect of the penalty function on the 3-pair correlations is evidently quite small, and the fact that TIP with the penalty function yields better agreement with the CC values for the same set of amplitudes suggests that the parameters chosen are reasonable.

Table 3.2 presents the same set of data at using a different set of fixed orbitals – this time the orbitals used are those that minimize the energy of the pilot TIP model. This time the

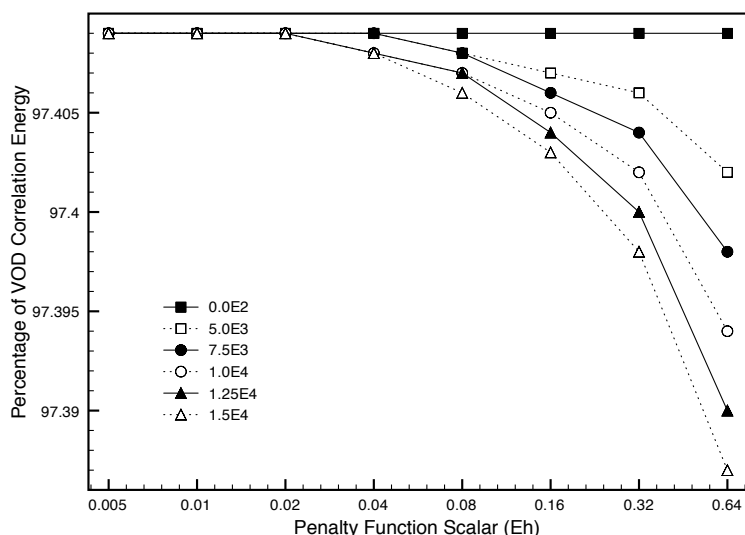


Figure 3.9: A plot of the percent of the VOD correlation energy recovered by TIP for propane, C_3H_8 , at the MP2/6-31G* optimized geometry. Each curve represents a single choice of the amplitude scaling parameter, with the x-axis being the values of the penalty function scalar in Hartrees. The percent of the VOD correlation energy recovered by TIP with no penalty function at all is 97.41, and the percent recovered with no 2^{nd} -order perturbation theory is 94.88.

picture is completely different, and this table illustrates the importance of employing the penalty function in order to ensure a stable method. The pilot TIP method overestimates the correlation energy for a majority of these simple test cases (negative mean signed error). While we have not investigated the optimized orbitals for each case individually, it is a reasonable assumption that most of the problem cases arise for reasons similar to the overestimation in N_2 illustrated in Fig. 3.4 – namely changes in active orbital ordering within either the occupied or virtual spaces to interchange the roles of CC and PT so that the latter is used to overestimate the strong correlations. Comparing the first two columns of Table 3.2, it is evident that the penalty function approach combined with the removal of the SIP amplitudes to define the present TIP model has satisfactorily resolved this issue. The modified TIP method now yields notably higher energies than the full CC models because the PT amplitudes are subject to significant penalties (compare the mean signed errors for TIP with and without the penalty function). This will cause orbital optimization in the penalty function TIP to retain treatment of strong correlations in the CC amplitudes, and weak correlations in the PT amplitudes, as we are seeking to do. We can see the effect of this in Table 3.3. When each method is allowed to let their orbitals fully relax, we see the same trend as in Table 3.2, the present TIP is a marked improvement cutting the error with respect to VOD by around a factor of five in comparison to the original TIP method,

	TIP ^{a,b,d}	TIP ^{a,c}	CC-TIP	CC-3P ^d	VOD ^d
N ₂	-0.1748	-0.1727	-0.1658	-0.1740	-0.1740
F ₂	-0.2402	-0.2373	-0.2368	-0.2381	-0.2383
CO	-0.1593	-0.1567	-0.1578	-0.1598	-0.1598
CS	-0.1137	-0.1115	-0.1138	-0.1167	-0.1167
NP	-0.1568	-0.1532	-0.1544	-0.1573	-0.1573
P ₂	-0.1082	-0.1040	-0.1059	-0.1085	-0.1085
NaF	-0.1301	-0.1294	-0.1301	-0.1318	-0.1318
ClF	-0.1575	-0.1543	-0.1567	-0.1618	-0.1626
Cl ₂	-0.0808	-0.0771	-0.0788	-0.0850	-0.0850
HCN	-0.1653	-0.1633	-0.1632	-0.1647	-0.1647
HNC	-0.1447	-0.1433	-0.1430	-0.1445	-0.1445
HCP	-0.1316	-0.1287	-0.1299	-0.1370	-0.1377
HNO	-0.2003	-0.1969	-0.1978	-0.2010	-0.2012
HPO	-0.1620	-0.1569	-0.1583	-0.1663	-0.1669
HOF	-0.2298	-0.2253	-0.2259	-0.2304	-0.2307
HOCl	-0.1565	-0.1525	-0.1540	-0.1593	-0.1601
H ₂ CO	-0.1771	-0.1736	-0.1734	-0.1771	-0.1773
H ₂ CS	-0.1177	-0.1144	-0.1162	-0.1201	-0.1203
H ₂ O ₂	-0.2224	-0.2187	-0.2206	-0.2249	-0.2257
H ₂ S ₂	-0.0929	-0.0905	-0.0924	-0.0974	-0.0984
N ₂ H ₂	-0.1877	-0.1838	-0.1838	-0.1885	-0.1889
RMS error vs. VOD	0.0030	0.0057	0.0049	0.0004	
MAX error vs. VOD	0.0061	0.0099	0.0086	0.0010	
MSE error vs. VOD	0.0024	0.0056	0.0044	0.0003	

Table 3.1: Correlation energies in Hartrees for a fixed geometry using the PP orbitals. ^aWith the RI approximation in the 6-31G* basis (RIMP2-VDZ auxiliary basis). ^bOriginal formulation of TIP. ^cRe-Formulation of TIP. ^dIncludes SIP amplitudes.

and eliminating the overestimation of correlation effects.

3.3.2 Equilibrium Bond-Lengths and Correlation Energies

A valence correlation method such as TIP or more accurate valence active space methods such as VOD or ultimately CASSCF cannot yield quantitative values for energy differences due to neglect of dynamic correlation. However they should nonetheless be sufficiently balanced that they yield reasonable values for molecular properties such as equilibrium geometries. To this end, Table 3.4 shows a comparison of HF, PP, IP, IP+DIP, TIP and VOD against experimental bond length values [152] for 21 small molecules with 33 unique bond lengths. Every method used its own orbitals and analytical gradient to compute these bond lengths. It is noteworthy that all the pairing methods yield molecular structures that are substantially more accurate than HF: this validates the importance of defining all valence electrons as active. Species with lone pairs in the active space and halogens (such as: F₂, ClF, Cl₂, HOF, and HOCl) are troublesome for PP; typically PP over-estimates these bond lengths by at least 0.05 Å. PP also under-estimates the length of the ionic bond of NaF by 0.035 Å. The more non-local methods tend to work better for these species, with the fully non-local VOD model being best, as would be anticipated.

	TIP ^{a,b,d}	TIP ^{a,c}	CC-TIP	CC-3P ^d	VOD ^d
N ₂	-0.2210	-0.1561	-0.1760	-0.1772	-0.1772
F ₂	-0.2719	-0.2216	-0.2318	-0.2377	-0.2398
CO	-0.1893	-0.1513	-0.1594	-0.1620	-0.1620
CS	-0.1399	-0.1087	-0.1167	-0.1210	-0.1218
NP	-0.2109	-0.1434	-0.1575	-0.1618	-0.1621
P ₂	-0.1298	-0.0976	-0.1097	-0.1123	-0.1123
NaF	-0.1467	-0.1136	-0.1322	-0.1326	-0.1326
ClF	-0.1931	-0.1685	-0.1743	-0.1800	-0.1825
Cl ₂	-0.1214	-0.1111	-0.1200	-0.1204	-0.1213
HCN	-0.1933	-0.1547	-0.1621	-0.1685	-0.1685
HNC	-0.1648	-0.1356	-0.1410	-0.1476	-0.1476
HCP	-0.1576	-0.1175	-0.1335	-0.1350	-0.1353
HNO	-0.2385	-0.1848	-0.1910	-0.2037	-0.2047
HPO	-0.2034	-0.1530	-0.1629	-0.1747	-0.1759
HOF	-0.2569	-0.2176	-0.2146	-0.2314	-0.2337
HOCl	-0.1932	-0.1621	-0.1732	-0.1784	-0.1809
H ₂ CO	-0.2085	-0.1643	-0.1730	-0.1804	-0.1816
H ₂ CS	-0.1456	-0.1231	-0.1282	-0.1324	-0.1335
H ₂ O ₂	-0.2499	-0.2081	-0.2203	-0.2276	-0.2305
H ₂ S ₂	-0.1096	-0.1032	-0.1110	-0.1130	-0.1154
N ₂ H ₂	-0.2153	-0.1804	-0.1855	-0.1913	-0.1930
RMS error vs. VOD	0.0239	0.0165	0.0080	0.0015	
MAX error vs. VOD	0.0488	0.0229	0.0191	0.0029	
MSE error vs. VOD	-0.0192	0.0159	0.0070	0.0012	

Table 3.2: Correlation energies in Hartrees for a fixed geometry using the original formulation of TIP’s orbitals in the 6-31G* basis (RIMP2-VDZ auxiliary basis). ^aWith the RI approximation. ^bOriginal formulation of TIP. ^cRe-Formulation of TIP. ^dIncludes SIP amplitudes.

The most relevant comparison here between the GVB-CC approximations and VOD, which is essentially their parent theory. The effect of truncating the \hat{T}_2 operator is generally quite small, as one might hope for well-balanced local correlation methods. As the most complete of the local correlation methods, TIP yields the lowest RMS and max errors of the CC-GVB methods. The worst case is F₂. For H₂S₂, TIP exhibits very slight symmetry-breaking, giving inequivalent S-H bond-distances. We also note that multiple (wavefunction) solutions exist for some molecules using these methods: the lowest energy solutions are the ones shown in all cases.

3.3.3 Aromatic Hydrocarbons and Symmetry-Breaking

The next test for the improved TIP is whether the very good performance of its predecessor for reducing SB can be retained with the changes we have made. We briefly re-examine the same aromatic hydrocarbons, benzene, naphthalene, and phenalenyl cation and anion, that we examined previously, using the 6-31G* basis set and the RIMP2-VDZ auxiliary basis set in the an all-valence electron PP active space. The classic example of SB is the distortion of D_{6h} benzene along a D_{3h} coordinate. Figure 3.10 shows that TIP recovers a curve similar to that of VOD without the un-physical cusp at the D_{6h} geometry as predicted by PP and IP. Figure 3.11 reinforces this by showing that the re-formulation

	TIP ^{a,b,d}	TIP ^{a,c}	CC-TIP	CC-3P ^d	VOD ^d
N ₂	-0.2210	-0.1805	-0.1722	-0.1759	-0.1789
F ₂	-0.2719	-0.2424	-0.2342	-0.2354	-0.2420
CO	-0.1893	-0.1644	-0.1574	-0.1637	-0.1637
CS	-0.1399	-0.1213	-0.1176	-0.1240	-0.1240
NP	-0.2109	-0.1640	-0.1588	-0.1621	-0.1668
P ₂	-0.1298	-0.1122	-0.1101	-0.1126	-0.1129
NaF	-0.1467	-0.1332	-0.1323	-0.1331	-0.1333
ClF	-0.1931	-0.1814	-0.1731	-0.1828	-0.1852
Cl ₂	-0.1214	-0.1128	-0.0846*	-0.0878*	-0.1149
HCN	-0.1933	-0.1708	-0.1649	-0.1690	-0.1706
HNC	-0.1648	-0.1490	-0.1420	-0.1493	-0.1493
HCP	-0.1576	-0.1375	-0.1326	-0.1392	-0.1394
HNO	-0.2385	-0.2053	-0.2041	-0.2071	-0.2073
HPO	-0.2034	-0.1755	-0.1754	-0.1754	-0.1794
HOF	-0.2569	-0.2324	-0.2260	-0.2348	-0.2350
HOCl	-0.1932	-0.1784	-0.1599*	-0.1621*	-0.1826
H ₂ CO	-0.2085	-0.1826	-0.1775	-0.1845	-0.1847
H ₂ CS	-0.1456	-0.1336	-0.1175	-0.1243	-0.1278
H ₂ O ₂	-0.2499	-0.2282	-0.2258	-0.2278	-0.2321
H ₂ S ₂	-0.1096	-0.1043	-0.1119	-0.0991*	-0.1131
N ₂ H ₂	-0.2153	-0.1908	-0.1847	-0.1952	-0.1954
RMS error vs. VOD	0.0221	0.0033	0.0070	0.0027	
MAX error vs. VOD	0.0441	0.0088	0.0120	0.0065	
MSE error vs. VOD	-0.0197	0.0017	0.0064	0.0016	

Table 3.3: Correlation and orbital relaxation energies in Hartrees for a fixed geometry using each method’s own orbitals in the 6-31G* basis (RIMP2-VDZ auxiliary basis). ^aWith the RI approximation. ^bOriginal formulation of TIP. ^cRe-Formulation of TIP. ^dIncludes SIP amplitudes. *Converged to a different orbital solution, excluded from statistics.

actually *improves* the TIP predicted geometry for benzene. The bond lengths predicted by modified TIP show a factor of three less bond alternation than previously reported, only 0.0009 Å, and the average bond length is now only 0.0017 Å longer than that predicted by VOD, previously it was 0.0087 Å longer. The other cases studied in our previous work are re-examined in the Supplementary Material with generally similar conclusions. The reformulation of TIP yields comparable or reduced SB relative to the pilot version, with results that are typically more than an order of magnitude better than the PP and IP methods which suffer from artifacts as dramatic as false bond isomers for the individual resonance structure of naphthalene.

We next consider Li₂C₄H₄, C₄H₄²⁻, and N₂S₂ [153] which are all four membered aromatic rings that all contain 6π electrons like benzene. The different CC-GVB methods predicted geometries for Li₂C₄H₄ can be seen in Table 3.5. VOD predicts a bond length of 1.491 Å which is very close to the experimental value [154] of 1.495 Å. There is significant symmetry-breaking in PP (D_{2h} structure), and IP and IP+DIP (C_{2v} structure), and the electronic wavefunctions for these methods are doubly degenerate giving a cusp at the desired D_{4h} symmetry. The addition of the three pair correlations results in a large reduction in the SB observed. The bond alternation of around .036 Å as seen in IP is brought down

	bond	HF	PP	IP	IP+DIP	TIP	VOD	Expt. ^a
N ₂	rNN	1.066	1.090	1.097	1.098	1.110	1.099	1.098
F ₂	rFF	1.324	1.480	1.408	1.407	1.430	1.398	1.412
CO	rCO	1.102	1.118	1.126	1.127	1.127	1.128	1.128
CS	rCS	1.511	1.524	1.532	1.536	1.532	1.531	1.535
NP	rNP	1.446	1.485	1.492	1.493	1.491	1.491	1.491
P ₂	rPP	1.851	1.900	1.919	1.916	1.910	1.915	1.893
NaF	rNaF	1.908	1.919	1.928	1.928	1.928	1.929	1.926
ClF	rClF	1.587	1.659	1.634	1.637	1.619	1.625	1.628
Cl ₂	rClCl	1.974	2.032	2.019	2.054	2.006	2.032	1.988
HCN	rHC	1.057	1.071	1.073	1.073	1.077	1.077	1.065
	rCN	1.124	1.148	1.155	1.155	1.158	1.158	1.152
HNC	rHN	0.982	0.996	0.999	0.999	1.003	1.003	0.994
	rNC	1.144	1.160	1.168	1.170	1.171	1.171	1.169
HCP	rHC	1.062	1.078	1.081	1.081	1.084	1.085	1.069
	rCP	1.508	1.543	1.550	1.549	1.549	1.549	1.540
HNO	rHN	1.031	1.045	1.048	1.050	1.062	1.063	1.063
	rNO	1.165	1.210	1.210	1.212	1.204	1.207	1.212
HPO	rHP	1.441	1.457	1.458	1.459	1.466	1.476	-
	rPO	1.442	1.471	1.473	1.474	1.470	1.476	1.512
HOF	rHO	0.944	0.967	0.967	0.966	0.971	0.968	0.966
	rOF	1.359	1.466	1.423	1.426	1.442	1.418	1.442
HOCl	rHO	0.942	0.964	0.965	0.964	0.965	0.966	0.975
	rOCl	1.647	1.732	1.696	1.708	1.700	1.692	1.690
H ₂ CO	rCO	1.176	1.204	1.208	1.208	1.206	1.205	1.208
	rCH	1.094	1.105	1.106	1.107	1.114	1.117	1.116
H ₂ CS	rCS	1.589	1.622	1.627	1.625	1.619	1.617	1.611
	rCH	1.077	1.093	1.095	1.095	1.100	1.101	1.093
H ₂ O ₂	rHO	0.941	0.963	0.964	0.962	0.967	0.965	0.965
	rOO	1.383	1.482	1.446	1.451	1.459	1.442	1.452
H ₂ S ₂ ^b	rHS	1.327	1.348(50)	1.350(52)	1.348	1.338(40)	1.350	1.345
	rSS	2.052	2.090	2.095	2.105	2.081	2.058	2.058
N ₂ H ₂	rHN	1.012	1.029	1.032	1.033	1.037	1.038	1.028
	rNN	1.209	1.245	1.250	1.251	1.249	1.251	1.252
RMS error vs. Expt.		0.038	0.022	0.014	0.018	0.012	0.013	
Max. error vs. Expt.		0.088	0.068	0.039	0.066	0.042	0.044	
MSE error vs. Expt.		-0.032	0.005	0.002	0.004	0.003	0.002	
RMS error vs. VOD		0.037	0.022	0.009	0.012	0.010		
Max. error vs. VOD		0.074	0.082	0.037	0.047	0.032		
MSE error vs. VOD		-0.034	0.003	0.000	0.002	0.001		

Table 3.4: Predicted equilibrium geometries in the 6-311g(3df,2p) basis (cc-pVTZ RI auxiliary basis) as compared to experiment. ^aRef. [152], ^bSome structures asymmetric on the milliAngstrom scale, both bond lengths are listed.

to only .003 Å. TIP also deviates by only .005 Å from the VOD answer. We note that SB is associated with the Li atoms, and when they are removed so is the SB problem for all methods, as illustrated by the results in Table 3.6 for the dianion, C₄H₄²⁻. We note that TIP predicts almost exactly the VOD bond length, overshooting by only 0.001 Å. The Li atoms should be symmetrically oriented along the z-axis if the molecule lies in the xy plane, as seen in the cartesian coordinates of the Li atoms as predicted by HF and VOD. The GVB-CC models skew this orientation with IP and IP+DIP shifting the axis the Li's are aligned on closer to one of the corners of the ring. TIP substantially reduces this problem: it is again an order of magnitude better than the other CC-GVB methods, but is still not

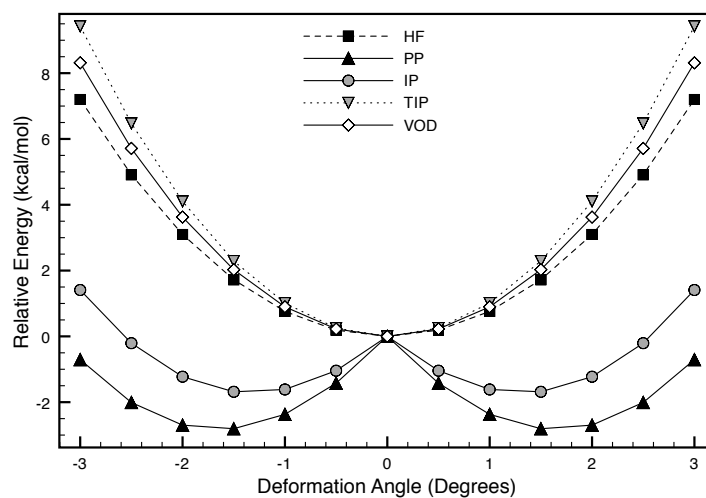
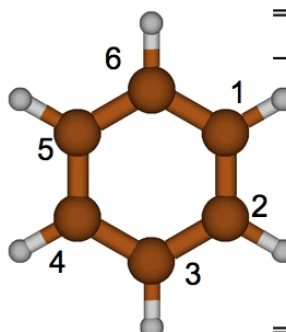


Figure 3.10: Potential energy curve for the distortion of benzene along a D_{3h} to D_{6h} coordinate axis. The PP and IP models exhibit SB, whereas the HF, TIP, and VOD methods do not. Absolute energies at the D_{6h} are: -230.702049 H for HF, -230.902841 H for PP, -231.014028 H for IP, -231.075839 H for TIP, and -231.089623 H for VOD.



	IP	TIP(a)	TIP(b)	VOD
C1-C2	1.3796	1.4194	1.4146	1.4123
C2-C3	1.4535	1.4218	1.4137	1.4123
C3-C4	1.3796	1.4218	1.4137	1.4123
C4-C5	1.4535	1.4194	1.4146	1.4123
C5-C6	1.3796	1.4218	1.4137	1.4123
C6-C1	1.4535	1.4218	1.4137	1.4123

Figure 3.11: A chart of the optimized bond lengths for benzene as solved by TIP with the 6-31G* basis set. The TIP (a) bond lengths are without any penalty function. The TIP (b) bond lengths are with the re-formulation and penalty function. All bond lengths are in Å.

completely cured of SB.

N_2S_2 is isoelectronic in the valence space to $C_4H_4^{2-}$. As seen in Table 3.7, VOD predicts a D_{4h} species with bond lengths 0.015 Å longer than experiment. This deviation from experiment is about what should be expected from VOD as can be seen in the VOD RMS

	HF	PP	IP	IP+DIP	TIP	VOD	Expt. ^a
C1-C2	1.461	1.483	1.468	1.469	1.488	1.491	1.495
C2-C3	1.461	1.455	1.468	1.469	1.485	1.491	1.495
C3-C4	1.461	1.483	1.504	1.504	1.488	1.491	1.495
C4-C1	1.461	1.455	1.504	1.504	1.485	1.491	1.495
Li Cart. Coords	HF	PP	IP	IP+DIP	TIP	VOD	
x_{Li_1}	0.000	0.000	0.030	0.030	-0.003	0.000	
y_{Li_1}	0.000	0.080	0.030	0.030	0.003	0.000	
z_{Li_1}	1.770	1.761	1.779	1.778	1.774	1.767	
x_{Li_2}	0.000	0.000	0.030	0.030	-0.003	0.000	
y_{Li_2}	0.000	-0.020	0.030	0.030	0.003	0.000	
z_{Li_2}	-1.770	-1.797	-1.779	-1.778	-1.774	-1.767	

Table 3.5: Predicted Structures for $\text{Li}_2\text{C}_4\text{H}_4$ in the 6-31G* basis. All bond lengths are in Å. ^aRef. [154]

	HF	PP	IP	IP+DIP	TIP	VOD
C-C	1.454	1.475	1.464	1.464	1.484	1.483

Table 3.6: Predicted C-C Bond Lengths in $\text{C}_4\text{H}_4^{2-}$ in the 6-31G* basis. All bond lengths are in Å.

error versus experiment in Table 3.4. HF underestimates the bond length, but surprisingly PP, IP, and IP+DIP approach very nearly the accuracy of VOD. IP+DIP is almost exactly VOD except for a slight shift towards D_{2h} symmetry. TIP keeps the same D_{2h} character of the IP+DIP solution while predicting an average bond length 0.008 Å longer than VOD’s. The pilot version of TIP exhibited nearly pathological behavior for this molecule – with multiple symmetry-broken solutions possible. The moderate errors observed for the penalty function TIP effectively removes these problems.

	HF	PP	IP	IP+DIP	TIP	VOD	Expt. ^a
N1-S1	1.614	1.663	1.666	1.669	1.674	1.669	1.651
S1-N2	1.614	1.663	1.666	1.671	1.680	1.669	1.657
N2-S2	1.614	1.663	1.666	1.669	1.674	1.669	1.651
S2-N2	1.614	1.663	1.666	1.671	1.680	1.669	1.657

Table 3.7: Predicted N-S Bond Lengths in N_2S_2 in the 6-31G* basis. All bond lengths are in Å. ^aRef. [155]

Borazine, $\text{B}_3\text{N}_3\text{H}_6$, is isoelectronic to benzene. Borazine, like N_2S_2 , has a resonance structure where the π electrons can localize as lone pairs on the nitrogen atoms along the ring. Table 3.8 shows the bond lengths for borazine as predicted the family of CC-GVB methods. All GVB-CC methods yield very good reproductions of the VOD structure. All of the CC-GVB methods reproduce the D_{3h} nature of the VOD solution with the internal bond angles alternating between around 117.28 and 122.72 degrees. The original version of TIP slightly over-estimates the B-N bond length and the bond angle alternation for

borazine. Fig. 3.12 compares the TIP occupied and correlating π benzene orbitals against those of borazine. In benzene, the π orbitals de-localize across the entire ring much like the VOD orbitals. For borazine, the electronic structure clearly shows donation from N to B, but the orbitals are essentially localized on the N sites. The other orbitals not shown for benzene and borazine strongly localized C-C σ , C-H σ , and carbon s orbitals. The penalty function version of TIP for benzene still produces a very desirable mix of local and de-localized orbitals, which leads to the large reduction in SB relative to the simpler CC-GVB methods.

	HF	PP	IP	IP+DIP	TIP ^a	TIP ^b	VOD
B-N	1.4265	1.4400	1.4462	1.4464	1.4513	1.4460	1.4465
\angle N-B-N	117.59	117.37	117.37	117.34	117.11	117.27	117.28
\angle B-N-B	122.41	122.63	122.63	122.66	122.88	122.73	122.72

Table 3.8: Predicted D_{3h} structures for $B_3N_3H_6$ in the 6-31G* basis. All bond lengths are in Å. ^aOriginal formulation of TIP. ^bRe-Formulation of TIP.

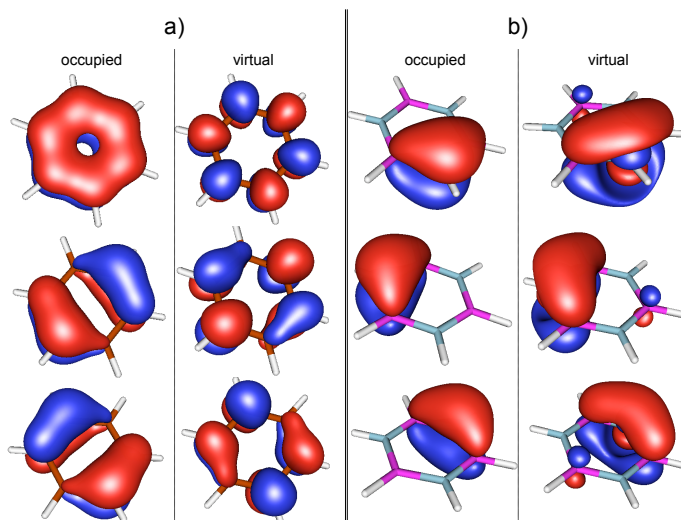


Figure 3.12: The TIP occupied and corresponding virtual orbitals for a) benzene and b) borazine.

3.3.4 Linear Polyenes

Another interesting set of molecules with complicated electronic structures are the linear polyenes. Hirao et al. [37] did a very informative study where they compared CASSCF results for the bond lengths of a series of trans linear polyenes against experimentally

observed [156–159] bond lengths. Using these CASSCF results as a benchmark, Table 3.9 compares the C-C bonds observed by TIP and VOD versus those presented by Hirao et al. Some discrepancies in the basis sets utilized are seen in the case of ethene, where the π active space is the one pair space where PP is exact. VOD and TIP are the same here, and agree almost perfectly with experiment. Butadiene is the case where the two pair model (full DIP) is exactly correct. TIP is the same as IP+DIP here, and we see that the lack of the SIP amplitudes has a big effect in these systems. VOD reproduces experiment almost exactly, but TIP has too much bond alternation owing to a higher degree of localization of the π bonds. In the larger polyenes, VOD clearly becomes an incomplete description of the true physical picture, but it mirrors the trends observed in CASSCF quite well. TIP recovers about 60% of these trends as observed by VOD. However TIP routinely overestimates the single bond lengths and under-estimates the double bond lengths, showing that there is a greater degree of localization in the model than VOD for these systems. Table 3.4 states that TIP is expected to exceed the experimental bond length on average by about 0.025 Å. This puts the TIP results into the same degree of agreement with experiment here as observed before. The problem with CASSCF is that it is computationally limited for most of these molecules to use only a π bonding active space that includes up to fourteen electrons. CASSCF can only be used to predict as far as C₁₄H₁₆. TIP is capable of running much larger systems, including C₄₀H₄₂ with the full valence active space! Diradicaloid character has been attributed to the behavior in these polyenes. TIP predicts a somewhat stagnant diradicaloid character of 7.9% for all the larger polyenes, with the note that each π bond has around 7% diradicaloid character. For decapentaene, the LUMO, LUMO+1, LUMO+2, LUMO+3 and LUMO+4 each have about the 7% diradicaloid character. This result is identical to the diradicaloid characters as predicted by VOD. The very promising results of TIP in this case strongly motivate a fuller study into this topic. An unrestricted TIP would be useful in computing the singlet-triple gaps and vertical excitations of these molecules. Since TIP can do chains with at least twenty π bonds in it, the question of how long must the chain be in order for all the interior bonds to assume the same length can be looked at.

3.3.5 Multiple Minima

Local valence correlation models (and nonlocal ones sometimes as well) have the problem that they tend to exhibit multiple orbital solutions that are local minima within the space of wave function variables. In practice, multiple solutions can often be found by changing the initial guess orbitals. This seems to be particularly true for molecules with many lone pairs, when using the perfect pairing active space. Figure 3.13 illustrates the issue for F₂ (with the 6-311g(3df,2p) basis) showing the difference between optimized TIP orbitals using canonical Hartree-Fock and the Pipek-Mezey [66] (PM) localized orbitals respectively as the initial guess. The TIP solution from the HF orbitals is 0.005 Hartrees lower in energy than that from the PM guess. Despite being higher in energy, the PM-derived lone pairs look

		C1-C2	C2-C3	C3-C4	C4-C5	C5-C6
Ethene	CASSCF ^a (Expt.) ^b	1.334 (1.339)				
Ethene	PP [IP]	1.338 [1.338]				
Ethene	TIP [VOD]	1.338 [1.338]				
Butadiene	CASSCF ^a (Expt.) ^c	1.335 (1.343)	1.463 (1.467)			
Butadiene	PP [IP]	1.339 [1.340]	1.481 [1.478]			
Butadiene	TIP [VOD]	1.340 [1.344]	1.478 [1.465]			
Hexatriene	CASSCF ^a (Expt.) ^c	1.338 (1.337)	1.469 (1.457)	1.345 (1.367)		
Hexatriene	PP [IP]	1.339 [1.340]	1.478 [1.475]	1.340 [1.342]		
Hexatriene	TIP [VOD]	1.341 [1.345]	1.474 [1.461]	1.342 [1.351]		
Octatetraene	CASSCF ^a (Expt.) ^d	1.345 (1.336)	1.457 (1.451)	1.351 (1.327)	1.451 (1.451)	
Octatetraene	PP [IP]	1.339 [1.340]	1.478 [1.475]	1.341 [1.342]	1.475 [1.472]	
Octatetraene	TIP [VOD]	1.341 [1.345]	1.473 [1.460]	1.343 [1.352]	1.470 [1.457]	
Decapentaene	CASSCF ^a	1.346	1.454	1.351	1.450	1.352
Decapentaene	PP [IP]	1.339 [1.340]	1.478 [1.475]	1.341 [1.342]	1.475 [1.471]	1.341 [1.343]
Decapentaene	TIP [VOD]	1.341 [1.345]	1.473 [1.460]	1.343 [1.352]	1.469 [1.456]	1.344 [1.353]
% Diradicaloid	Eth.	Buta.	Hexa.	Octa.	Deca.	
PP	9.1	7.7	7.8	7.8	7.7	
IP	9.1	7.9	7.9	7.9	7.9	
TIP	9.1	7.9	7.9	7.9	7.9	
VOD	9.1	7.9	7.9	7.9	7.9	

Table 3.9: Predicted Bond Lengths of the first five conjugated polyenes in the 6-31G* basis. All bond lengths are in Å. ^aRef. [37] ^bRef. [156,157] ^cRef. [158] ^dRef. [159]

more physical: they are fluorine *s* and *p* functions. There is accordingly some ambiguity as to which solution to prefer. We suggest that when a TIP or CC-GVB job is performed, the resulting orbitals should always be inspected, and if they do not appear physical, then it is desirable to also employ a smaller active space (for instance correlating only the bond orbitals) and compare results – both should be consistent. In the tables presented in this paper, to present a balanced comparison, we have always simply taken the lowest energy solutions for all methods.

3.4 Conclusions

Local correlation methods yield significantly increased efficiency by either truncating amplitudes based on spatial criteria, or using simple approximations such as perturbation theory (PT) to treat those amplitudes that are considered to be small. We apply both of these techniques to define an improved generalized valence bond (GVB)coupled cluster (CC) method for valence correlations. This approach, called 3-pair corrected imperfect pairing (TIP) was proposed recently to address the well-known symmetry-breaking problems of more approximate GVB-CC methods such as perfect pairing and imperfect pairing. SB often arises because correlation energy associated with geometries where electronic structure is delocalized (e.g. D_{6h} benzene) cannot be as effectively recovered by a

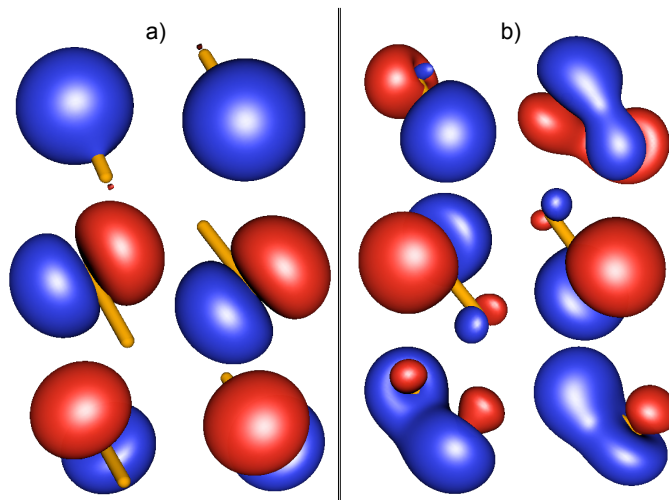


Figure 3.13: The TIP lone pair orbitals for F_2 computed with a) Pipek-Mezzey [66] localized orbitals for the guess and b) the canonical orbitals for the guess.

local correlation model as those geometries where electronic structure is localized (e.g. D_{3h} benzene). The addition of correlation amplitudes coupling 3 pairs can restore appropriate balance as illustrated in Fig. 3.11.

However, methods that combine PT for (numerous) weak amplitudes and CC for (a small number of) strong correlations are fraught with difficulty because the two methods give incompatible estimates for the energy-lowering associated with a given amplitude. Combined with orbital optimization, as we do in the TIP method, one can obtain very undesirable artifacts such as PT describing the strong correlations (when it overestimates them) and CC theory describing weaker amplitudes. We discuss how to address these difficulties by modifying the energy expressions for PT amplitudes with a penalty function that is zero for small amplitudes ($< t_c$, a critical value) but rises very strongly when this threshold is exceeded. Two other changes are made to the design of our pilot method, to treat one other class of amplitudes by CC theory (which can be done efficiently), and to entirely remove another class of amplitudes that couple two pairs which was previously treated by perturbation theory.

The resulting improved TIP method is tested on a range of problems, and when assessed alongside its GVB predecessors, TIP continually out-performs them in terms of correlation energy recovery, reduction of symmetry-breaking and quality of property-predictions. The

reduction of error for many properties compared its GVB predecessors and many of the other good features of TIP make it a very useful method for obtaining static local correlations for many types of molecular systems. It is now appears to be a superior replacement for the imperfect pairing method for chemical applications. Finally we believe that the penalty function approach to perturbation theory tested here may also be useful in other methods where it is desirable to ensure that amplitudes evaluated by perturbation theory should be small.

Chapter 4

The numerical condition of electron correlation theories when only active pairs of electrons are spin-unrestricted

4.1 Introduction

Many electron models often sidestep the complicated structure of separating electron pairs by allowing approximate wavefunctions to break spin symmetry. The spin-unrestricted wavefunction [160] has the strength that it matches the energy of non-interacting molecular fragments in the limit of dissociation. As a consequence, spin-unrestricted Hartree-Fock has become a standard reference for many sorts of correlated treatments including high-quality coupled-cluster (CC) methods [161]. When correlated models are used to optimize unrestricted orbitals [86] strong correlations between paired electrons are described redundantly, and the two competing descriptions can cause difficulties. Multiple solutions are one manifestation, and another which we have unfortunately encountered while developing orbital-optimized cluster models [81] is singular behavior of the amplitude equations.

Because of their great physical impact, the existence and character of solutions to the coupled cluster equations are of interest in themselves. Despite the non-linearity and high dimension of these equations much is now known about their solutions thanks to the efforts of several groups [162–169]. Our focus in this paper is much more quotidian, we simply explore why we were unable to combine valence-space CC with orbital optimization when only active pairs of electrons are spin-unrestricted. These unrestricted in active pairs (UAP) orbitals lead to the high spin ROHF wavefunctions for molecular fragments at dissociation. We find, to our surprise, that the CC equations are quite generally singular in the UAP

space.

Poor numerical condition of the CC amplitude equations at restricted dissociation is not new to any practitioner, but with unrestricted orbitals they are usually well-behaved. The UAP case is noteworthy for a few reasons: it is a general feature of combining unrestricted orbitals for dissociation with a correlation model in the unrestricted space, it is easy to find "false solutions", and we can offer a possible solution. The Jacobian and closely related stability matrix [170] of the CC equations will be examined for these purposes. The former has been examined before for the case of restricted linear [163] and multi-reference [165] cluster theories.

4.2 Results

In all that follows CC calculations were performed in the minimal Perfect Pairing active space formed by the geminal pairs relevant to a bond-dissociation process. The orbitals were unrestricted in the UAP sense, as is demonstrated in Figure 4.1. It is important to stress that our conclusions only hold for a cluster model in this UAP basis where all singly occupied spin-orbitals are spin parallel on a given fragment and all other orbitals are restricted. Our conclusions do not hold for the usual UHF orbitals because of the partial spin-polarization of inactive spectator pairs which would be restricted in the ROHF case.

Our analysis begins with a curious set of calculations on the N_2 molecule. Orbitals were prepared such that only the 6 active valence electrons were unrestricted and localized on each fragment so that a dissociation curve could be followed inwards from the correct asymptote at a separation of a few Ångströms. We attempted to apply CCD in the active space, and with simple amplitude iterations convergence was sluggish. Inspection of the amplitudes revealed that they were a scaled unit vector. Employing a standard DIIS [171] solver the correction vector was zeroed in a few iterations, but again the amplitudes appeared unphysical and the simple iteration residual was non-zero. The gradient obtained from these amplitudes took strange orbital optimization steps, and the same results were found independently in our two totally independent implementations of the theory, and so we proceeded to examine them further.

Many attempts were made to obtain a solution by continuation. At N-N separations of less than 1.7 \AA , $\langle \hat{S}^2 \rangle$ of the reference determinant is well below the spin-polarized limit (3) even for simple Hartree-Fock orbitals and the coupled cluster equations can be solved easily. This solution however cannot be followed to the dissociation limit. Even at the dissociation limit, one can easily solve the CC equations if a single term linear in the amplitudes is neglected. We attempted to continue this solution by introducing a simple continuous deformation parameter λ as the coefficient of the single linear term and solving the equations

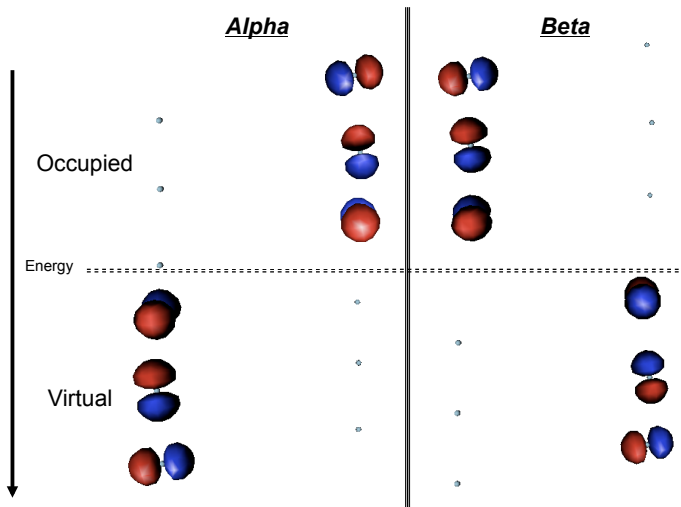


Figure 4.1: Unrestricted in active pairs orbitals at the dissociation limit for N_2 .

along the real axis between $\lambda = [0, 1]$, but were unsuccessful. Convergence stagnated, but no single element of the amplitude diverged. A similar situation has been observed in some other studies of singular CC equations [164]. The same attempts were made for several other dissociation problems (Ethene, H_2 , etc.) with the same results. Further analysis of homotopies [166–169] can completely characterize the solutions of non-linear equations should they exist, and can establish the precise identity of a non-linear singularity (pole, branch, pinch etc.), but any such distinction is of mathematical (not physical) concern, as was established in the pioneering work of others [162] (c.f. Section IV(d)). We will instead focus on firmly establishing the singularity of the Jacobian, the scope of the problem, developing a similar set of well-conditioned equations, and heuristic understanding of this situation.

The Jacobian characterizes the response of the coupled cluster equations to a linear perturbation:

$$\frac{\partial^2 \tilde{E}}{\partial T \partial \Lambda} = \frac{\partial \langle \Phi_{uv}^{\beta\gamma} | \{ \hat{H} e^T \}_c | \Phi_0 \rangle}{\partial t_{lm}^{\lambda\mu}}. \quad (4.1)$$

This matrix is the size of the amplitude vector squared; if one of its eigenvalues should become non-positive either the equations have no well-behaved solution, or solutions will meet at this point. In either of the previous cases the amplitude vector to which the Jacobian belongs should not be regarded as a good approximation to a physical ground state.

Furthermore one might say the "condition number" (the ratio of the Jacobian's smallest and largest eigenvalues) can be used to measure how rapidly the equations can be solved by iteration as it is a linear approximation to the amplitude iteration step. This non-Hermitian matrix has been derived and coded into programs many times [172–174] in the history of quantum chemistry. For the purposes of this paper we produced a computer-generated implementation, as have others [175,176]. The results of the automatic implementation are complemented by a separate program derived and coded by hand for the cases of our local cluster models with which all stability matrix calculations were performed. In all cases the Jacobian was explicitly constructed and diagonalized to avoid the art of guess construction.

Figure 4.2 depicts the lowest eigenvalue of the CC Jacobian for the case of ethene dissociation as obtained by explicit diagonalization. The orbitals were prepared as the dissociation limit UAP orbitals, then allowed to restrict as the fragments coalesce. Several sets of amplitudes were examined: the null guess (alternatively this can be considered the Linearized Coupled Cluster (LCC) Jacobian), the MP2 guess, the best amplitudes which can be reached by simple iteration (as seen in the figure), those produced by DIIS, and even amplitudes iterated from random noise, all to the same effect. The increase of the lowest eigenvalue around the unrestricted point on the inclusion of single excitations is noteworthy (shown here as a comparison of CCD versus CCSD for ethene in the (4,4) active space). Performing the same exercise for analogous dissociation problems produces the same results. By 5 Å the condition numbers of all of these dissociation processes are so large that convergence seems impossible with double precision arithmetic. Of the cases examined Mo₂ is the most stable, with a smallest Jacobian eigenvalue of roughly 0.0001 at 7 Å.

If the active space is expanded with the same orbitals so that not all the active orbitals are completely spin-polarized at dissociation, the equations become immediately well-behaved. The resulting Jacobian eigenvalues are strictly positive at any displacement. The reader is undoubtedly familiar with the reasonable condition of UCC calculations and so this should be evidence enough. Having converged these amplitudes for the case of ethene in the (12,12) active space at dissociation, they were projected on the minimal UAP (4,4) active space as a guess (the orbitals are unchanged between these two calculations; only the amplitude space is altered). The singularity remains whether one tries to converge from this guess or immediately diagonalizes the Jacobian. Based on these results and the previous observations we argue that the singularity can be understood with the linear part of the Jacobian which does not depend on the amplitudes. Inspection of the fragment orbitals provides another simple argument, all non-linear CCD terms depend on integrals of the sort $\langle ov||ov \rangle$ and for these fragment localized spin-orbitals (Figure 4.1) these are separated across space and vanishing.

The coupled cluster stability matrix contains information very similar to the Jacobian, but can be used to understand the convergence properties of the iterative process we rely

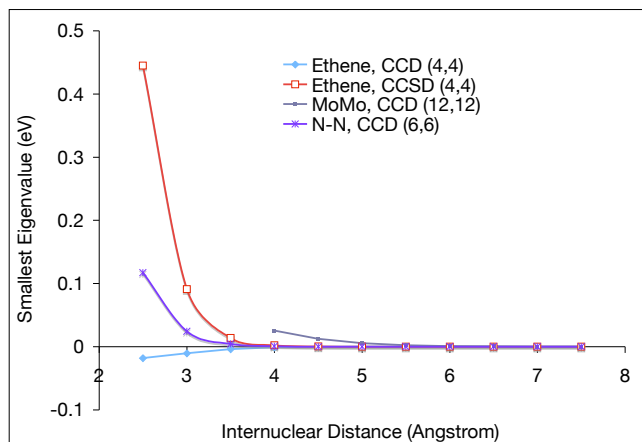


Figure 4.2: Smallest Jacobian eigenvalue for various fragment dissociations, in the 6-31G basis for all cases except Mo₂ which is in the CRENBS ECP [177].

upon to solve these equations. Surján [170] and coworkers recently published work examining this matrix for several solutions of the CC equations along dissociation curves. Their results showed that the CC equations may exhibit a diverse range of iterative behavior (convergence, chaos and divergence) if manipulated by a denominator shift, and that extrapolative methods like DIIS [171] can be misleading as they seem to converge on what appear to be stable fixed points. We reiterate the formulas for this matrix given CCD and the usual partitioning. One can see that it is essentially the Jacobian dressed by factors which reflect the conventional form we use to solve the CC equations.

$$J_{uv\beta\gamma,lm\lambda\mu}^{22} = \delta_{ul}\delta_{vm}\delta_{\beta\lambda}\delta_{\gamma\mu} - \frac{\partial\langle\Phi_{uv}^{\beta\gamma}|\{\hat{H}e^T\}_c|\Phi_0\rangle/\partial t_{lm}^{\lambda\mu}}{f_{\beta}^{\beta} + f_{\gamma}^{\gamma} - f_u^u - f_v^v} \quad (4.2)$$

The Lyapunov exponents are the central object of this analysis, which are the logarithm of the stability matrix's eigenvalues. If these should equal or exceed zero, the iterations are non-convergent. We turned to this tool because we wanted to understand what was occurring when simple iterations would stagnate at very small residual values. Figure 4.3 depicts the results for several small molecules obtained with a hybrid of our local CC methods: The Perfect Pairing ($\hat{T}_{PP} = \sum_{i\bar{i}} t_{i\bar{i}}^{i\bar{i}*} \hat{a}_{i*}^{\dagger} \hat{a}_{i*}^{\dagger} \hat{a}_i \hat{a}_i$) [56, 57, 86, 131], and Imperfect Pairing ($\hat{T}_{IP} = \hat{T}_{PP} + \sum_{i\neq j} t_{ij}^{i^*j^*} \hat{a}_{j*}^{\dagger} \hat{a}_{i*}^{\dagger} \hat{a}_j \hat{a}_i + t_{ij}^{j^*i^*} \hat{a}_{i*}^{\dagger} \hat{a}_{j*}^{\dagger} \hat{a}_j \hat{a}_i$) [78, 79, 82, 83] models. Note that even if the species is asymmetrical the same trend is observed.

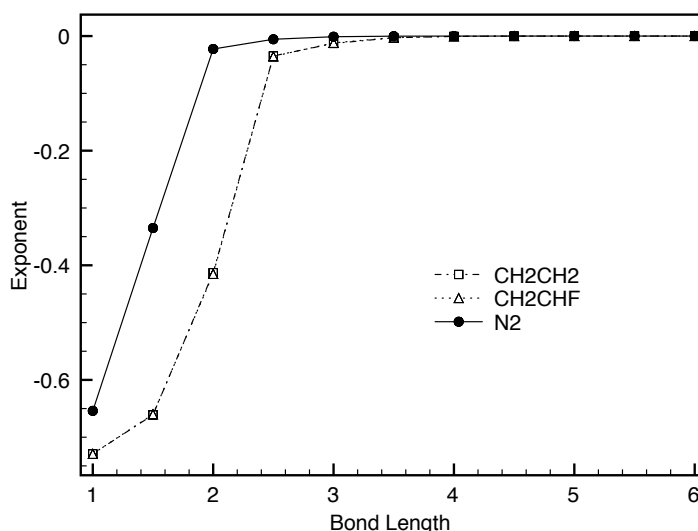


Figure 4.3: The largest Lyapunov exponent as a function of bond length for a stability analysis of PP and IP exchange type amplitudes for 3 molecules using the IP energy ansatz with the UAP PP orbitals in a minimal active space [(4,4) for C_2H_4 and C_2H_3F , (6,6) for N_2] with the 6-31G* basis.

These results firmly establish the singularity of the CC equations using the UAP orbitals at dissociation, but what meaning, if any, does this have for UCC as it is practiced when the UAP style spin polarization is almost never the case? Many situations could be imagined where this construction would be the case. One such situation is if the restricted core electrons are cut from the calculation by a pseudo-potential the results are essentially the same as those which would be obtained from the minimal active space. Another example is N_2 in a minimal basis where there are no virtual orbitals beyond those utilized in the (6,6) active space. Figure 4.2 depicts the CCD Jacobian's lowest eigenvalue for the dissociation of Mo_2 with the CRENBS basis and matching pseudo-potential.

4.3 Modified Equations Which are Well-Conditioned

Since the instability and ill-conditioning of the CC amplitude equations at the UAP dissociation limit has been established, we seek to restore solubility to these cluster models in this case. Here we will discuss a few possible solutions based on the idea of regularization [178, 179]. We will rate them based on a simple set of criteria: a) does it stabilize the CC amplitudes, b) is it simple to define and implement, c) how heavily does it affect the energetics of the molecular system at equilibrium, and d) will it allow us to optimize

orbitals with active space CC Lagrangian methods.

The first and simplest correction is to add a constant denominator shift. As shown by Surján et al. [170], this enables us to make the amplitude equations stable. However, it requires a constant shift of at least 12 kcal/mol to be able to optimize the orbitals along the entire ethene dissociation curve. This is a very strong penalty near equilibrium bond lengths where the amplitude equations are usually well-conditioned. We also took a non-linear equation solving approach and tried to identify the source of the singularity, eliminate it, solve the system when it is non-singular, and follow a homotopy back closely [180]. In the next section we attribute the singularity to the structure of the block of the linear coupling matrix containing the PP and the IP exchange type amplitudes. We can create a stable nonlinear system and solution by eliminating the off-diagonal matrix elements. The CC amplitude equations are easily solved in that diagonal representation, and the homotopy can be followed in very closely to the original problem. However the homotopy could only be followed in to a scaling parameter of at maximum around 80.0% for the IP level of correlation, and it is prohibitively expensive to follow the homotopy properly.

Another approach can be taken from our recent work [119]. A dynamic denominator shift reminiscent of amplitude regularization with a form reminiscent of a damping function, $-\gamma(e^{(t/t_c)^{2n}} - 1)$, can be constructed to affect the amplitudes similarly to a static denominator shift. The t_c critical amplitude parameter defines the largest desired value an amplitude can take before it becomes heavily regularized. The power $2n$ is designed to require the power of the argument to the exponent to be an even integer and the dynamic penalty function to be invariant of the phase of the amplitude. The coefficient γ is there to help scale the magnitude of the dynamic penalty when amplitudes are not small, but not as large as the critical amplitude parameter. Unlike the static denominator shift the dynamic penalty function approach is flexible enough to be very small before the unrestriction point on the dissociation PES where amplitudes are typically small, and large when amplitudes become large (typically on non-variational surfaces the amplitudes are greater than one). Of course to evaluate a gradient in the presence of such a penalty we must propagate this modification through the derivatives of the Lagrangian, so that it can be used to optimize orbitals and geometries.

A reasonable choice for the critical amplitude parameter, t_c , is one, since that prevents a complete inversion of the reference and the doubly excited states. The other parameters (γ and n) should be chosen to balance making the corrections small at equilibrium, with ensuring that orbitals can be optimized towards dissociation. A dynamic penalty function that we have found to work well by numerical experiment is $-8(e^{t^6} - 1) E_h$ in the amplitude equations with a corresponding penalty function of $-8(e^{t^6}(1 + 6t^6) - 1) E_h$ for the Lagrange multipliers. There is only a cost in correlation energy of $9.1 \mu E_h$ for ethene at its equilibrium geometry with the IP+DIP method, and a mean absolute error of $11.5 \mu E_h$ for

the full PP active space G2a and G2b sets [181, 182] done with 6-31G*. These parameter values are of course not unique: a choice of a γ of 2 and a power of 4 also works quite well with an energy cost around twice as large (both RMS and MAE) as the above parameters.

4.4 Heuristic Understanding of the Problem

There is a very simple argument for linear dependence in the basis composed of excitations from the UAP orbitals in the dissociation limit. The molecular fragments with the UAP orbitals are completely degenerate with respect to complete spin inversion. The divergent unphysical amplitudes connect these two solutions, and the energy changes along the path connecting these solutions are either negligible or zero. The resulting physical consequence is that a degenerate subspace of solutions has been created and a linear dependence arises when the amplitudes and spin polarization compete to describe the spin-unrestriction. One can also ask how this is manifest in the representation of the Hamiltonian in this basis explicitly, and this is much less straightforward. The results demonstrate that generally this singularity is present in the coupled cluster equations and strongly suggest that it lies in the linear part of the Jacobian. There is a possibility that both the linear and non-linear equations are singular but for different reasons. In this work we will assume that their conditions stem from the same problem.

The simplest possible case is the dissociation of a hydrogen molecule in the minimal STO-3G basis. There is only one unique amplitude in the wavefunction, and one unique orbital unrestricted parameter which reflects the rotation of the beta bonding MO into the beta anti-bonding MO. The coupled cluster equations for the amplitude have the simple form of a quadratic equation, whose coefficients can be constructed for any distance, R and any orbital rotation, θ , the surfaces representing these coefficients and their resulting amplitudes and energetics are plotted in Figure 4.4.

$$0 = A + B\hat{T} + C\hat{T}^2 \quad (4.3)$$

First notice on the plot of energy that variational determination of the orbitals would not unrestricted at any distance. The simple 1-amplitude CCD expansion can handle the open-shell singlet. Next focus on the line passing through 45° , both the constant and quadratic terms vanish, but the linear term doesn't, so one of the two roots diverges in this unrestricted limit, while the other goes to zero. We can dissect the linear term further and find that there is a single diagram responsible for the non-vanishing term with the usual algebraic form:

$$\sum_{kc} \langle ka || ic \rangle \hat{T}_{cb}^{kj} \Rightarrow B\hat{T}_2 \quad (4.4)$$

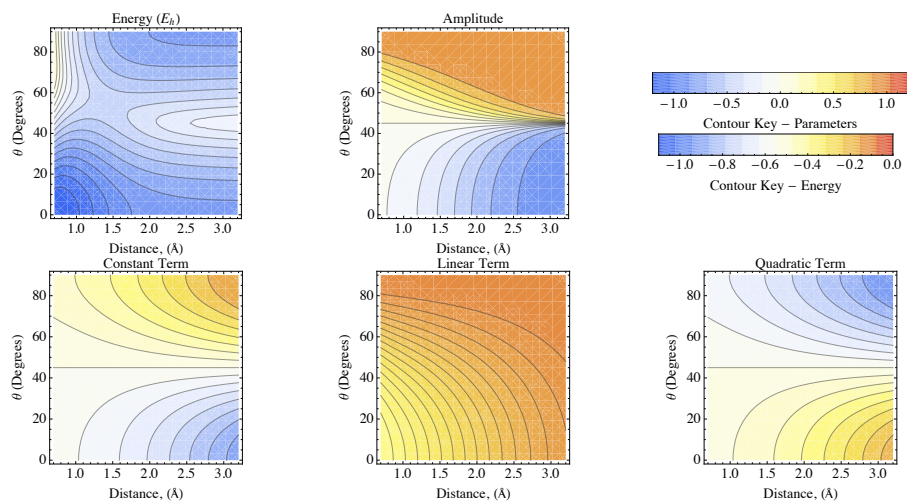


Figure 4.4: CCD parameters for H_2 in STO-3G basis, horizontal axis θ , vertical axis R (Å).

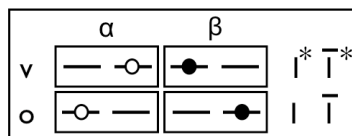


Figure 4.5: Orbital labeling for H_2 dissociation.

In the numbering of Figure 4.5 the 2-electron integral that appears in this term is $(11|\bar{1}^*\bar{1}^*)$. The Coulomb operator lies between orbitals lying on the same atom, and so it fails to decay as the bond is broken. If the description of the correlation is expanded to include singles, i.e. CCSD, the problem remains singular.

Considering a more general case, such as ethene dissociation, the CCD equations are now of much higher dimension, but we maintain that the essential features of this singularity are the same. The linear part of the equations is now multidimensional, and the coefficient of the linear term is a matrix which is precisely the well-known LCCD Jacobian [163]

(which is alternatively the CCD Jacobian for the null guess, also known as the matrix \hat{U} in the notation of some other papers [81]). For complete CCD the dimension is too large to permit direct inspection, but we can examine the truncated block of amplitudes (Table 4.1) spanned by a local model for physical insight, remembering that they exhibit the same behavior seen in the full active-space CC models examined in Section 4.2 and were the root of our interest in this problem. A figure labeling the relevant 1 particle functions is also included for clarity (Figure 4.6).

	$t_{1\bar{1}}^{1^*1^*}$	$t_{1\bar{2}}^{2^*1^*}$	$t_{2\bar{1}}^{1^*2^*}$	$t_{2\bar{2}}^{2^*2^*}$
$t_{1\bar{1}}^{1^*1^*}$	0.093	-0.047	-0.047	0.000
$t_{1\bar{2}}^{2^*1^*}$	-0.047	0.093	0.000	-0.047
$t_{2\bar{1}}^{1^*2^*}$	-0.047	0.000	0.093	-0.047
$t_{2\bar{2}}^{2^*2^*}$	0.000	-0.047	-0.047	0.093

Table 4.1: Linear coupling matrix for the PP and IP exchange amplitudes for ethene ($\text{H}_2\text{C}=\text{CH}_2$) at a C-C bond length of 7.50 Å with unrestricted PP orbitals in the minimal active space in the 6-31G* basis.

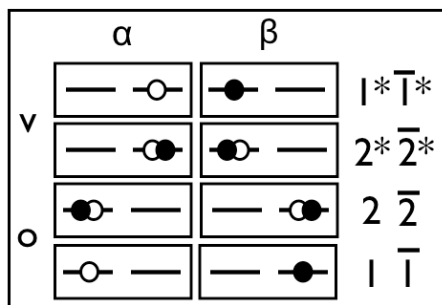


Figure 4.6: Orbital labeling for ethene dissociation.

Ironically, orbitals that lack any spin-symmetry impart a fragment symmetry onto this matrix which causes its determinant to vanish. The off-diagonal matrix elements are found to arise in the same diagram examined above and the troublesome ($oo||vv$) integral. It can also be shown algebraically that this block of the linear coupling matrix must have

this structure in general. Introducing asymmetry in to the molecules, i.e. fluorinated ethene or the molecule NP, does not alleviate this problem and the structure of the linear coupling matrix is identical with some slight asymmetry in the off-diagonal elements. In the appendix we provide further argument for the structure of this matrix for our local models (again because the number of amplitudes is manageable) and general formulas for the determinant given this structure for the interested reader.

4.5 Conclusions

Recently an interesting study was directed at the question, "Do broken-symmetry references contain more physics than the symmetry adapted ones?" [183]. In that case the concern was for RHF orbitals with broken spatial symmetries, and it was found that it was difficult for single-reference CC theories to correct the symmetry-broken wavefunction. In a similar vein, we have found that in the case of completely broken spin symmetry, the physics of spin correlation is removed from the cluster equations such that they are singular. This manifests itself in poor numerical condition of the cluster equations which prevents us from finding physical solutions and hampers orbital optimization. Ad-hoc manipulation of the Lagrangian using a dynamic penalty of the form $-\gamma(e^{(t/t_c)^{2n}} - 1)$ can render the equations soluble, even in this situation, and it seems that the remaining correlations are relatively unperturbed. Philosophically, our results suggest that CC based on UHF references succeeds (in the sense that most dissociation curves are reasonable even in the intermediate region) largely through the independence of strong spin correlations from the others. This bodes well for correlation models designed on the principle of dividing these problems. This ill-conditioning is striking at first sight, just as the poor values of $\langle \hat{S}^2 \rangle$ usually observed with spin-unrestricted orbitals are also striking. However the physical properties at dissociation with the UAP fragment orbitals are absolutely fine. Amplitude regularization breaks the degeneracy between amplitudes which are zero and those which are divergent, in favor of the former, which can then be readily obtained.

Chapter 5

Orbitals that are unrestricted in active pairs for GVB-CC methods

5.1 Introduction

Generalized Valence Bond (GVB) methods are active space electron correlation methods. The simplest model is GVB Perfect Pairing (PP) [56,57] which can correctly describe the making and breaking of isolated single bonds with spin-restricted orbitals since it allows one bonding and one anti-bonding orbital to describe each pair of electrons. The PP method can be extended within the framework of spin-coupled valence bond (SC-VB) theory, although due to computational expense which is higher than even Complete Active Space (CAS) methods for a given number of electrons, such calculations are not common. Recently a low-order polynomial-scaling approximation to SC-VB has been proposed [184], which appears very promising, but its strengths and weaknesses have not yet been fully characterized. It is also possible to view PP as a rough approximation to the Complete Active Space Self-Consistent Field (CASSCF) [50,51,53,54] treatment of all electron correlations in the valence space that includes one active orbital per valence electron.

The PP wave function has direct connections with the coupled cluster (CC) formalism [78,79,86]; PP is an approximation to active space CC with double excitations, where only 1 double excitation is retained per electron pair. The CC connection allows for the creation of new GVB-CC methods that are more accurate than PP (closer to CASSCF) but still computationally efficient. A variety of approaches have been explored including imperfect pairing (IP) [83], imperfect pairing with doubly ionic pairing amplitudes (IP+DIP) [119], and doubly ionic pairing [84]. These methods are subsets of the next logical stopping point, which is a cluster approximation that is exact for two pairs of electrons, fully extensive – this is perfect quadruples (PQ) model [85], which neglects all correlations that couple more than two different electron pairs. Inclusion of pair correlations that

couple three electron pairs as an augmentation to IP+DIP has also been explored by us, and shown to be crucial in the reduction of symmetry-breaking in molecules with multiple resonance structures [118, 119]. The resolution of the identity (RI) [61–63] approximation can also be used with the GVB-CC methods [131] without any significant loss of accuracy to further reduce the computational cost.

The focus of this paper is the form of optimized orbitals to employ in GVB-CC methods. As for CASSCF, the orbitals should be optimized to minimize the energy. Should the orbitals be spin-restricted or spin-unrestricted? If there is no truncation of correlations in the active space correlation method, then restricted orbitals can be employed to ensure a spin-eigenstate is obtained. If the correlation treatment is approximate, as in GVB-CC methods, then spin-unrestricted orbitals may be essential in order to obtain correct dissociation products, although this will introduce spin-contamination. For instance PP cannot separate multiple bonds correctly with restricted orbitals. For this reason, Unrestricted PP (UPP) has been implemented [86], with some promising results such as molecular properties for open shell systems that are significantly improved over Hartree-Fock theory. Additionally the valence orbital optimized CC doubles (VOO-CCD, or simply VOD) method has been implemented with unrestricted orbitals [81].

However, some serious problems have also been identified as a consequence of allowing orbitals to freely spin-unrestrict within an active space description of the electron correlation [87]. The most undesirable artifact that is associated with spin-unrestriction in active spaces is the rotation of pairs out of the active space as they dissociate in favor of orbitals that still produce some correlation energy. For example, the dissociation of methane to methyl and H leads to a valence active space that consists of 4 bond pairs at equilibrium, but 3 bond pairs, and the 1s core pair at separation [87]. This means the resulting energies will not be properly size-consistent: dissociated methyl and H with 4 pairs has lower energy than the energy of separate calculations on methyl with 3 active pairs, and H atom. In other cases, the character of the active space may change suddenly along a reaction coordinate, leading to discontinuous potential energy surfaces. These problems apply equally to unrestricted orbitals from active space methods more sophisticated than PP, such as VOD [81].

With intent to both remedy the artifacts found with freely spin-unrestricting PP and to make the approach workable with higher order GVB-CC methods (IP, IP+DIP, 2P, etc.), we will introduce in this paper a new model for spin-polarization in GVB-CC methods that we term unrestricted in active pairs (UAP). The UAP orbitals are defined so that two spatial orbitals span the space describing each active orbital pair (i.e. one bonding and one anti-bonding level) just as for restricted orbitals, and, subject to this constraint, the two alpha orbitals can differ from the two beta orbitals. This strongly limits the extent to which spin polarization is possible. Thus when dissociating molecules into fragments such

that all active pairs separate, the UAP procedure will directly yield fragment orbitals and energies which are high spin restricted open shell Hartree-Fock.

The UAP approach very strongly limits the spin polarization that is possible in GVB-CC methods relative to the unconstrained approach suggested originally. However, there is a close relation between the spin polarization allowed in UAP, and unrestricted orbitals at the HF level, which is revealed by comparing the UAP construction with the so-called corresponding HF orbitals [185]. The coupled cluster valence bond (CC-VB) approach [184] also yields orbitals that are non-orthogonal within a pair, while being strongly orthogonal between pairs, though in this case the wave function is spin-pure.

The outline of the remainder of this paper is as follows. In Sec. 2, the UAP approach is developed, and a practical implementation of the UAP orbitals is described for GVB-CC models including PP itself as well as extensions to include interpair correlations. The connection to the corresponding orbitals of UHF theory is discussed. In Sec. 3 we compare UAP calculations with unconstrained unrestricted calculations on a variety of sample cases to assess the extent of improvement. Finally, in Sec. 4 we will present our conclusions.

5.2 Theory

5.2.1 Unrestricted in Active Pairs (UAP) orbitals

The UAP method begins with a set of restricted molecular orbital (MO) coefficients, \mathbf{C} . They must be optimized with respect to all rotation angles that mix orbitals in the 4 spaces (core, active occupied, active virtual, and virtual). They must also be optimized with respect to mixings of the active occupied orbitals amongst themselves and the active virtual orbitals amongst themselves, since one of each is used to describe each electron pair. Collectively, these mixings define the orbital rotation, θ , degrees of freedom. They are typically solved for as successive unitary orbital rotations [30, 82, 186] in the GVB-CC methods, such that the i^{th} orbital update is $\mathbf{C}_{i+1} = \mathbf{C}_i \mathbf{e}^{\theta_i}$, where a full set of $N(N-1)/2$ rotations (i.e. both non-redundant and redundant rotations) are used for θ on each iteration.

In truncated GVB-CC theory (e.g. breaking a double bond with methods such as PP or IP) the use of restricted orbitals causes the energy to behave non-variationally towards dissociation. We seek to avoid this problem by permitting the orbitals to spin-polarize so that α and β orbitals are different. This is done by making both the α and β molecular orbitals a unitary transformation of the restricted reference orbitals, \mathbf{C} ,

$$\mathbf{C}^\alpha = \mathbf{C}\mathbf{U} \quad (5.1)$$

$$\mathbf{C}^\beta = \mathbf{C}\mathbf{U}^\dagger. \quad (5.2)$$

In previous work [81, 86], the spin polarization transformation, \mathbf{U} , was optimized as generally as possible. In the UAP approach, instead the spin-polarization transformation is defined on a pair by pair basis via a 2x2 Givens rotation matrix that mixes only the two orbitals describing each geminal pair: the bonding orbital, i , and the corresponding correlating orbital, i^* . This will prevent the artifacts that have been reported previously [87] from occurring. Additionally, inactive occupied orbitals, inactive virtual orbitals, and any half-occupied orbitals are constrained to remain restricted. The unitary transformation matrix, \mathbf{U} , is therefore a tensor product of 2x2 Givens rotation matrices that only interact within the pair, \mathbf{G}_i ,

$$\mathbf{U} = \prod_{i=1}^{\text{Npairs}} \mathbf{G}_i. \quad (5.3)$$

For example, a 2-pair case will be composed of two Givens matrices for the pairs and the identity elsewhere:

$$\begin{bmatrix} 1 & & & & & & \\ & \cos\phi_i & & & & & \\ & & \cos\phi_j & & & & \\ & & & 1 & & & \\ & & & & -\sin\phi_j & & \\ & -\sin\phi_i & & & \cos\phi_j & & \\ & & & & & \cos\phi_i & \\ & & & & & & 1 \end{bmatrix},$$

and more specifically these equations emerge for the UAP MOs:

$$C_{\mu i}^\alpha = C_{\mu i} U_{ii} + C_{\mu i^*} U_{i^* i} \quad (5.4)$$

$$C_{\mu i^*}^\alpha = C_{\mu i} U_{ii^*} + C_{\mu i^*} U_{i^* i^*} \quad (5.5)$$

$$C_{\mu i}^\beta = C_{\mu i} U_{ii} + C_{\mu i^*} U_{ii^*} \quad (5.6)$$

$$C_{\mu i^*}^\beta = C_{\mu i} U_{i^* i} + C_{\mu i^*} U_{i^* i^*}. \quad (5.7)$$

With the UAP definition of spin polarization, there is a single unrestriction angle, ϕ , for each pair, which permits dissociating bond orbitals to spin-unrestrict along reaction coordinates, without solving for excessive numbers of degrees of freedom (in principle there could be $N(N-1)/2$ variables associated with U). The UAP model has a resemblance to

the corresponding orbitals of self-consistent field theory [185]. The corresponding orbitals are those which diagonalize the overlap matrix between α and β molecular orbitals, while retaining orthonormality amongst themselves. The result is that a given α orbital has non-zero overlap with only one β orbital. These two orbitals will then span a subspace that is 2-dimensional if there is spin polarization (α β overlap of less than 1). The UAP orbitals have exactly the same property.

5.2.2 Algorithm

In the current implementation of UPP and related GVB-CC methods [82] in Q-Chem [142] spin-polarized orbital optimization is performed by independently varying all $2N(N-1)$ orbital rotation degrees of freedom with the Geometric Direct Minimization (GDM) procedure [30, 82]. For the UAP model, we choose to optimize the restricted orbital variables, θ , and the spin-polarization degrees of freedom, ϕ , together with GDM as $N(N-1) + N_{\text{pairs}}$ degrees of freedom. The $N(N-1)$ θ degrees of freedom are treated just as in the existing restricted GVB-CC implementations. The additional N_{pairs} ϕ degrees of freedom associated with UAP are treated as a series of 2x2 rotations. It is also possible to converge θ and ϕ disjointly, and this appears potentially very promising for some implementations (such as using only exact integrals). However, for our implementation (exact integrals for mean field, and resolution of the identity for electron correlation), it is most economical to employ combined optimization with GDM to minimize the total number of iterations.

The main computational steps in a GVB-CC calculation are MO basis integral transformations and forming an MO derivative, $\frac{\partial E}{\partial C_{\mu}^p}$, on each orbital iteration. Both steps involve the half transformed Coulomb and exchange integral quantities $J_{\mu\nu}^{[ii]}$ and $K_{\mu\nu}^{[ii]}$, where the untransformed indexes μ and ν are in the AO basis. In a spin-restricted calculation this step scales with the fourth power of molecule size and requires $6N_{\text{pairs}}N^2$ (3J and 3K) total space. For implementation of spin-polarization in GVB-CC without constraints, $16N_{\text{pairs}}N^2$ of these half-transformed quantities are needed, which requires fourth order computational effort on each ϕ and θ iteration.

By contrast, to implement spin polarization via the UAP model, the three-quarters transformed quantities, $J_{\mu p}^{[ii]}$ and $K_{\mu p}^{[ii]}$, (the new index, p runs over all core occupied and active MO's) can be formed and written to disk in the reference restricted basis. This requires only $7N_{\text{pairs}}NN_p$ (3J and 4K) space on disk, which is more than a 2-fold reduction. The target spin-unrestricted quantities and final transformations can be performed on the fly with only quadratic memory and third order computational effort. For instance to create an active space integral, $(\bar{i}\bar{i}|\mu\bar{p}^*)$, two simple steps are needed:

$$(\bar{i}\bar{i}|\mu p) = U_{ii}U_{ii}(ii|\mu p) + U_{ii^*}U_{ii^*}(i^*i^*|\mu p)$$

$$+ U_{ii^*}U_{ii}(i^*i|\mu p) + U_{ii}U_{ii^*}(ii^*|\mu p), \quad (5.8)$$

$$(\bar{i}\bar{i}|\mu\bar{p}^*) = U_{p^*p}(\bar{i}\bar{i}|\mu p) + U_{p^*p^*}(\bar{i}\bar{i}|\mu p^*). \quad (5.9)$$

The restricted open-shell integrals need to be updated every time a step in θ is made. That is the only expensive step in our new process, as the number of θ iterations in an UAP calculation is comparable with that of a restricted calculation. When compared side by side, this three-quarters transformation algorithm rivals our restricted algorithm on a per step basis as will be shown later in the Results section.

To obtain the solution in practice it is recommended to start a computation at a point with strongly spin-polarized unrestricing pairs (i.e a broken bond at dissociation or by just looking at the primary bonding orbitals for a radical). The spin-polarization gives the unrestriction angle gradient for the other pairs the appropriate direction. The corresponding orbitals guess [185] is constructed by forming the α and β overlap matrix, $S_{\alpha\beta}$, for the occupied space and then diagonalizing it to obtain the unrestriction angles. From here the orbitals are localized and the procedure of Sano [68] is used to form the guess for the active virtual space. It is also useful to pre-converge the θ degrees of freedom as typically there is enough of a difference between the desired restricted reference orbitals and those produced by a spin-unrestricted Hartree-Fock calculation to be noticeable. This is done in our algorithm by taking a few PP iterations in θ at the fixed guess values of the unrestriction angles. This approach is particularly helpful when running UAP-2P calculations.

5.2.3 Amplitude Regularization

Perhaps the simplest possible model problem is H_2 in the STO-3G basis. The two restricted orbitals are determined by symmetry as σ and σ^* , so there are no rotation angles to optimize, and it has only one unrestriction angle, ϕ , and one PP amplitude. If we optimize the amplitude for each value of ϕ , we obtain the results shown in Figure 5.1, where each curve corresponds to a different bond-length. The equilibrium geometry curve shows that spin-polarization is energetically unfavorable, as we should expect. What may not be expected is that as the angle is varied from 0° to 90° , representing the change from standard orbital configuration to a complete inversion of the occupied and virtual orbitals, the potential surface exhibits cusps and takes the form of periodically repeated parabolas. The cusps arise from the PP amplitude becoming too large (>1) to be reliably described by the non-variational CC method past $\phi = 45^\circ$.

We have also shown recently [120] that the iterator for the non-PP GVB-CC methods does not produce stable amplitude solutions [170] at dissociation without amplitude regularization. The unrestricted CC equations are effectively singular, and this problem must be remedied by adding an additional term to the equations which regularizes the solutions [120]. For all subsequent calculations in this paper, we use a modification of our

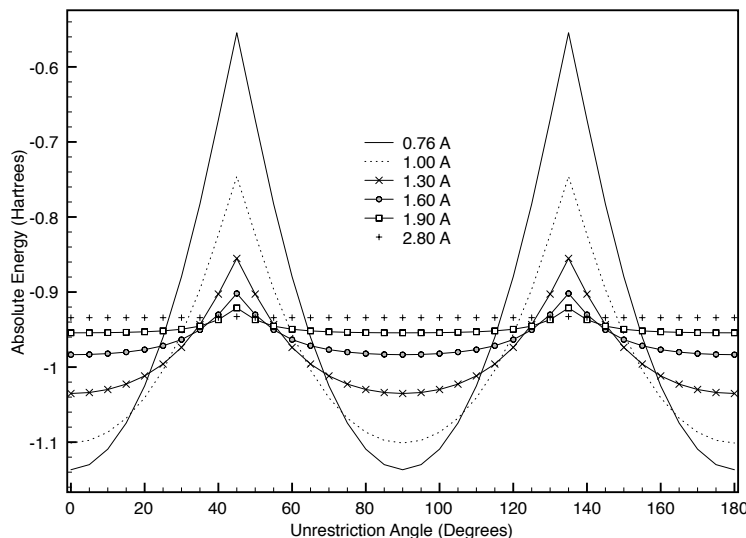


Figure 5.1: The unrestriction angle PES for (2,2) H_2 using PP (choosing most energy lowering amplitudes) with the STO-3G basis.

original penalty function that is even smaller in magnitude but still effective. A PP amplitude, $t_{ii}^{i^* \bar{i}^*}$, always bear a penalty of the form $-0.01(\exp(t_{ii}^{i^* \bar{i}^* 6}) - 1)/(e^1 - 1)$ Eh which has a maximum value of -0.01 Eh. The imperfect pairing [83] exchange amplitudes, $t_{ij}^{j^* \bar{i}^*}$, also need to be penalized if they are present in the correlation model [120]. They are penalized by the values of the PP amplitudes they are directly connected to:

$$-0.05(\exp((2t_{ii}^{i^* \bar{i}^*})^6) - 1)/(e^1 - 1)\text{Eh} + -0.05(\exp((2t_{ij}^{j^* \bar{i}^*})^6) - 1)/(e^1 - 1)\text{Eh} \quad (5.10)$$

with each term being restricted to a maximum value of -0.05 Eh.

While the precise form of the penalty function is not unique, it has the important property that its effect on GVB-CC energies is very small, both for weakly and not so weakly correlated systems. For example, for the absolute energies of the molecules in the G2a and G2b data sets [181, 182], using the 6-31G* basis, the penalty functions give a mean absolute error of $0.35 \mu\text{Eh}$ and a root-mean square error of $4.07 \mu\text{Eh}$. The largest outlier in this set is O_3 , which has an error of $49.5 \mu\text{Eh}$. By removing this piece of data, the RMS error reduces to $.03 \mu\text{Eh}$. For the two pair (2P) model [84], the mean absolute error is $.04 \mu\text{Eh}$ and the RMS error is $.10 \mu\text{Eh}$ for the G2a and G2b sets done with 6-31G*. This choice of penalty function works well in the usual domain of ϕ where the angles and amplitudes can be well guessed and solved for easily.

5.3 Results

5.3.1 Performance and Timings

After the presentation of our improved algorithm for the GVB-CC methods utilizing the UAP model, it is necessary to demonstrate its computational efficiency and its overall predictive performance. First, we will examine the computational efficiency of the UAP approximation as the algorithm is significantly changed compared to previous implementations of GVB-CC in Q-Chem [142]. Table 5.1 shows the performance of UAP-PP compared to both restricted PP and freely unrestricing PP (UPP) for polyenyl radicals of three different lengths in the 6-31G* basis set using the geometries listed in Table 5.4 as the alternating guess, "a", geometries. For the following timings we utilize the exact integrals with a cut-off threshold of 10^{-14} . Our implementation includes both exact and RI [61–63] integrals. The previous GVB-CC implementations utilized the RI integrals for the mean-field contributions to the orbital rotation gradient, whereas the UAP implementation formulates those contributions with exact integrals. using the exact integrals to form the mean-field contributions to the orbital rotation gradient means slower iterations, but the orbital rotation gradient is numerically correct which is important for difficult to converge systems.

	Method	Initial Guess (s)	Time per Iter. (s)	Num. of Iter.
Allyl	Free Unrest.	2.34	5.27	24
Allyl	UAP	1.17	2.95	22
Pentadienyl	Free Unrest.	14.73	38.73	36
Pentadienyl	UAP	7.23	21.23	54
Heptatrienyl	Free Unrest.	50.77	145.11	40
Heptatrienyl	UAP	25.03	77.05	47

Table 5.1: A timing comparison of both spin-unrestricted implementations of PP for various sized radicals. All calculations are performed in the 6-31G* basis using exact (analytical) integrals with a convergence criterion of 10^{-5} for the orbitals and an integral threshold of 10^{-14} . The timings were done on an Apple Mac Pro with 3 GHz Quad-Core Intel Xeon processors.

In comparing per-iteration timings for UAP to free spin-polarization in Table 5.1, it is clear that the ability to exploit the reduction in the number of degrees of freedom in the UAP integral transformation algorithm is very advantageous. Each iteration of UAP only takes about 50 to 60 percent of the time of an iteration of freely unrestricted PP takes with this percentage diminishing towards a limit as system size increases. In essence UAP-PP timings per iteration are very close to restricted PP timings, as a result of the implementation strategy developed in the previous section. There is a similar nearly 2-fold reduction in UAP versus freely unrestricing calculations in the amount of time needed for the initial guess. The UAP initial guess timings are nearly comparable with restricted timings, as the additional work needed to do the diagonalization of $S_{\alpha\beta}$ in the initial guess for UAP is

relatively small.

Both types of calculations take roughly similar numbers of iterations. Perhaps surprisingly the freely unrestricting UPP calculations take slightly fewer iterations than UAP-PP. This is not because UPP is an easier optimization problem than UAP-PP (in fact, the opposite is generally true). Instead it is because a more approximate diagonal hessian is used for the UAP methods. Only components coming from the 1-particle density matrix terms are used, whereas the existing RPP and UPP implementations utilize both 1 and 2-particle density matrix contributions to the hessian. The diagonal hessian becomes quite complicated to compute for all the GVB-CC methods if all the 2-particle density matrix components are included, and therefore we have not done so at this time.

5.3.2 Minimal Active Space Homolytic Bond Dissociation

Figure 5.2 shows the potential energy surfaces for pulling apart the carbon-carbon double bond in ethene in the minimal (4,4) active space, which leads to triplet methylene fragments at dissociation. As PP cannot correctly break two interacting bonds simultaneously, spin-polarization is essential, leading to a lowest energy asymptotic solution with two spins of one type on one fragment, and those of the other on the opposite fragment. The zero of Fig. 5.2 has been set to just that limit of two triplet methylene fragments. It is evident that UAP-PP smoothly dissociates to this limit. By contrast, freely unrestricting PP (UPP) goes to a different asymptote about 25 kcal/mol lower in energy than the correct dissociation limit. If the orbitals are examined as in Figure 5.3, we can see that this lower asymptote spuriously includes the correlation energy of one C-H bond in ethene. Around 2.0 Å the UPP solution begins to rotate out the C-C fragment orbitals that are not yielding enough correlation energy in favor of the C-H σ bonding orbitals which lower the overall correlation energy. By contrast, the UAP orbitals as seen in Figure 5.3, cleanly dissociate to the desired fragments. The uncontrollable switching of active space orbitals with UPP (or other truncated active space methods with unconstrained unrestricted orbitals) shows that the freely spin-unrestricting approach is not size-consistent. By contrast the UAP approach is perfectly size-consistent.

Just how smooth is the UAP-PP potential energy surface? This question can be answered numerically by examining the derivatives on both sides of the geometry (about 2.0 Å) at which spin-polarization occurs point need to be examined to verify the smoothness of the UAP potential surface. The force on the C atoms as a function of geometry is plotted in Figure 5.4. It is evident that the force is continuous but changes slope at the geometry where spin-polarization first occurs. In other words, at the point where spin-polarization first occurs, the second derivative of the energy exhibits a discontinuity. This is exactly the same as spin-polarization in the Hartree-Fock and Kohn-Sham density functional theory (at least with present day approximations), as has been recently discussed [187], and

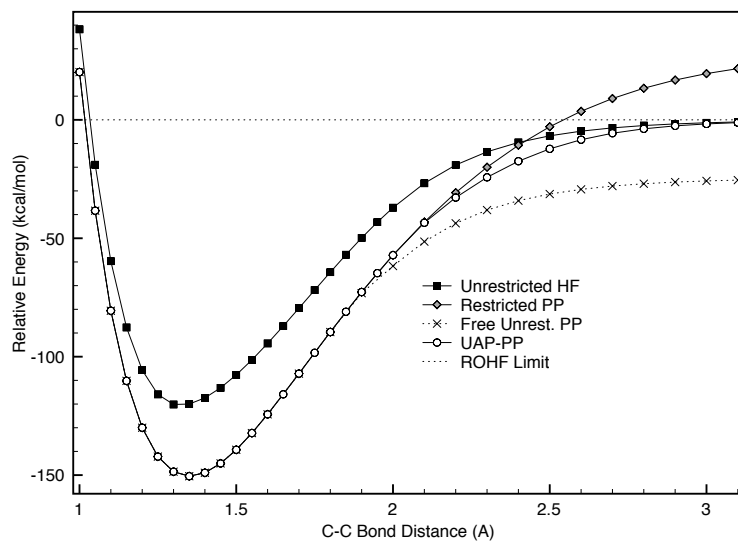


Figure 5.2: The C-C dissociation PES for ethene in the (4,4) active space in the 6-31G* basis.

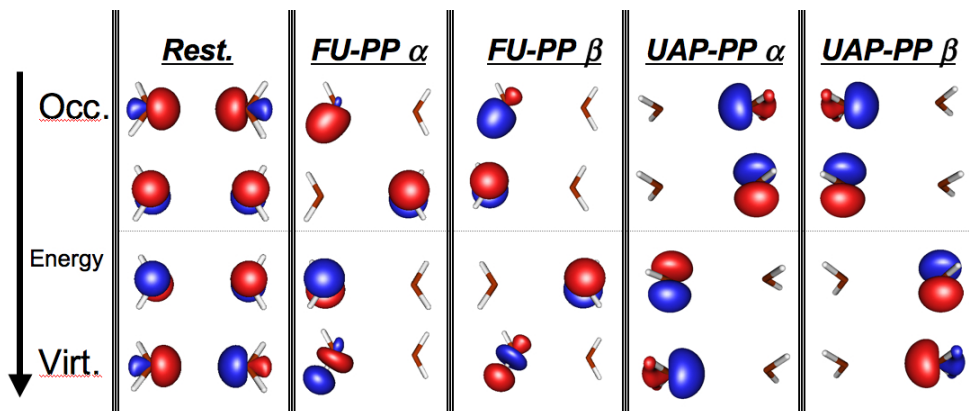


Figure 5.3: The orbitals at 3.5 Å C-C separation in ethene using restricted, freely unrestricting, and UAP PP.

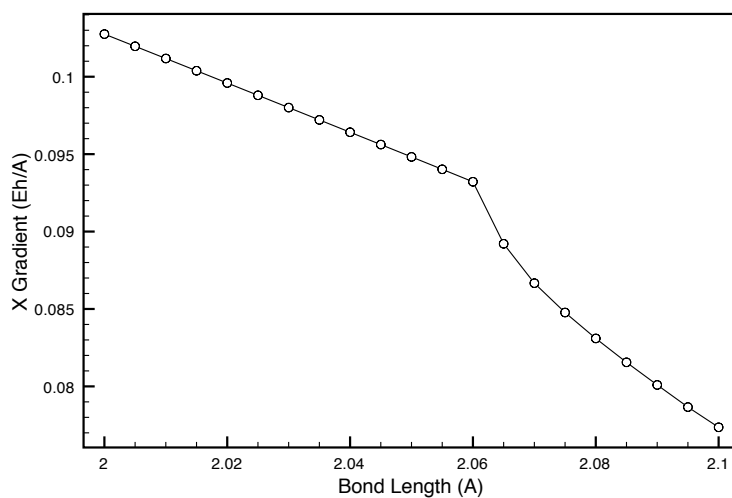


Figure 5.4: The absolute value of the nuclear gradient along the C-C bonding axis for ethene in the (4,4) active space in the 6-31G* basis.

occurs for the same reason (the derivative of the spin-polarization variables, ϕ , exhibits a discontinuity when spin-polarization occurs).

In Figure 5.5 a series of dissociation curves for N_2 in the (6,6) active space can be seen. The zero limit of this curve represents the ROHF dissociation limit of two quartet nitrogen atoms, and once again UAP-PP approach cleanly dissociates to this limit whereas the free spin-unrestriction does not. The freely spin-unrestricting approach once again reorganizes the active space to lower the correlation energy at dissociation. As is evident in the potential energy surface, not only does this yield an incorrect asymptote (again a size-consistency violation), but there are multiple changes in active space character on the path to dissociation which leaves the UPP PES visibly discontinuous at the level of first derivatives. Not only is this unsatisfactory for chemical applications, it also leads to considerable difficulties in converging the orbital optimization across the PES. By and large, all of these difficulties are resolved with the UAP approach. The UAP orbitals change character from molecular to atomic gradually and smoothly, and are prevented by the constraints from involving spectator orbitals. UAP-PP yields a smooth potential energy surface with a greatly reduced hump around 2.0 Å.

5.3.3 Full Active Space Bond Dissociation in Methane

We will re-examine the model system studied by Beran et al. [87]; a single hydrogen abstraction from methane in the full (8,8) PP active space. In ethene, a carbon-hydrogen

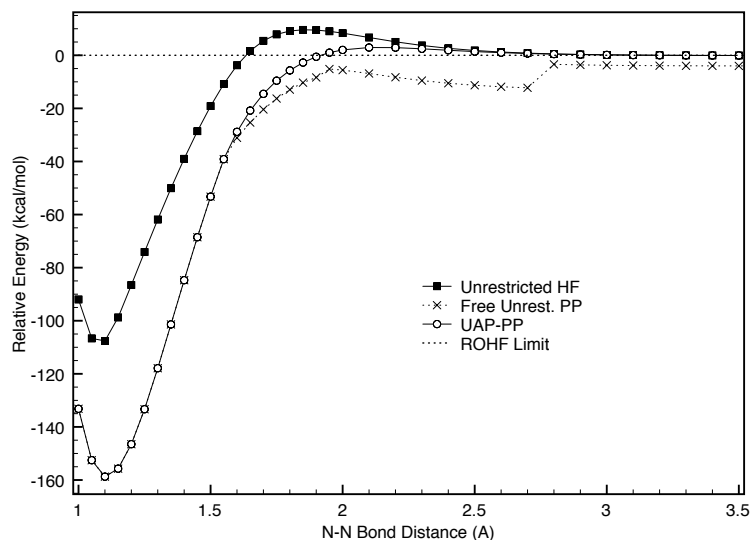


Figure 5.5: The N-N dissociation PES for N_2 in the (6,6) active space in the 6-31G* basis.

bond rotated into our active space as the carbon-carbon bond orbitals began to assume methylene fragment character. In the methane case, all the possible carbon-hydrogen bonds are being correlated and they hypothetically follow the single hydrogen abstraction until the fragments are a doublet methyl radical and doublet hydrogen. RPP, UPP and UAP-PP curves are equivalent from 1.0 to about 2.8 Å, and then differences are seen towards the dissociation limit as shown in Figure 5.6. The energy of the dissociation limit is hydrogen plus 3-pair UAP-PP for CH_3 . Freely unrestricing PP branches off to a lower energy solution, where as UAP-PP and restricted PP both stay about the same. The energy for restricted PP becomes slightly higher than UAP-PP as it approaches a limit where the CH_3 pays an energy penalty for not having any spin-polarization.

The freely unrestricing PP asymptote at dissociation is around 3 kcal/mol lower in energy than the appropriate UAP-PP asymptote. Instead of rotating in a different bond to correlate, Figure 5.7 shows that with freely unrestricing PP the system has rotated out the hydrogen-centered virtual orbital (it can no longer provide any correlation energy) and rotated in an orbital centered on the CH_3 fragment. Fig. 5.6 shows that if the UAP approximation is used, the potential energy surface does not branch to that lower asymptote and instead goes to the desired molecular fragments as can be seen in the orbitals shown in Figure 5.7. As a consequence of the constraint which permits only spin-polarization within the 2-dimensional subspace describing a pair, the bond has dissociated to have one electron on each fragment and its corresponding pairing virtual on the opposite fragment. Including the full PP active space is not sufficient to prevent artifacts with free spin-unrestriction; the

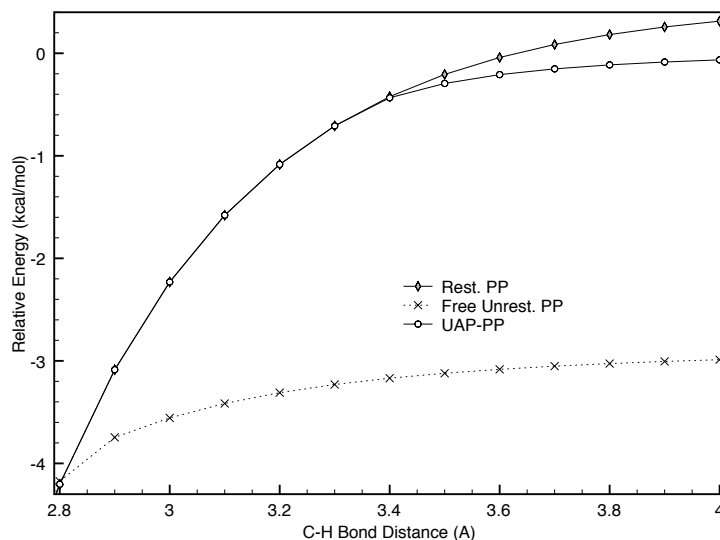


Figure 5.6: The spin-unrestriction point along the single hydrogen abstraction PES for CH_4 in the (8,8) active space in the 6-31G* basis. The zero in energy is the UAP dissociation limit.

UAP approach is again necessary to keep the appropriate orbitals in the active space and ensure size-consistency. Together with the results of the previous section, this establishes that all of the main artifacts associated with freely unrestricted PP identified in earlier work [87] are resolved with the UAP model for spin polarization.

5.3.4 Radical Properties

Radicals can also be examined with the UAP approach, beginning with equilibrium properties calculated from these static correlation models. The biggest problem in dealing with radical properties is sorting out all the different low-lying minima and a preference for symmetry breaking solutions. To compute these properties the UAP-2P method with the cc-pVTZ basis (with the RIMP2-cc-pVTZ auxiliary basis) is employed. The 2P method includes all the doubles amplitudes that connect two pairs and also removes all the integrals with indices spanning more than two pairs. This method corresponds to a truncation of the PQ method discussed elsewhere [85] at the level of double excitations. 2P includes as many doubles amplitudes as can be done with quadratic memory and quartic computational effort. The basic properties we are examining are the optimized equilibrium bond length of the radical, $\langle \hat{S}^2 \rangle$ for the correlated wave function, and the Mulliken charge and spin populations for the diatoms at the equilibrium bond length. Tables 5.2 and 5.3 shows the properties of the wavefunction for 7 of the worst cases for the freely spin-unrestricted PP [86]: BO, CN, CO^+ , N_2^+ , O_2^+ , OF and F_2^+ . Table 5.2 contains UAP-PP results while

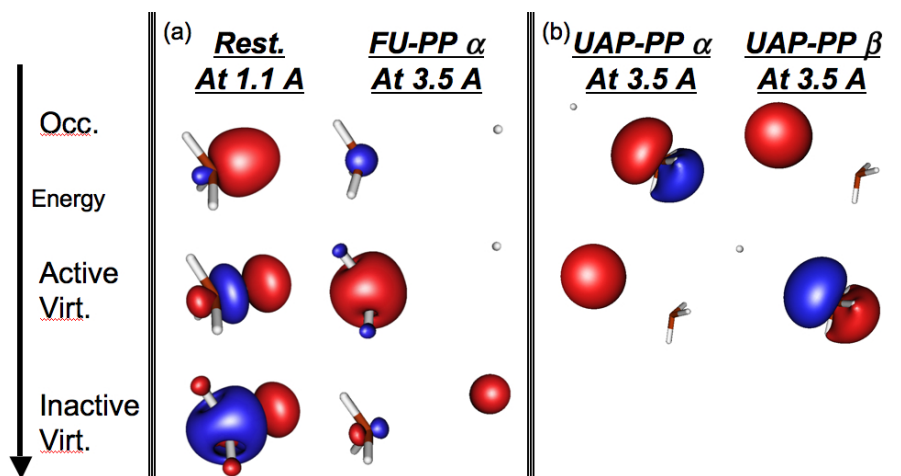


Figure 5.7: C-H bonding and anti-bonding orbitals from the $\text{CH}_3 + \text{H}$ reaction using a) freely unrestricting PP and b) UAP-PP. a) Includes an inactive virtual orbital to indicate re-arrangement of active space.

Table 5.3 contains UAP-2P results.

	R_{eq} Expt.	R_{eq} Predicted	$\langle \hat{S}^2 \rangle$	Charge	Spin
BO	1.205	1.193	0.7553	0.153/-0.153	1.079/-0.079
CN	1.172	1.155	0.7925	0.044/-0.044	1.300/-0.300
CO^+	1.115	1.098	0.7727	0.704/0.296	1.196/-0.196
N_2^+	1.116	1.155	0.7958	0.628/0.372	1.235/-0.235
O_2^+	1.116	1.094	0.7576	0.500/0.500	0.500/0.500
OF	1.358	1.418	0.7544	0.089/-0.089	1.054/-0.054
F_2^+	1.322	1.428	0.7615	0.713/0.287	1.089/-0.089
	MAD Expt.	0.039			
	RMS Expt.	0.050			

Table 5.2: Properties of some diatomic radicals in the cc-pVTZ basis (with the rimp2-cc-pVTZ auxiliary basis) using the UAP-PP method. The Mulliken charge and spin populations are given in the order of the molecular formula. The bond lengths are expressed in Angstroms.

Comparing the predicted bond lengths against the known experimental bond lengths, it can be seen in Table 5.2 that UAP-PP does a fairly poor job relative to our usual expectations of an accuracy of perhaps 0.01 \AA . This demonstrates that regardless of the treatment of spin-polarization, the PP level of correlation is insufficient for modeling the equilibrium properties of these radicals. Table 5.3 demonstrates that UAP-2P improves greatly over UAP-PP: it still has large errors in bond lengths for the halogenated species, but for all other species it performs superbly. Thus inter-pair correlations help significantly to reduce the PP error.

	R_{eq} Expt.	R_{eq} Predicted	$\langle \hat{S}^2 \rangle$	Charge	Spin
BO	1.205	1.204	0.7500	0.136/-0.136	1.030/-0.030
CN	1.172	1.161	0.7503	0.024/-0.024	1.129/-0.129
CO ⁺	1.115	1.107	0.7502	0.691/0.309	1.085/-0.085
N ₂ ⁺	1.116	1.106	0.7506	0.633/0.367	1.083/-0.083
O ₂ ⁺	1.116	1.105	0.7500	0.500/0.500	0.500/0.500
OF	1.358	1.391	0.7500	0.100/-0.100	1.018/-0.018
F ₂ ⁺	1.322	1.399	0.7501	0.700/0.300	1.032/-0.032
	MAD Expt.	0.022			
	RMS Expt.	0.033			

Table 5.3: Properties of some diatomic radicals in the cc-pVTZ basis (with the rimp2-cc-pVTZ auxiliary basis) using the UAP-2P method. The Mulliken charge and spin populations are given in the order of the molecular formula. The bond lengths are expressed in Angstroms.

The values of $\langle \hat{S}^2 \rangle$ for the correlated wave function indicate that an almost pure doublet has been found for each of these cases at the UAP-2P level, with reduced contamination relative to UAP-PP. The improved description of electron correlations in UAP-2P leads to more symmetric solutions than obtained with PP. However the Mulliken spin and charge densities tell us that a symmetry broken state is still the preferred one for all molecules except O₂⁺. The more symmetric states for CN and N₂⁺ are on the order of 10 kcal/mol higher in energy for UAP-2P than the solution presented at their optimized geometry. The predicted bond length for the more spin-symmetric species are also around 0.04 Å longer than the ones for the spin symmetry broken solutions. This means that although the spin symmetry is wrong, the spin-polarized symmetry broken solutions agree better with experiment. The leading spin-unrestriction angles for each of these cases is for the bonding orbital pairs, and they are typically small values ranging from 1 to 5 degrees.

The allyl radical is a well-known problem for both HF and GVB methods because of its propensity to exhibit artificial symmetry breaking. UB3LYP predicts a structure that has symmetric C-C bonds of 1.386 Å in the cc-pVDZ basis and Beran et al. [86] showed that unconstrained UPP breaks symmetry along a distortion coordinate. The distortion coordinate is defined as the difference in the two C-C bond lengths, with UPP yielding an optimized geometry with a distortion of around 0.06 Å. If the PP optimized geometries are computed with both types of spin-unrestriction, we find that UPP predicts C-C bond lengths of 1.3735 and 1.4393 Å and UAP-PP predicts a nearly symmetric structure with C-C bond lengths of 1.4005 and 1.4008 Å. Figure 5.8 shows a plot along the C-C bond distortion coordinate. The 0 Å distortion point is defined as the average of the two equilibrium C-C bond lengths at the optimized symmetry-broken geometry. The UAP method produces a curve that is virtually flat around the symmetric geometry, showing that in this case artificial symmetry breaking can be significantly reduced simply by our constrained treatment of spin-polarization.

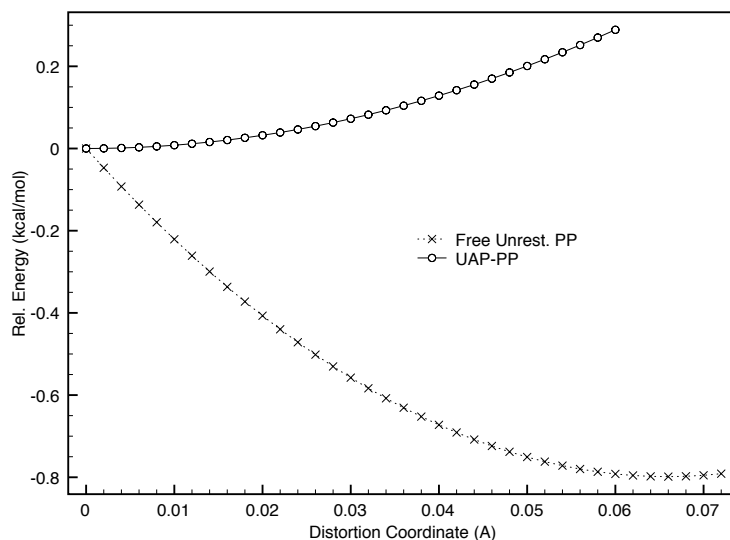


Figure 5.8: PP using different forms of spin-unrestriction potential energy surfaces along a distortion coordinate from their optimized structures in the cc-pVDZ basis.

Continuing from allyl radical, Table 5.4 shows predicted bond lengths for the next two larger polyenyl radicals, pentadienyl, C_5H_7 , and heptadienyl, C_7H_9 . Two initial geometries were used for each molecule done with each method. The "a" geometry has the radical electron localized on a terminal carbon with alternating single and double carbon-carbon bonds, and the "b" geometry is a C_{2v} structure with the radical electron in the center of the molecule. Each calculation is done in the full PP active space with the cc-pVDZ basis set (with its corresponding auxiliary basis). For pentadienyl radical, both UAP-PP and UAP-2P predict the appropriate location for the radical electron (centered around the central carbon atom of the chain), but freely unrestricing PP keeps the alternating geometry regardless of the guess used. Overall, the UAP-PP vs UPP results for pentadienyl resemble those discussed above for allyl: the UAP approach to spin polarization diminishes artificial symmetry breaking significantly. It is noteworthy that UAP-2P obtains the correct symmetry, whereas UAP-PP still yields some distortion.

The bond length difference (outer vs inner CC distance) for this species was found to be 0.054 Å for CASSCF and 0.053 Å for UCCSD(T) [188]. UAP-2P has bond alternation that is about two times too large at 0.090 Å with UAP-PP roughly the same at 0.095 Å. This suggests that the radical electron is too localized in these methods, and that correlations coupling more than 2 pairs and/or higher than double substitutions are important to obtain the correct extent of localization/delocalization in this case.

		C1-C2	C2-C3	C3-C4	C4-C5	C5-C6	C6-C7
Pentadienyl	Guess (a)	1.338	1.444	1.341	1.436		
	Free-UPP	1.360	1.472	1.394	1.415		
	UAP-PP	1.367	1.444	1.468	1.355		
	UAP-2P	1.374	1.464	1.464	1.374		
Pentadienyl	Guess (b)	1.389	1.403	1.402	1.387		
	Free-UPP	1.360	1.472	1.394	1.415		
	UAP-PP	1.370	1.439	1.471	1.354		
	UAP-2P	1.374	1.464	1.464	1.374		
Heptatrienyl	Guess (a)	1.338	1.445	1.342	1.447	1.341	1.436
	Free-UPP	1.353	1.488	1.365	1.463	1.398	1.412
	UAP-PP	1.353	1.494	1.353	1.477	1.422	1.382
	UAP-2P	1.360	1.493	1.378	1.460	1.464	1.374
Heptatrienyl	Guess (b)	1.378	1.447	1.395	1.395	1.447	1.378
	Free-UPP	1.358	1.475	1.387	1.428	1.460	1.364
	UAP-PP	1.350	1.485	1.401	1.401	1.485	1.350
	UAP-2P	1.360	1.493	1.378	1.461	1.464	1.374

Table 5.4: Optimized geometries of pentadienyl and heptatrienyl radicals. The calculations were performed with the cc-pVDZ basis (with the rimp2-cc-pVDZ auxiliary basis) with the 3 spin-polarized correlation methods. The a) guess geometries are alternating single and double bonds with the radical electron on a terminal carbon. The b) guess geometries are structures of the appropriate C_{2v} geometry with the radical electron centered on the central carbon of the chain.

For the heptadienyl radical, UAP-2P was able to move the radical electron inwards from the terminal carbon, but it did not return the whole molecule to a C_{2v} geometry. Instead it produced a geometry similar to pentadienyl, with another carbon single and double bond attached to one end of it. UAP-PP can find two solutions, one of the appropriate C_{2v} structure, and one similar to the structure predicted by UAP-2P, with the asymmetric structure being lower in energy by around 0.19 kcal/mol. Freely unrestriciting PP also predicts two structures. The structure with a pentadienyl-like subunit is 3.65 kcal/mol lower in energy than the bond alternating structure that closely resembles guess structure "a". Therefore, while UAP is again a clear improvement over unconstrained spin-polarization at the PP level, it is an interesting question for future investigation as to how delocalized the correlations must be permitted to be in order to correctly reproduce CASSCF results.

5.4 Conclusions

Spin-polarization is essential for describing strongly correlated problems like multiple bond dissociation with truncated descriptions of electron correlation, such as coupled cluster generalized valence bond (CC-GVB) methods which use an active space of one orbital per active electron. When using active space methods to describe the static electron correlation of a molecular system, the normal definition of spin-unrestriction which allows the α and β variables to vary independently becomes unacceptable [87]. The resulting artifacts

include orbitals completely rotating out of the active space so that the system described by the correlation at equilibrium is no longer the same as the one described at dissociation [87].

The spin-polarization method described in this paper constrains orbitals to only be unrestricted within active pairs (UAP). In UAP, spin-polarization occurs only with the space of two orbitals (one bonding, and one antibonding) used to describe each active electron pair, giving one degree of freedom per pair. The smaller number of degrees of freedom and the strict pair-by-pair definition of spin-polarization of orbitals can be utilized to make an efficient implementation of UAP with PP or more advanced CC-GVB methods. Most importantly, UAP produces orbitals that smoothly transition from the restricted bonding orbitals at R_{eq} to appropriate spin-polarized orbital fragments at dissociation. To ensure well-behaved amplitudes, we additionally add a penalty function term to the CC-GVB equations. Based on a variety of test calculations, the resulting UAP methods are a great improvement over the spin-polarization without constraints. It will be interesting and desirable to combine the UAP approach with further systematic improvement of the cluster operator [85, 118, 119] in the future.

Chapter 6

Analysis of multi-configurational Kohn-Sham methods: Theory and model application to bond-breaking.

6.1 Introduction

Density functional theory (DFT) [121] is considered to be the most applicable and useful method to determine the ground-state (GS) physical properties of microscopic electronic systems. Given a system of N particles, bound in an external potential, v_{ext} , the main idea of DFT is to search for their GS density, n , rather than the full GS wave function (WF), Ψ . The former can be obtained, in principle, by solving the highly complicated $3N$ dimensional Schrödinger equation (SE). DFT, on the other hand, takes advantage of the Hohenberg-Kohn theorem [121], which proves that; first, the interacting particles' energy functional, $\varepsilon[\Psi]$, can be replaced by a density functional, $E[n]$, thanks to a 1-1 map between GS WFs and densities; $\Psi \leftrightarrow n$:

$$\begin{aligned}
 E[n] &\equiv \varepsilon[\Psi[n]] = F_{HK}[n] + \int dr v_{ext} n \\
 F_{HK}[n] &\equiv \langle \Psi[n] | \hat{T} + \hat{V}_{ee} | \Psi[n] \rangle \\
 \hat{T} &= - \sum_{i=1}^N \frac{1}{2} \nabla_i^2, \quad \hat{V}_{ee} = \frac{1}{2} \sum_{i \neq j=1}^N \frac{1}{|r_i - r_j|}
 \end{aligned} \tag{6.1}$$

(we use atomic units: $m_e = e^2 = \hbar = 1$) and second, the GS energy and density can be obtained from the variational principle of $E[n]$ with respect to the density

$$\delta E[n] |_{n=n_{gs}} = 0$$

However, since the exact, explicit one-to-one map $\Psi \leftrightarrow n$ is unknown, approximations are required in order to estimate the universal HK functional part of the energy functional, $F_{HK}[n]$.

Therefore Kohn and Sham [189] (KS) suggested mapping the real interacting system onto an auxiliary fictitious system of N noninteracting particles, described by a WF, $\Psi_S[n]$, which restores the exact interacting GS density. Consequently, the HK functional $F_{HK}[n]$ is partitioned as

$$F_{HK}[n] = \langle \Psi[n] | \hat{T} | \Psi[n] \rangle + E_H[n] + E_{XC}[n] \quad (6.2)$$

where the Hartree energy, E_H , and the exchange-correlation (XC) energy, E_{XC} , are defined as

$$\begin{aligned} E_H[n] &= \frac{1}{2} \iint dr dr' \frac{n(r)n(r')}{|r-r'|} \\ E_{XC}[n] &\equiv F_{HK}[n] - E_H[n] - T_S[n] \\ T_S[n] &= \langle \Psi_S[n] | \hat{T} | \Psi_S[n] \rangle \end{aligned} \quad (6.3)$$

It remains to model E_{XC} as an explicit density *functional*, for instance, based on the homogeneous electron gas (the so-called local density approximation (LDA)). The KS fictitious WF, Ψ_S , is taken as a Slater determinant of N orbitals, $\{\phi_i\}_{i=1}^N$. They are determined by the KS method, as is explained later on, such that their density is in principle identical to the exact GS density of the (real) interacting electrons. The density-WF relation is exploited then:

$$n(r) = N \frac{\int dr_2 \dots dr_N |\Psi_S(r, r_2 \dots r_N)|^2}{\langle \Psi_S | \Psi_S \rangle}$$

While the DFT-KS method yields very good results for GS energy in many equilibrium cases, [190] it still exhibits several severe problems. These problems mainly arise from the local density nature of E_{XC} (LDA/GGA), and the very simple fictitious wave function, Ψ_S . For instance, it is well known that KS method is unable to describe complete dissociation curves [191], static linear and non-linear polarizability [192], 3-electron bonding [193], or bond twisting [194], properly. Also, the various XC LDA/GGA functionals include undesired self-interaction energy, [195, 196] spin contamination [197], and lack of derivative discontinuity of the derived XC potential [190]. The former is critical for band-gap calculations in semiconductor and dielectric materials. It is also recognized that for strongly correlated systems (some of the above examples are in this class also), the KS method yields poor results [198, 199]. Furthermore, it is not clear how to systematically improve the LDA/GGA XC functionals, taken from the homogeneous electron gas (HEG), for atomic and molecular finite systems to address these problems, although progress has been made

on self-interaction in particular [200, 201].

It is therefore a present-day grand challenge in DFT to go beyond the regular KS method and the various widely used XC functionals. One direction to improve the regular KS method is searching for the energy minimum using an auxiliary multi-determinantal/multi-configuration (MC) fictitious WF, $\Psi_S^{MC}[n]$, where the energy functional is partitioned similarly to the KS partition, as

$$E = \langle \Psi_S^{MC}[n] | \hat{T} + \hat{V}_{ee} | \Psi_S^{MC}[n] \rangle + E_C^{dyn}[n] + \int dr v_{ext} n, \quad (6.4)$$

where $E_C^{dyn} \equiv F_{HK}[n] - \langle \Psi_S^{MC}[n] | \hat{T} + \hat{V}_{ee} | \Psi_S^{MC}[n] \rangle$ is to be modeled as an *explicit functional* of the density (it is called the ‘dynamical’ or ‘residual’ correlation). The interacting system is now mapped onto a *partially* interacting system, where the corresponding KS equations contain both effective local and nonlocal potentials. We are able, in this way, to address the abovementioned problems by incorporating static (strong) correlations via $\langle \Psi_S^{MC} | \hat{V}_{ee} | \Psi_S^{MC} \rangle$, and at the same time to reduce the dynamical correlation effects, taken for instance from HEG. It is clear that the various aspects of the chemical bond can be described in a more realistic and reliable manner, thanks to the nonlocal and long-range nature of such correlation. Also, this method is much more flexible than the regular KS method, and intelligent choice of the WF, Ψ_S^{MC} , may yield good results still with cheaper computational cost than the standard WF methods. Indeed, proposed multi-determinantal methods like multi-reference (MR) DFT/CAS-DFT, [104–113] and MC-optimized effective potential (OEP) [114, 115] do exhibit feasibility and improvement over the regular KS method.

It is the aim of this article to examine the basis of such theories, while extending the rigorous regular KS method to the case of a MC auxiliary WF. By this we mean we are interested in an effective local potential map between interacting and auxiliary systems, $v_S: \Psi \mapsto \Psi_S^{MC}$, without any prior assumption for the auxiliary WF form, Ψ_S^{MC} . We show that a consistent rigorous MCKS method will always yield a single-determinant (SD) WF at the end of the KS-SCF procedure. We also discuss the connection between the above MC methods and our analysis. Finally we illustrate the use of a partly interacting reference system, and the associated challenge of treating residual correlation for bond-breaking in the hydrogen molecule, using a perfect pairing reference wave function.

6.2 The Standard Kohn-Sham Method

To briefly summarize, the KS method [189] introduces an auxiliary system of non-interacting particles, bound in an effective local external potential, $v_S(r)$, described by the auxiliary (SD) wave function, Ψ_S . A fundamental assumption is that the non-interacting

GS density is identical to the interacting GS density, and that this can be restored by v_S (v-representability). Since Ψ_S is a Slater determinant of N orbitals $\{\phi_i\}_{i=1}^N$, the energy functional of the non-interacting system can be written as

$$E_S[n] = T_S + \int dr v_S(r) n(r), \quad (6.5)$$

where $T_S = \sum_{i=1}^N \langle \phi_i | -\frac{1}{2} \nabla^2 | \phi_i \rangle$ is the non-interacting kinetic energy functional, the density is given by $n(r) = \sum_{i=1}^N |\phi_i(r)|^2$, and v_S should be determined. At the same time one can write the interacting energy as

$$E[n] = T_S[n] + \int dr v_{ext}(r) n(r) + E_H[n] + E_{XC}[n]. \quad (6.6)$$

We require that the non-interacting and interacting systems have the same density at their GS, restored by v_S , i.e.

$$\delta E[n_{gs}] = \delta E_S[n_{gs}] = 0. \quad (6.7)$$

A crucial part of the KS method is determining the non-interacting potential, v_S . The assumption that both interacting and non-interacting systems have the same density at their GS enables us to determine v_S rigorously. At the GS density, both variational principles with respect to the density together with the particle number constraint, yield expressions for the constrained variations:

$$\begin{aligned} \delta E[n_{gs}] &= \delta T_S[n_{gs}] + (v_{ext} + v_H[n_{gs}] + v_{XC}[n_{gs}] + \mu) \delta n \\ \delta E[n_{gs}] &= \delta T_S[n_{gs}] + v_S[n_{gs}] \delta n + \mu \delta n \end{aligned} \quad (6.8)$$

where μ is the Lagrange multiplier for the particle number constraint, and,

$$\begin{aligned} v_H[n_0](r) &= \int dr' n_0(r') |r - r'| \\ v_{XC}[n_0](r) &= \delta E_{XC}[n] / \delta n(r) |_{n=n_0} \end{aligned} \quad (6.9)$$

Employing Eq. 6.8 in Eq. 6.7, we obtain v_S (up to a constant):

$$v_S[n_{gs}](r) = v_{ext}(r) + v_H[n_{gs}](r) + v_{XC}[n_{gs}](r). \quad (6.10)$$

The potential v_S in Eq. 6.10 defines a map $v_S : \Psi \mapsto \Psi_S^{MC}$ between the interacting and the non-interacting systems. Furthermore, since $\Psi_S = \det(\{\phi_i\}) / \sqrt{N!}$, the non-interacting energy minimum can also be obtained from the following constrained variation via the orbitals:

$$\delta \left\{ E_S + \sum_{i,j} [\varepsilon_{ij} (\langle \phi_i | \phi_j \rangle - \delta_{ij})] \right\} = 0$$

$$\delta E_S = \delta T_S + v_S \delta n \quad (6.11)$$

Eq. 6.11 yields the celebrated KS equations [189] for the orbitals:

$$\hat{h}_S(r) \phi_i(r) = \varepsilon_i \phi_i(r),$$

$$\hat{h}_S(r) \equiv -\frac{1}{2} \nabla^2 + v_S(r),$$

$$n(r) = \sum_{i=1}^N |\phi_i|^2 \quad (6.12)$$

Together with Eq. 6.12, the KS self-consistent field (SCF) has a closed form. The KS-SCF ends when v_S yields a set of orbitals that minimizes E_S .

6.3 Mapping the Interacting System onto an Auxiliary System via an Effective Local Potential

In this section we prove that mapping an interacting system onto an auxiliary system, the latter described by a multi-configuration (MC) WF, Ψ_S^{MC} , will always yield a single-determinant WF, like in the regular KS method. Given a set of orbitals, $\{\phi_i\}_{i=1}^M$, we define the MC WF as $\Psi_S^{MC} = \sum_i c_i D_i$, where $D_i = \det(\{\phi_k\}) / \sqrt{N!}$ is a normalized determinant of N orbitals chosen from the orthogonal set $\{\phi_i\}_{i=1}^M$ ($N < M \leq \infty$), and $\{c_i\}$ are complex coefficients. At first glance, it might seem obvious that such an auxiliary system should be described by a SD WF. Indeed this is the final result, but, unlike a physical fixed potential, the MC-KS effective potential is changed during the SCF procedure. Furthermore, it is possible, at each SCF cycle, to obtain first the configuration coefficients, $\{c_i\}$, and then calculate the orbitals $\{\phi_i\}_{i=1}^M$ via the proper KS equations with frozen coefficients $\{c_i\}$. In this case a collapse into a SD WF is unlikely. However, as we will explain in Sec. 6.4, there is no consistent map between interacting and auxiliary systems in this latter case.

Let us repeat the KS analysis for the case of Ψ_S^{MC} . Again, we assume that there is a local potential, v_S , which at the auxiliary system's GS, generates the GS density of the interacting system. We have to find the GS energy of the auxiliary system (analogously to Eq. 6.5):

$$E_S^{MC} = \langle \Psi_S^{MC} | \hat{T} + \hat{V}_{ee} | \Psi_S^{MC} \rangle / \langle \Psi_S^{MC} | \Psi_S^{MC} \rangle$$

$$\begin{aligned}
 &= \sum_{i,j} c_i^* c_j \langle D_i | \hat{H}_S | D_j \rangle / \sum_i |c_i|^2 \\
 &\equiv \sum_{i,j} P_{ij}(\{c_k\}) \langle \phi_i | \hat{h}_S | \phi_j \rangle
 \end{aligned} \tag{6.13}$$

where P_{ij} is the $M \times M$ Hermitian one-particle density matrix and $\hat{H}_S(r_1..r_N) = \sum_i \hat{h}_S(r_i) \equiv \sum_i [-\frac{1}{2}\nabla^2 + v_s(r_i)]$. Correspondingly, we can define the interacting energy and XC functionals as:

$$\begin{aligned}
 E &= T_S^{MC}[n] + \langle \Psi_S^{MC} | \hat{V}_{ee} | \Psi_S^{MC} \rangle + \int dr v_{ext}(r) n(r) + E_C^{dyn}[n], \\
 T_S^{MC}[n] &= \langle \Psi_S^{MC}[n] | \hat{T} | \Psi_S^{MC}[n] \rangle, \\
 E_C^{dyn}[n] &\equiv F_{HK}[n] - \langle \Psi_S^{MC}[n] | \hat{T} + \hat{V}_{ee} | \Psi_S^{MC}[n] \rangle,
 \end{aligned} \tag{6.14}$$

where

$$\begin{aligned}
 T_S^{MC} &= -\frac{1}{2} \sum_{ij} P_{ij}(\{c_k\}) \langle \phi_i | \nabla^2 | \phi_j \rangle \\
 n(r) &= \sum_{ij} P_{ij}(\{c_k\}) \phi_i^*(r) \phi_j(r).
 \end{aligned} \tag{6.15}$$

From Eq. 6.15 the density is now a functional of the orbitals and the amplitudes, $\{c_k\}$, so the variation should be done, correspondingly, with respect to each of them. Furthermore, the same trial wavefunction Ψ_S^{MC} must be used in the interacting and the auxiliary energy functionals, since the variation is done with respect to the density, and the density is a functional of both the orbitals and the amplitudes. The objective is again to find a closed form for v_S by equating the constrained variations:

$$\delta E_S^{MC} = \delta E = 0, \tag{6.16}$$

in direct analogy to Eq. 6.7. From Eqs. 6.14 and 6.16 we obtain, similarly to the regular KS method:

$$\begin{aligned}
 v_S &= v_{ext} + v_{XC}^{MC} \\
 v_{XC}^{MC} &= \delta \left\{ \langle \Psi_S^{MC}[n] | \hat{V}_{ee} | \Psi_S^{MC}[n] \rangle + E_C^{dyn}[n] \right\} / \delta n
 \end{aligned} \tag{6.17}$$

Note that v_{XC}^{MC} can be found similarly to the extended OEP method [115]. The MCKS equations are obtained now from the constrained variation principle

$$\delta E_S^{MC} + \sum_{i,j} [\tilde{\epsilon}_{ij} \delta(\langle \phi_i | \phi_j \rangle - \delta_{ij})] = 0, \tag{6.18}$$

with respect to each orbital and amplitude (v_S is not varied of course). The final result is

$$\begin{aligned} \sum_j P_{ij}(\{c_k\}) \hat{h}_S(r) \phi_j(r) &= \sum_i \tilde{\varepsilon}_{ij} \phi_j(r), \\ \partial E_S^{MC} / \partial c_k &= 0. \end{aligned} \quad (6.19)$$

Since \hat{h}_S is a 1-body Hamiltonian, orbitals $\{\phi_i^d\}$ can be chosen that diagonalize it:

$$\hat{h}_S \phi_i^d = \varepsilon_i \phi_i^d \quad (6.20)$$

Therefore each determinant, $D^d = \det(\{\phi_i^d\}) / \sqrt{N!}$, is automatically an eigenfunction of \hat{H}_S (defined in Eq. 6.13):

$$\begin{aligned} \hat{H}_S D_i^d &= E_i D_i^d, \\ E_i &= \sum_{j=1}^N \varepsilon_{ij}. \end{aligned} \quad (6.21)$$

For any such determinant, $E_i \geq E_{min}^d \equiv \sum_{i=1}^N \varepsilon_i$ (assuming that $\{\varepsilon_i\}$ are ordered from lower to higher). We now expand the MC-WF in the determinants $\{D_i^d\}$: $\Psi_S^{MC} = \sum_i c_i D_i = \sum_i b_i D_i$. Employing the first equality in Eq. 6.13 and the fact that \hat{H}_S is a sum of single-particle operators (i.e. unitarily invariant), one can see that $E_S^{MC} = \vec{b}^\dagger \overleftrightarrow{H}^d \vec{b} / |\vec{b}|^2$ where $(\vec{b}_i) = b_i$ and \overleftrightarrow{H}^d is the diagonal matrix $H_{ij} \equiv \langle D_i^d | \hat{H}_S | D_j^d \rangle \delta_{ij} \equiv E_i \delta_{ij}$. Therefore, the non-interacting MC energy is

$$E_S^{MC} = \frac{\sum_i |b_i|^2 E_i}{\sum_i |b_i|^2} = E_0 + \frac{\sum_i |b_i|^2 \Delta E_i}{\sum_i |b_i|^2} \quad (6.22)$$

where $E_0 = \min \{E_i | b_i \neq 0\}$ and $\Delta E_i = E_i - E_0$. Thus, provided that Ψ_S^{MC} contains more than one nonzero b_i , and $E_0 = \sum_{j=1}^N \varepsilon_{ij} \geq E_{min}^d$ as we concluded above, we obtain:

$$E_{min}^d \leq E_0 < E_S^{MC} \quad (6.23)$$

Therefore, for any given local potential, v_S , the MC-WF will never minimize E_S^{MC} unless it collapses into a single determinant (in the case of degeneracy, the MC-WF will collapse into a sum of determinants containing non-excited orbitals). We conclude that Eqs. 6.16 and 6.17 can never be satisfied rigorously by a nontrivial MC-WF.

6.4 Mapping the Interacting Systems onto Partially Interacting Systems

Despite the fact that a rigorous MC-KS construction simply collapses to the standard KS method, there are MC-DFT methods that do not exhibit such a WF collapse. For instance, the CAS-DFT/MR-DFT approach [105, 106, 113] uses the partition 4 to model the total energy by a MC-WF. The energy functional is then mapped onto a ‘partially’ interacting system via an effective local potential, w , $w : \Psi \mapsto \Psi_S^{MC}$, where the interacting and partially-interacting energy functionals are (respectively)

$$\begin{aligned} E &= \langle \Psi_S^{MC} | \hat{T} + \hat{V}_{ee} | \Psi_S^{MC} \rangle + E_C^{dyn} [n] + \int dr v_{ext}(r) n(r) \\ \bar{E} &= \langle \Psi_S^{MC} | \hat{T} + \hat{V}_{ee} | \Psi_S^{MC} \rangle + \int dr w(r) n(r). \end{aligned}$$

The assumption here is that there is a local potential, w , that at the GS of the partially interacting \bar{E} , generates the same fully interacting GS density of E . w is determined from the HK variational principle (with total particle number constraint):

$$\delta E = \delta \bar{E} = 0 \tag{6.24}$$

to yield $w(r) = v_{ext}(r) + \delta E_C^{dyn} / \delta n(r)$. This equality defines a consistent map between the fully interacting and partially interacting systems, if the variation of \bar{E} is done with respect to both orbitals and amplitudes. Hence the amplitudes and the orbitals are determined by the SCF equations for the orbitals and the amplitudes:

$$\begin{aligned} \delta \left[\bar{E} + \sum_{j,k} (\langle \phi_j | \phi_k \rangle - \delta_{jk}) \right] / \delta \phi_i &= 0, \\ \partial \bar{E} / \partial c_i &= 0 \end{aligned} \tag{6.25}$$

The first set of equations are extended KS equations, containing both effective local and nonlocal potentials (see Eq. 6.20 in Ref. [113]). WF collapse is not likely here, since the KS equations contain a nonlocal potential, reflecting partial treatment of electron-electron interactions in $\langle \Psi_S^{MC} | \hat{T} + \hat{V}_{ee} | \Psi_S^{MC} \rangle$. Therefore, our analysis of Sec. 6.3 does not hold here: \bar{E} cannot be written as a pure bilinear form of the amplitudes as was done for E_S^{MC} in Eq. 6.13.

Another method is the MC-OEP [115], a variation of CAS-DFT/MR-DFT, with a difference regarding the evaluation of the orbitals. Here, three systems and functionals are defined, the fully interacting $E[n]$, a partially interacting $\bar{E}[n]$ and a noninteracting $E_S[n]$. At each iterative cycle, the amplitudes are determined, first, from the variation $\partial \bar{E} / \partial c_i = 0$, as in Eqs. 6.25 (w is obtained from Eq. 6.24). Then, the local potential is calculated from the variation $\partial \bar{E} / \partial v_s = 0$ (an extended OEP equation), which is equivalent

to $\partial\bar{E}/\partial n = 0$ [202]. Finally, the orbitals are obtained from the regular KS equations (Eqs. 6.12) with the calculated local $v_S(\delta\bar{E} = \delta E_S = 0$ should be assumed in order to obtain a consistent map). Therefore MC effects enter the KS equations only implicitly, through v_S . Here, again, MC-WF collapse is unlikely, since the amplitudes are calculated for the partially interacting system, and then, with frozen values of the amplitudes, only the orbitals have to minimize a non-interacting energy. Furthermore, the assumption, $\delta\bar{E} = \delta E_S = 0$, where the variation should be done with respect to the density, is not fully satisfied, since δE_S is done with respect to the orbitals only and not for the amplitudes. Therefore, the orbitals are not calculated from a fully consistent local potential map, v_S . In fact, this inconsistency keeps the MC WF from collapsing into a SD WF.

6.5 Perfect Pairing as a Partially Interacting Reference

The purpose of this paper is not to assess MC-DFT schemes based on partially interacting reference wavefunctions. Nevertheless, a simple practical example can serve to illustrate the central issues that arise. For this purpose, we will employ the perfect pairing (PP) wavefunction as the MC-DFT reference wave function. PP is exact for isolated electron pairs using a 2 electron-in-2 orbital active space, and thus gives perhaps the simplest possible account of static correlations. The wavefunction is:

$$|\Psi_{PP}\rangle = \exp\left(\hat{T}_{PP}\right)|\Phi_0\rangle \propto \hat{A} \prod_{j=1}^{n/2} G_j. \quad (6.26)$$

\hat{A} is the antisymmetrizer and there is one cluster amplitude, t_j , for each 2-electron geminal function, G_j , which is composed of a superposition of two electrons in a bonding orbital and two electrons in an antibonding orbital:

$$G_j = (1 + t_j^2)^{-1/2} \left\{ \det [\phi_j \bar{\phi}_j] + t_j \det [\phi_j^* \bar{\phi}_j^*] \right\} \quad (6.27)$$

Discussions of PP, the defining equations, and its relation to more advanced static correlation methods are available elsewhere [56, 78, 79].

Following the discussion of the previous section, the PP energy is to be augmented with a functional of the electron density to describe residual dynamic correlation:

$$E = E_{PP} + E_C^{dyn} \quad (6.28)$$

The residual correlation correction depends upon the electron density and its gradients. The PP electron density is:

$$n(r) = \sum_{j=1}^{N/2} \left[(2 - u_j) |\phi_j(r)|^2 + u_j |\phi_j^*(r)|^2 \right] \quad (6.29)$$

where the scalar $u_j \in [0, 1]$ measures the occupation number of the correlating orbital for the j th pair (and the reduction from double occupation of the bonding orbital):

$$u_j = \frac{2t_j^2}{1 + t_j^2} \quad (6.30)$$

To address the double-counting problem, it is convenient to associate part of the density with unpaired electrons. From Eq. 6.29, there are no unpaired electrons when $u_j = 0$ while both electrons are unpaired when $u_j = 1$. These two known points can be smoothly connected by defining the distribution of unpaired electrons to be:

$$n_u^m(r) = \sum_{j=1}^{N/2} (u_j)^m \left[|\phi_j(r)|^2 + |\phi_j^*(r)|^2 \right] \quad (6.31)$$

The integer m is taken as 2 in the definition due to Yamaguchi [203], and 1 in the definition of Head-Gordon [204]. In fact any positive value of m is potentially acceptable.

The unpaired electron density can be used as a basis for correcting the double counting problem associated with evaluating the residual correlation energy, following the suggestion of Pérez-Jiménez et al [116,117]. The idea is to construct fictitious polarized densities (even though no spin polarization has occurred) such that no double counting correction is applied when there are no unpaired electrons ($u_j = 0$), and a maximal correction is applied if the electron density associated with a pair of electrons is completely unpaired ($u_j = 1$). These densities are defined by adding and subtracting half the unpaired electron density from half the total density:

$$\begin{aligned} n_+(r) &= \frac{1}{2}n(r) + \frac{1}{2}n_u^m(r) \\ n_-(r) &= \frac{1}{2}n(r) - \frac{1}{2}n_u^m(r) \end{aligned} \quad (6.32)$$

They are used to evaluate the residual dynamic correlation energy in place of the usual alpha and beta densities, within a conventional correlation energy functional (the LYP functional [122]).

$$E_C^{\text{dyn}} = E_C^{\text{LYP}}(n_+, n_-) \quad (6.33)$$

This construction correctly yields no opposite spin correlation energy in the limit of separating bonds ($u_j = 1$), as well as full opposite-spin correlation when there is no MC character ($u_j = 0$).

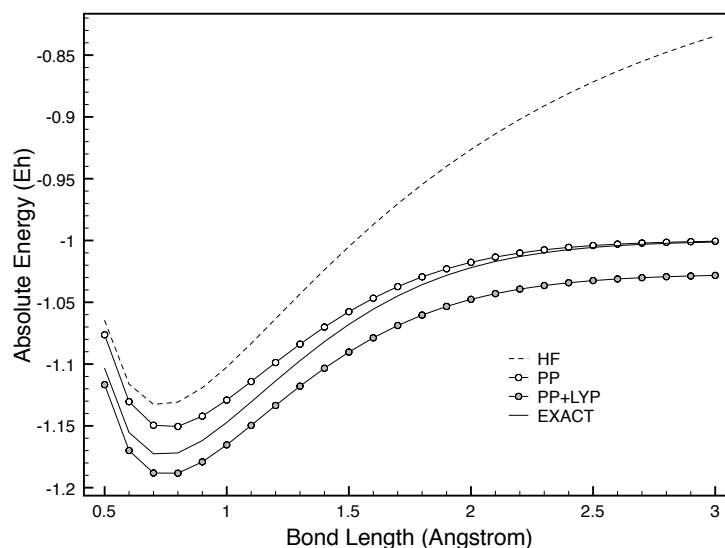


Figure 6.1: Energy (in Hartrees) as a function of H-H separation in the hydrogen molecule by the restricted Hartree-Fock method, the perfect pairing (PP) method (PP for this case is identical to CASSCF with 2 electrons in 2 orbitals), the PP method with the LYP correction for dynamic correlation (uncompensated for double counting), and the exact answer. All calculations are performed in the aug-cc-pVTZ basis.

As a very simple illustration of the behavior of this model for the dissociation of a single bond, we consider the H₂ molecule, using the aug-cc-pVTZ basis set. Figure 6.1 shows potential energy curves for 4 different approaches: from highest to lowest are restricted Hartree-Fock (RHF), PP, the exact wavefunction, and then PP directly augmented with LYP correlation, as $E_C^{dyn} = E_C^{LYP}(n/2, n/2)$. All these methods are spin-pure. The first point to note is that the multi-configurational character of PP allows it to separate correctly, unlike RHF, but relative to the exact solution (in this quite large basis), it is missing a significant fraction of the correlation energy near the equilibrium geometry. However, when corrected directly for residual dynamic correlation using LYP correlation, the result is a curve that not only is significantly lower than the exact result, it no longer reaches the correct asymptote of independent hydrogen atoms. The error relative to the exact wavefunction is a good measure of the double-counting problem associated with treating residual correlation with an existing correlation functional such as LYP, which itself derives from correcting the helium atom [205].

The improvements that are possible using Eq. 6.33 to evaluate residual correlation can be assessed from Figure 6.2, which shows the PP curve, the exact curve, and PP with residual corrections for correlation via Eq. 6.33 using $m = 1, 0.5, 0.2$ and 0.1 . First consider

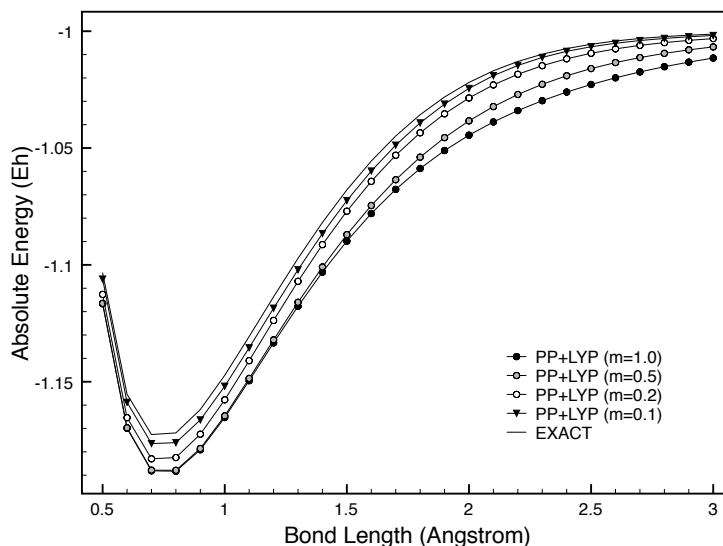


Figure 6.2: Energy (in Hartrees) as a function of H-H separation in the hydrogen molecule by the PP method with the compensated correction for residual dynamic correlation defined by Eq. 6.33 using several values of m , as defined in Eq. 6.31, as compared to the exact energy. All calculations are performed in the aug-cc-pVTZ basis.

the $m = 1$ curve relative to the lowest curve of Figure 6.1. This is the method that was suggested by Pérez-Jiménez and Pérez-Jordá [117]. As they already discussed, the results obtained show that the double counting problem is now correctly resolved in the dissociation limit of large H-H separations: in that limit $n_+ \rightarrow n$ and $n_- \rightarrow 0$. However, inspection of the equilibrium region shows that the double counting problem there is not adequately resolved – in fact there is only a very slight difference relative to the lowest curve on Figure 6.1. The reason for inadequate compensation is the very small t amplitude value in the reference wave function around equilibrium (less than 0.1, in contrast to approaching 1 at dissociation), which, when substituted into Eq. 6.31 yields nearly negligible unpaired electron density, with $m = 1$. Furthermore, for a similar reason, the approach of the curve to the zero asymptote is too slow. So, while this approach is a qualitative improvement on the uncompensated LYP correction shown in Figure 6.1, it is not a complete panacea.

It is possible to simultaneously ameliorate the two deficiencies associated with residual correlation by reducing the value of m employed in Eq. 6.31. The curves on Figure 6.2 with smaller values of m illustrate the extent to which this is possible. A value of $m = 0.5$ visibly improves over $m = 1$ by approaching the correct dissociation limit more quickly, but it does not significantly reduce the double counting error around equilibrium. A value of $m = 0.2$ further improves the approach to dissociation and, intriguingly, also reduces

the double counting error at equilibrium. The $m = 0.1$ curve is roughly optimal: there is a reduction of the double counting error by at least 75% for all geometries, and the curve is satisfyingly parallel to the exact one. Still smaller exponents probably cannot be justified and furthermore do not further improve the results. While this is a toy model case, it suggests that this very simple approach may have promise for yielding computationally tractable, and reasonably accurate residual correlation corrections. We intend to explore this in more detail in the future, with the additional important refinement that the residual correlation correction is included properly in the self-consistent iterations, rather than as a one-shot final correction, as we have done here. It will be particularly interesting to explore whether known deficiencies of PP for molecular problems, such as symmetry-breaking in benzene [118, 119], can be improved with this approach.

6.6 Discussion and Conclusions

We have analyzed the rigorous basis of various extended Kohn-Sham methods, where the auxiliary wave function (WF) contains multiple configurations (MC) rather than the regular single determinant Kohn-Sham (KS) approach. We showed that the auxiliary MC WF in a consistent map between interacting and auxiliary systems would always collapse into the single determinant KS WF. We explained the non-collapse of the auxiliary MC WF in the case of an interacting – to partially interacting mapping of systems. Partially interacting system approaches have been used to combine MC WF treatments (particularly CASSCF) of static correlation with DFT treatments of the residual dynamic correlations [105, 106, 113]. We also showed that the MC-OEP method [115] does not have a fully consistent map between its partially-interacting and non-interacting systems (the latter determines the orbitals).

Partially interacting system approaches are promising extensions to KS DFT for strongly correlated systems but face two main challenges. First, there is significant double counting between DFT dynamical correlation functionals and CASSCF treatments of static correlation. Second, the computational cost of the MC WF can increase very strongly (exponentially for CASSCF) with the number of valence electrons that are statically correlated. We presented some very simple illustrative calculations on bond-separation in H₂ to address aspects of the double counting problem, using perfect pairing (which for H₂ is equivalent to CASSCF with 2 electrons in 2 active orbitals). The results show that while obtaining a residual correlation functional that is free from double counting problems is very difficult in general, there are simple possibilities that appear to be quite promising for practical applications. We have explored just one here – others have been presented elsewhere [106, 111, 113, 206], and further progress seems likely.

It is far from clear how to address the steep increase of cost of CASSCF methods with

molecular size, but there are some interesting possibilities. One possibility is to approximate CASSCF with polynomial scaling models – perfect pairing itself is one of these, but more sophisticated examples exist [85,128]. A second possibility involves a partially interacting system that is related to the conventional spin-polarized KS method. It is possible to construct the MC WF, Ψ_S^{MC} as a spin-coupled valence bond (VB) WF, with one spatial orbital ϕ_j per valence electron [207]:

$$\Psi_S^{MC} = \hat{A} \left\{ \prod_{j=1}^N [\phi_j] \Theta(1\dots N) \right\} \quad (6.34)$$

coupled together by a spin-coupling function, Θ . If all valence electron pairs are separated (as in dissociation to high spin fragments), then the VB WF provides no correlation beyond the KS WF, but simply corrects the WF to a spin eigenfunction. Therefore it provides the ability to reach dissociation (or antiferromagnetically couple) without spin polarization (which introduces a second derivative discontinuity in the energy at the unrestricted point with all current functionals [187]). Recently it has been shown that the spin coupling function, Θ , while formally exponentially expensive with the number of coupled pairs [207], can correctly recover the dissociation limit with only pairwise re-coupling (i.e. a quadratic number of spin coupling coefficients) [184]. Therefore a VB WF can also be a computationally efficient reference wave function for describing a partially interacting system, and thereby potentially offer a new route towards a tractable MC DFT.

Chapter 7

Conclusions & Outlook

7.1 Summary

In the course of this research, many of the known failures of the generalized valence bond-coupled cluster (GVB-CC) methods have been addressed and thereby the GVB-CC methods have been improved. These improvements were made while keeping the computational efficiency of the GVB-CC methods. A broader range of a molecular systems can now be examined with the improved GVB-CC methods usually with better results than the previous generation of GVB-CC methods.

The issues with symmetry breaking (SB) in aromatic molecules such as benzene in GVB-CC methods such as perfect pairing (PP) and imperfect pairing (IP) were examined and a method to ameliorate them was proposed in chapter 2. The origin of the SB is identifiable as over correlation of localized structures due to omitted inter-pair correlations. PP only correlates electrons within one pair, and IP only correlates electrons between two pairs. Pilot orbital optimized active space Møller-Plesset second-order perturbation theory (MP2) calculations that coupled only one and two pairs of electrons produced results similar to those of PP and IP for the model system of distorting benzene from a D_{6h} structure to a D_{3h} structure. The orbital optimized active space MP2 calculations that coupled three pairs of electrons are the first that significantly reduce the SB in the benzene model system. Based on this data, a new mixed Lagrangian method known as three-pair corrected IP (TIP) was proposed. The TIP method treats the strong (IP-type) inter-pair correlations at the coupled cluster level, and the weaker and more numerous correlations coupling up to three pairs are treated with second-order perturbation theory. TIP reduces the magnitude of the over correlation of local structures error by a factor of 10 to 20, and reduces the magnitude of SB effects by a similar factor. Several aromatic hydrocarbons were analyzed with TIP, and for each case the SB effects of TIP were greatly reduced compared to IP. An interesting feature of the TIP optimized orbitals is that the σ bonding and core or-

bitals localize strongly into bonds while the aromatic π bonding orbitals delocalize over the molecule. TIP gives a better balanced description of local and non-local static correlations while still reducing SB compared to PP and IP.

The rotational invariance of the orbitals and the resulting artifacts in the TIP method was addressed in chapter 3. Methods that combine coupled cluster theory for strong correlations and perturbation theory for weaker correlations give incompatible estimates for the energy-lowering associated with a given amplitude. These differences can lead to re-ordering of the active space orbitals to fictitiously lower the energy of the system as is observed in the case of N_2 . This problem can be alleviated by the application of a penalty function to regularize the second-order perturbation theory amplitudes. The penalty function goes to zero when the perturbation theory amplitudes have small values and rises very strongly once a threshold for the amplitudes is exceeded, t_c . To improve the quality of the TIP calculation in general, it is necessary to include a new class of amplitudes, the doubly ionic pairing amplitudes, into the strong correlations and remove another class of amplitudes, the singly ionic pairing amplitudes, entirely. The resulting improved TIP method out-performs all of its GVB-CC predecessors in terms of correlation energy recovered and SB.

The nature of the coupled cluster amplitudes in the dissociation limit when using spin-unrestricted orbitals that resemble non-interacting restricted open-shell molecular fragments was explored in chapter 4. In this spin symmetry broken reference, the physics of spin correlation is removed from the cluster equations such that they become singular. This singularity manifests itself in poor numerical conditioning of the coupled cluster amplitudes. Poor numerical conditioning prevents the finding of physical solutions and makes the process of orbital optimization impossible even though by construction there should be no strong correlations. The offending amplitudes are coupled cluster doubles (CCD) amplitudes that can be described as the PP amplitudes and the IP exchange-type amplitudes. In this dissociation limit, a degenerate subspace of solutions is created and these particular amplitudes become linearly dependent. A solution to this poor numerical conditioning is to regularize the CCD amplitudes with a dynamic penalty function of the form $-\gamma(e^{(t/t_c)^{2n}} - 1)$. Amplitude regularization renders the coupled cluster amplitude equations soluble without affecting the physical properties of the GVB-CC wavefunction using the reference of non-interacting restricted open-shell molecular fragments at dissociation.

The Unrestricted-in-Active-Pairs (UAP) approximation for spin-unrestriction of valence active space correlation methods was formulated and its utility was assessed in chapter 5. For active space methods that truncate the included correlations, spin-unrestriction is a necessary tool to accurately describe the correlated wavefunction at dissociation. UAP limits the spin-unrestriction to occur only in within the space of two orbitals (one bonding, one anti-bonding) instead of the usual completely independent variation of α and β orbitals. UAP produces solutions which smoothly transition from a spin-restricted so-

lution at equilibrium to a spin-polarized solution of non-interacting restricted open-shell molecular fragments at dissociation. UAP is implemented to work with up to the 2P GVB-CC model, and the pair-by-pair definition of spin-unrestriction is utilized to make an efficient algorithm for spin-unrestricted orbital optimization. To ensure well-behaved amplitudes, a penalty function term is added only to the GVB-CC equations that caused the poor numerical conditioning observed in chapter 4. UAP removes the artifacts associated with spin-unrestriction in valence active space correlation methods [87]. UAP is shown to improve the description of spin polarized systems (dissociating molecules and radical) compared to free spin-unrestriction.

A rigorous analysis of combining Kohn-Sham density functional theory (KS DFT) methods with auxiliary wavefunctions containing multiple configurations instead of a single Slater determinant was performed in 6. It was shown that the auxiliary multi-configurational (MC) wavefunction in a consistent map between interacting and auxiliary systems will always collapse into the single determinant KS wavefunction. There is a non-collapse in the case of interacting to partially interacting mapping of systems. The partially interacting system approach is promising as it shows that KS DFT can be extended for strongly correlating systems. The main issues with using MC DFT is double counting of the correlation energy and coping with high computational cost of most MC wavefunction based methods. Results on combining DFT for residual correlation with a relatively inexpensive MC wavefunction method, PP, were presented. These results show promise for the improvement of methods combining GVB-CC and DFT with respect to both double counting and computational efficiency.

Some recommendations can be made based on this work regarding appropriate methods to treat strongly correlated systems. For any system that must describe non-local correlations, (like conjugated π systems like polyacenes [34,35] and polyenes [37]), the modified TIP method presented in chapter 3 should be used. The drawback to this method is that to date it is only fully developed and implemented in a spin-restricted formalism. For spin-polarized systems, the UAP approximation needs to be used with the GVB-CC methods to produce smooth potential energy surfaces and good molecular orbitals and properties. In instances where an orbital guess is desired for a higher-order CC calculation (such as valence active space optimized coupled cluster doubles (VOD) [81] or perfect quadruples (PQ) [85]), UAP-PP is recommended and is the default in the current implementation of Q-Chem [142]. The combination of GVB-CC with DFT for residual correlation is quite useful conceptually as it demonstrates that near chemical accuracy can be achieved without the complicated and laborious measures taken by other methods to approach that level of accuracy. The implementation of GVB-CC+DFT presented here is a proof of principle that very likely can be improved for general use on many types of molecular systems.

7.2 Future Research Directions

The research in this work has produced good results and can be extended in the future. First, the UAP approximation is of general value for approximate active space methods and can be implemented to work with all forms of valence active space orbital optimized quantum chemical methods. The methods that are correlation complete (ie. CASSCF or the appropriate higher order truncated orbital optimized CC models) do not need spin-unrestriction, but other truncated models such as valence active space optimized coupled cluster doubles (VOD) [81], perfect quadruples (PQ) [85], and perfect hexuples (PH) can benefit from the inclusion of UAP.

The TIP model could be improved and also extended to the UAP spin-unrestricted framework. A pilot spin-unrestricted version of the modified TIP has been implemented, but it exhibited convergence problems. Integrating the UAP model fully with GDM [30] to optimize all the necessary rotation angles should greatly fix these convergence problems. The original TIP models were constructed without a working implementation of the singly ionic pairing amplitudes being treated with CC theory. With the creation of the two pair doubles (2P) model, the TIP method can possibly be improved by the inclusion of the singly ionic pairing amplitudes treated with CC. The use of mixed coupled cluster/perturbation theory Lagrangians can also be expanded from the examples presented here. Even though it is computationally slower, the amplitudes coupling four different electron pairs could be included into the TIP second-order perturbation theory Lagrangian. Also, the TIP second-order perturbation theory Lagrangian can be integrated with the current implementation of PQ [85] to improve that method with regards to SB.

The combination of GVB-CC with DFT holds promising future prospects. The formulation presented in chapter 6 is only integrated with PP and only guaranteed to work for systems with one pair of active electrons. Preliminary work has been done to improve the residual energy to reduce double counting for PP by using a geminal form to construct the density used by the DFT correlation functional and incorporate more than one pair of electrons into the active space. The DFT residual correlation correction could be connected to any other static correlation model (such as imperfect pairing with doubly ionic pairing (IP+DIP) [119], 2P, PQ [85], VOD [81], or CC-VB [184]) with appropriately designed residual energy expressions to eliminate double counting. The DFT residual correlation correction is presented only utilizing the correlation function of Lee Yang and Parr [122], however a specifically designed DFT correlation function could substantially improve the performance of the method. The overall prospects resulting from the research described in this dissertation are therefore quite encouraging for future developments of fast, accurate quantum chemical methods.

Appendix A

Supporting Information

A.1 Chapter 3: Penalty functions for combining coupled cluster and perturbation amplitudes in local correlation methods with optimized orbitals

A.1.1 Amplitude Equations

Restricted closed-shell TIP infinite-order coupled-cluster amplitude equations

The TIP Lagrangian and \hat{T} amplitude equations for the restricted closed-shell coupled-cluster case are presented below. They were derived by eliminating the singles, non-local doubles and SIP type amplitudes from the spin-orbit CCSD equations [77]. The following definitions apply, with RHS being the right hand side of the amplitude equation:

$$D_{ij}^{ab} = f_{ii} + f_{jj} - f_{aa} - f_{bb} \quad (\text{A.1})$$

$$\omega_{ij}^{ab} = \text{RHS} - t_{ij}^{ab} D_{ij}^{ab} \quad (\text{A.2})$$

- The infinite-order Lagrangian is

$$L_{IP+DIP}^{(\infty)} = \sum_i^v \langle ii|i^*i^* \rangle t_{ii}^{i^*i^*} + \lambda_{ii}^{i^*i^*} \omega_{ii}^{i^*i^*} + \sum_{ij}^v (1 - \delta_{ij}) \left\{ \begin{aligned} & [2\langle ij|i^*j^* \rangle - \langle ij|j^*i^* \rangle] t_{ij}^{i^*j^*} + \lambda_{ij}^{i^*j^*} \omega_{ij}^{i^*j^*} \\ & + [2\langle ij|j^*i^* \rangle - \langle ij|i^*j^* \rangle] t_{ij}^{j^*i^*} + \lambda_{ij}^{j^*i^*} \omega_{ij}^{j^*i^*} \\ & + \langle ii|j^*j^* \rangle t_{ii}^{j^*j^*} + \lambda_{ii}^{j^*j^*} \omega_{ii}^{j^*j^*} \end{aligned} \right\}. \quad (\text{A.3})$$

- Opposite spin \hat{T} -amplitude equations including couplings via the Fock operator to the second-order perturbation theory amplitudes. For the $t_{ij}^{i^*j^*}$, $t_{ij}^{j^*i^*}$, and $t_{ii}^{j^*j^*}$ equations, $i \neq j$, and P_{ij} is defined as $P_{ij}(x_{ij}) = x_{ij} + x_{ji}$. All sums run over active electron pairs only.

$$\begin{aligned}
 D_{ii}^{i^*i^*} t_{ii}^{i^*i^*} &= \langle ii|i^*i^* \rangle - (a_{ii}^{ii} + \langle i^*i^*|i^*i^* \rangle) t_{ii}^{i^*i^*} - (2e_{i^*}^{i^*} + 2e_i^i) t_{ii}^{i^*i^*} \\
 &\quad + \sum_k \left\{ (1 - \delta_{ki}) [a_{ii}^{kk} t_{kk}^{i^*i^*} + \langle k^*k^*|i^*i^* \rangle t_{ii}^{k^*k^*}] \right. \\
 &\quad \left. + (2j_{ik^*}^{i^*k} - k_{ik^*}^{ki^*}) (2t_{ik^*}^{i^*k^*} - t_{ik^*}^{k^*i^*}) - 3k_{ik^*}^{ki^*} t_{ik^*}^{k^*i^*} \right\}
 \end{aligned} \tag{A.4}$$

$$\begin{aligned}
 D_{ij}^{i^*j^*} t_{ij}^{i^*j^*} &= \langle ij|i^*j^* \rangle + (a_{ij}^{ij} - e_{i^*}^{i^*} - e_{j^*}^{j^*} - e_i^i - e_j^j) t_{ij}^{i^*j^*} + a_{ij}^{ij} t_{ij}^{i^*j^*} \\
 &\quad + \sum_{k \neq i,j} \left\{ t_{ij}^{i^*k^*} f_{j^*k^*} + t_{ij}^{k^*j^*} f_{i^*k^*} - t_{kj}^{i^*j^*} f_{ki} - t_{ik}^{i^*j^*} f_{kj} \right\} \\
 &\quad + P_{ij} \left\{ \sum_k \frac{1}{2} \left[(2j_{ik^*}^{i^*k} - k_{ik^*}^{ki^*}) (2t_{kj}^{k^*j^*} - t_{kj}^{j^*k^*}) - k_{ik^*}^{ki^*} t_{kj}^{j^*k^*} \right] \right. \\
 &\quad \left. - k_{ij^*}^{ij^*} t_{ij}^{i^*j^*} - k_{ii^*}^{jj^*} t_{jj}^{i^*i^*} \right\}
 \end{aligned} \tag{A.5}$$

$$\begin{aligned}
 D_{ij}^{j^*i^*} t_{ij}^{j^*i^*} &= \langle ij|j^*i^* \rangle + (a_{ij}^{ij} - e_{j^*}^{j^*} - e_{i^*}^{i^*} - e_j^j - e_i^i) t_{ij}^{j^*i^*} + a_{ij}^{ij} t_{ij}^{j^*i^*} \\
 &\quad + \sum_{k \neq i,j} \left\{ t_{ij}^{j^*k^*} f_{i^*k^*} + t_{ij}^{k^*i^*} f_{j^*k^*} - t_{kj}^{j^*i^*} f_{ki} - t_{ik}^{j^*i^*} f_{kj} \right\} \\
 &\quad + P_{ij} \left\{ \frac{1}{2} (2j_{ij^*}^{j^*i} - k_{ij^*}^{ij^*}) (2t_{ij}^{j^*i^*} - t_{ij}^{i^*j^*}) + (j_{ii^*}^{j^*j} - k_{ii^*}^{jj^*}) t_{jj}^{i^*i^*} \right. \\
 &\quad \left. - \frac{1}{2} k_{ij^*}^{ij^*} t_{ij}^{i^*j^*} - \sum_k k_{ik^*}^{ki^*} t_{kj}^{j^*k^*} \right\}
 \end{aligned} \tag{A.6}$$

$$\begin{aligned}
 D_{ii}^{j^*j^*} t_{ii}^{j^*j^*} &= \langle ii|j^*j^* \rangle + \sum_k \left[a_{ii}^{kk} t_{kk}^{j^*j^*} + \langle j^*j^*|k^*k^* \rangle t_{ii}^{k^*k^*} \right] \\
 &\quad + \sum_{k \neq i,j} \left\{ (t_{ii}^{j^*k^*} + t_{ii}^{k^*j^*}) f_{j^*k^*} - (t_{ki}^{j^*j^*} + t_{ik}^{j^*j^*}) f_{ki} \right\} \\
 &\quad - 2(e_{j^*}^{j^*} + e_i^i) t_{ii}^{j^*j^*} + (2j_{ii^*}^{j^*j} - k_{ii^*}^{jj^*}) (2t_{ij}^{j^*i^*} - t_{ij}^{i^*j^*}) \\
 &\quad - 3k_{ii^*}^{jj^*} t_{ij}^{i^*j^*} + (2j_{ij^*}^{j^*i} - 4k_{ij^*}^{ij^*}) t_{ii}^{j^*j^*}
 \end{aligned} \tag{A.7}$$

where the following intermediates are defined:

$$a_{ii}^{jj} = \langle ij|ji \rangle + \sum_k \langle k^*j|jk^* \rangle t_{ii}^{k^*k^*} \tag{A.8}$$

$$\begin{aligned}
 \text{(for } i \neq j) \quad a_{ij}^{ij} &= \langle ij|ij \rangle + \langle i^*j^*|i^*j^* \rangle \\
 &\quad + \langle ij|i^*j^* \rangle t_{ij}^{j^*j^*} + \langle ij|j^*i^* \rangle t_{ij}^{j^*i^*}
 \end{aligned} \tag{A.9}$$

$$\begin{aligned}
 \text{(for } i \neq j) \quad a_{ij}^{ji} &= \langle ji|ij \rangle + \langle j^*i^*|i^*j^* \rangle \\
 &\quad + \langle ji|i^*j^* \rangle t_{ij}^{i^*j^*} + \langle ji|j^*i^* \rangle t_{ij}^{i^*i^*}
 \end{aligned} \tag{A.10}$$

$$e_i^i = \langle ii|i^*i^* \rangle t_{ii}^{i^*i^*} + \sum_k^v (1 - \delta_{ik}) \left\{ [2\langle ik|i^*k^* \rangle - \langle ik|k^*i^* \rangle] t_{ik}^{i^*k^*} + [2\langle ik|k^*i^* \rangle - \langle ik|i^*k^* \rangle] t_{ik}^{k^*i^*} + \langle ik|k^*k^* \rangle t_{ii}^{k^*k^*} \right\} \quad (\text{A.11})$$

$$e_{i^*}^{i^*} = \langle ii|i^*i^* \rangle t_{ii}^{i^*i^*} + \sum_k^v (1 - \delta_{ik}) \left\{ [2\langle ik|i^*k^* \rangle - \langle ik|k^*i^* \rangle] t_{ik}^{i^*k^*} + [2\langle ik|k^*i^* \rangle - \langle ik|i^*k^* \rangle] t_{ik}^{k^*i^*} + \langle kk|i^*i^* \rangle t_{kk}^{i^*i^*} \right\} \quad (\text{A.12})$$

$$j_{ij^*}^{j^*i} = \langle j^*i|ij^* \rangle + \frac{1}{2}(1 - \delta_{ji}) \left\{ -\langle ij|j^*i^* \rangle t_{ij}^{i^*j^*} + [2\langle ij|j^*i^* \rangle - \langle ij|i^*j^* \rangle] t_{ij}^{j^*i^*} \right\} \quad (\text{A.13})$$

$$j_{ij^*}^{i^*j} = \langle i^*j|ij^* \rangle + \frac{1}{2} \sum_k^v \left\{ -\langle jk|j^*k^* \rangle t_{ik}^{k^*i^*} + [2\langle jk|j^*k^* \rangle - \langle jk|k^*j^* \rangle] t_{ik}^{i^*k^*} \right\} \quad (\text{A.14})$$

$$j_{jj^*}^{i^*i} = \langle i^*i|jj^* \rangle + \frac{1}{2} \langle ii|j^*j^* \rangle (t_{ij}^{j^*i^*} - t_{ij}^{i^*j^*}) + \frac{1}{2} (\langle ij|j^*i^* \rangle - \langle ij|i^*j^* \rangle) t_{jj}^{i^*i^*} \quad (\text{A.15})$$

$$k_{ij^*}^{ji^*} = \langle ji^*|ij^* \rangle - \frac{1}{2} \sum_k^v \langle jk|k^*j^* \rangle t_{ik}^{k^*i^*} \quad (\text{A.16})$$

$$k_{ij^*}^{ij^*} = \langle ij^*|ij^* \rangle - \frac{1}{2}(1 - \delta_{ij}) \left[\langle ij|i^*j^* \rangle t_{ij}^{i^*j^*} + \langle ii|j^*j^* \rangle t_{ii}^{j^*j^*} \right] \quad (\text{A.17})$$

$$k_{jj^*}^{ii^*} = \langle ii^*|jj^* \rangle - \frac{1}{2}(1 - \delta_{ij}) \left[\langle ii|j^*j^* \rangle t_{ij}^{j^*j^*} + \langle ij|i^*j^* \rangle t_{jj}^{i^*i^*} \right] \quad (\text{A.18})$$

Restricted closed-shell TIP second-order perturbation theory amplitude equations

The TIP Lagrangian and \hat{T} amplitude equations for the restricted closed-shell second-order perturbation theory case are presented below. They include the necessary definitions for the penalty function.

- The second-order Lagrangian is

$$L_{3P}^{(2)} = \sum_i^v \sum_{j \neq i}^v \sum_{k \neq i, j}^v \left\{ \tau_{ij}^{i^*k^*} \langle ij|i^*k^* \rangle + \lambda_{ij}^{i^*k^*} \omega_{ij}^{i^*k^*} + \tau_{ij}^{k^*i^*} \langle ij|k^*i^* \rangle + \lambda_{ij}^{k^*i^*} \omega_{ij}^{k^*i^*} + \tau_{ij}^{j^*k^*} \langle ij|j^*k^* \rangle + \lambda_{ij}^{j^*k^*} \omega_{ij}^{j^*k^*} + \tau_{ij}^{k^*j^*} \langle ij|k^*j^* \rangle + \lambda_{ij}^{k^*j^*} \omega_{ij}^{k^*j^*} + t_{ii}^{j^*k^*} \langle ii|j^*k^* \rangle + \lambda_{ii}^{j^*k^*} \omega_{ii}^{j^*k^*} + t_{ij}^{k^*k^*} \langle ij|k^*k^* \rangle + \lambda_{ij}^{k^*k^*} \omega_{ij}^{k^*k^*} \right\}, \quad (\text{A.19})$$

• with the following amplitude definitions, γ and α are the penalty parameters for the TIP method.

$$(D_{ii}^{j^*k^*} - \gamma e^{\alpha t_{ii}^{j^*k^*2}}) t_{ii}^{j^*k^*} = \langle ii|j^*k^* \rangle \quad (\text{A.20})$$

$$(D_{ij}^{k^*k^*} - \gamma e^{\alpha t_{ij}^{k^*k^*2}}) t_{ij}^{k^*k^*} = \langle ij|k^*k^* \rangle \quad (\text{A.21})$$

$$(D_{i\bar{j}}^{i^*\bar{k}^*} - \gamma e^{\alpha t_{i\bar{j}}^{i^*\bar{k}^*2}}) t_{i\bar{j}}^{i^*\bar{k}^*} = \langle i\bar{j}|i^*\bar{k}^* \rangle \quad (\text{A.22})$$

$$(D_{ij}^{i^*k^*} - \gamma e^{\alpha t_{ij}^{i^*k^*2}}) t_{ij}^{i^*k^*} = \langle ij|i^*k^* \rangle - \langle ij|k^*i^* \rangle \quad (\text{A.23})$$

$$(D_{i\bar{j}}^{i^*\bar{i}^*} - \gamma e^{\alpha t_{i\bar{j}}^{i^*\bar{i}^*2}}) t_{i\bar{j}}^{i^*\bar{i}^*} = \langle i\bar{j}|k^*\bar{i}^* \rangle \quad (\text{A.24})$$

$$(D_{ij}^{k^*i^*} - \gamma e^{\alpha t_{ij}^{k^*i^*2}}) t_{ij}^{k^*i^*} = \langle ij|k^*i^* \rangle - \langle ij|i^*k^* \rangle \quad (\text{A.25})$$

$$(D_{i\bar{j}}^{j^*\bar{k}^*} - \gamma e^{\alpha t_{i\bar{j}}^{j^*\bar{k}^*2}}) t_{i\bar{j}}^{j^*\bar{k}^*} = \langle i\bar{j}|j^*\bar{k}^* \rangle \quad (\text{A.26})$$

$$(D_{ij}^{j^*k^*} - \gamma e^{\alpha t_{ij}^{j^*k^*2}}) t_{ij}^{j^*k^*} = \langle ij|j^*k^* \rangle - \langle ij|k^*j^* \rangle \quad (\text{A.27})$$

$$(D_{i\bar{j}}^{k^*\bar{j}^*} - \gamma e^{\alpha t_{i\bar{j}}^{k^*\bar{j}^*2}}) t_{i\bar{j}}^{k^*\bar{j}^*} = \langle i\bar{j}|k^*\bar{j}^* \rangle \quad (\text{A.28})$$

$$(D_{ij}^{k^*j^*} - \gamma e^{\alpha t_{ij}^{k^*j^*2}}) t_{ij}^{k^*j^*} = \langle ij|k^*j^* \rangle - \langle ij|j^*k^* \rangle \quad (\text{A.29})$$

$$\tau_{ij}^{i^*k^*} = t_{i\bar{j}}^{i^*\bar{k}^*} + t_{ij}^{i^*k^*} \quad (\text{A.30})$$

$$\tau_{ij}^{k^*i^*} = t_{i\bar{j}}^{k^*\bar{i}^*} + t_{ij}^{k^*i^*} \quad (\text{A.31})$$

$$\tau_{ij}^{j^*k^*} = t_{i\bar{j}}^{j^*\bar{k}^*} + t_{ij}^{j^*k^*} \quad (\text{A.32})$$

$$\tau_{ij}^{k^*j^*} = t_{i\bar{j}}^{k^*\bar{j}^*} + t_{ij}^{k^*j^*} \quad (\text{A.33})$$

A.1.2 Supplementary Figures

Presented here are the same larger molecules as explored in Chapter 2 with the penalized Mixed Lagrangian for TIP.

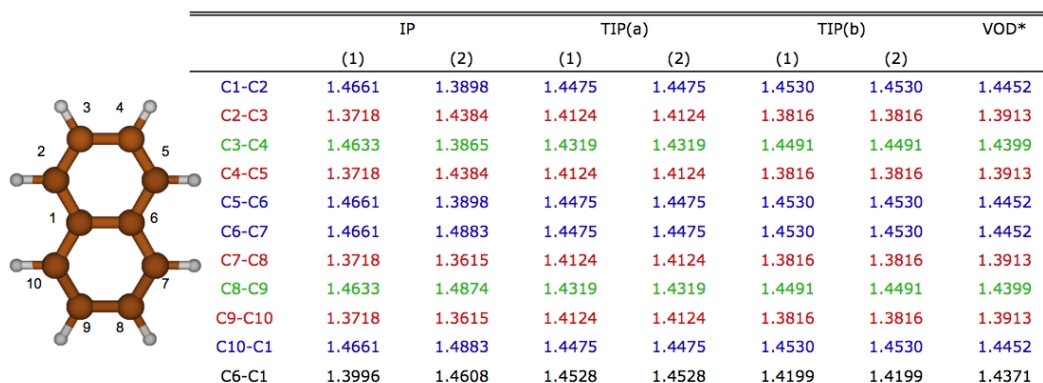


Figure A.1: A chart of the optimized bond lengths for naphthalene as solved by TIP with the 6-31G*. Structure (1) for each level of theory is a D_{2h} guess structure; structure (2) is from a C_{2v} guess. The TIP (a) bond lengths are without any penalty function. The TIP (b) bond lengths are with the re-formulation and penalty function. All bond lengths are in Å. *The VOD bond lengths are with the 6-31G basis set.

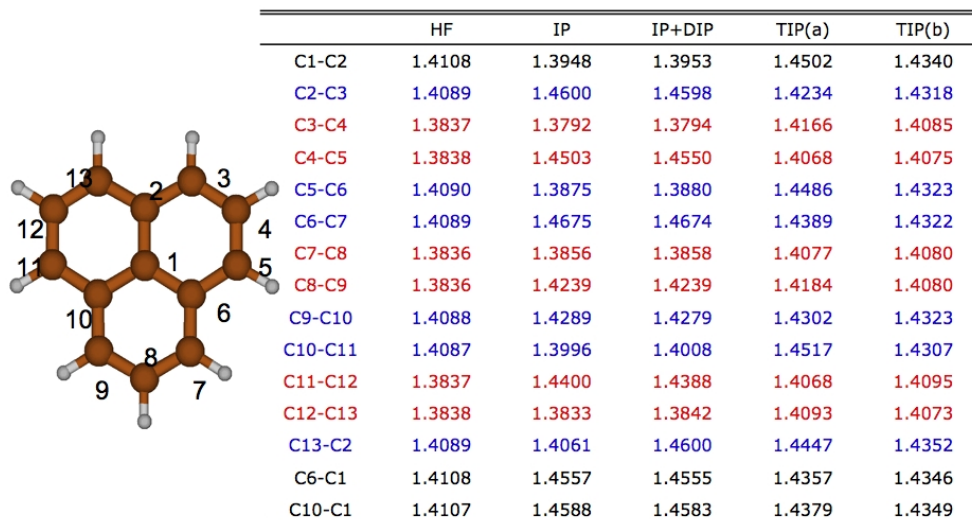


Figure A.2: A chart of the optimized bond lengths for phenalenyl cation as solved by TIP with the 6-31G*. The TIP (a) bond lengths are without any penalty function. The TIP (b) bond lengths are with the re-formulation and penalty function. All bond lengths are in Å.

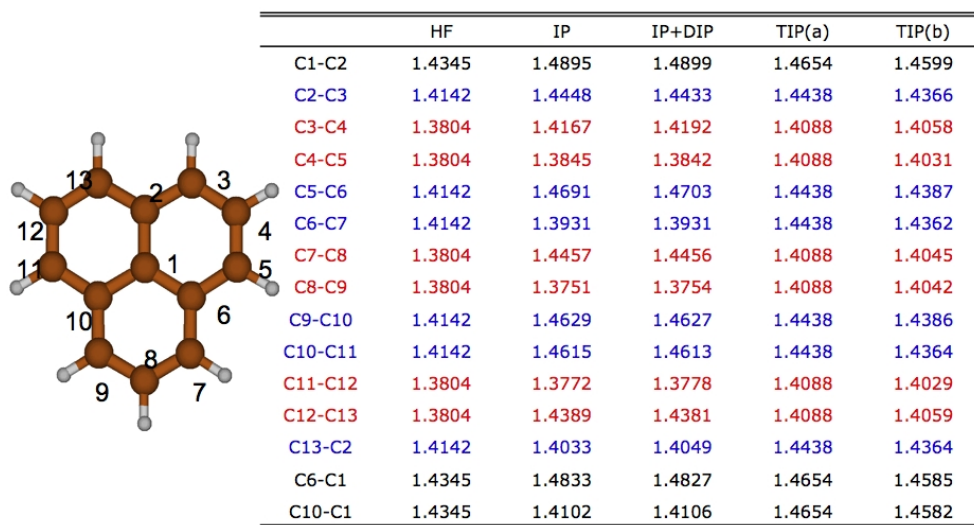


Figure A.3: A chart of the optimized bond lengths for phenalenyl anion as solved by TIP with the 6-31G*. The TIP (a) bond lengths are without any penalty function. The TIP (b) bond lengths are with the re-formulation and penalty function. All bond lengths are in Å.

A.2 Chapter 4: The numerical condition of electron correlation theories when only active pairs of electrons are spin-unrestricted

In the arguments that follow, a pair correspondence between alpha and beta spin orbitals will be assumed by our notation. We enforce such a correspondence on our constrained CC models, however we note that by the pairing theorem [208] it is valid to apply such language to unrestricted wave-functions generally, as they may be cast into this form. The electronic Hamiltonian is separable into operators affecting each fragment separately $\hat{H} = \hat{H}_1 + \hat{H}_2$, and because of the high-spin structure of our reference any opposite-spin doubles amplitude doesn't alter the number of electrons on a fragment (only their spin), and spatial symmetry dictates that the spatial parts of the orbital in each pair should be the same on both fragments.

A.2.1 The Two Electron-Pair Case.

	t_{11}^{1*1*}	t_{12}^{2*1*}	t_{21}^{1*2*}	t_{22}^{2*2*}
t_{11}^{1*1*}	0.102	-0.047	-0.056	0.000
t_{12}^{2*1*}	-0.047	0.102	0.000	-0.056
t_{21}^{1*2*}	-0.056	0.000	0.102	-0.047
t_{22}^{2*2*}	0.000	-0.056	-0.047	0.102

Table A.1: Linear coupling matrix for the PP and IP exchange amplitudes for fluoroethene (HFC=CH₂) at a C-C bond length of 7.50 Å with unrestricted PP orbitals in the minimal active space.

The situation of the 2-pair case of two-atom dissociation (an active space with 4 spatial, 8 spin orbitals) is similar physically to that of the 1-pair case. However, instead of two degenerate states that we can use the amplitudes to decide between, there is a larger degenerate subspace leading to far more zeroes in our Hamiltonian. The couplings between these degenerate states again leads to potentially infinite amplitudes, and the necessity of solving the CC equations iteratively leads to quite a problem here. A simple description of these degenerate doubly excited references can be obtained with the pairing notion, as there are amplitudes that show coupling within a pair (PP), ie: \hat{T}_{11}^{1*1*} , and opposite spin (OS) exchange-type amplitudes that couple the two pairs (IP), ie: \hat{T}_{12}^{2*1*} . Because the determinants generated by all of these amplitudes only differ from the reference by flipping the spins of two of the spin-orbitals, the diagonal of the doubles-doubles block of the Hamiltonian is some value, a . Breaking down the off-diagonal matrix element coupling a PP amplitude to an IP amplitude, $\langle \Phi_{11}^{1*1*} | \hat{H} | \Phi_{12}^{2*1*} \rangle$, over the two fragments, we see that on one fragment the projections of these determinants are the same as generated on the diagonal

of \hat{H} . Because the two determinants differ by 2 spin-orbitals the matrix element is a single integral, $(12|\bar{1}^*\bar{2}^*)$ which may be identified with the integral examined in the 1-pair case. These matrix elements which share a single index may be denoted b . Matrix elements which share no indices, ie. PP of one pair with PP of the other, differ by more than two spin orbitals and are thus zero. The result is that the Hamiltonian has the following structure (in the basis: $\hat{T}_{1\bar{1}}^{1^*1^*}$, $\hat{T}_{1\bar{2}}^{2^*1^*}$, $\hat{T}_{2\bar{1}}^{1^*2^*}$, $\hat{T}_{2\bar{2}}^{2^*2^*}$):

$$\hat{H} = (\hat{H}_1 + \hat{H}_2) = \begin{pmatrix} a & b & b & 0 \\ b & a & 0 & b \\ b & 0 & a & b \\ 0 & b & b & a \end{pmatrix} \quad (\text{A.34})$$

This matrix is singular if $b = -a/2$ which is empirically found to be the case, and explained below. Of course this is only a sub-block of the linear coupling matrix, U, which would occur in complete CCD, and we affirm with calculations that in unrestricted CCD as it is usually practiced this is not a concern.

A.2.2 The Many-Pair Case.

	$t_{1\bar{1}}^{1^*1^*}$	$t_{1\bar{2}}^{2^*1^*}$	$t_{1\bar{3}}^{3^*1^*}$	$t_{2\bar{1}}^{1^*2^*}$	$t_{2\bar{2}}^{2^*2^*}$	$t_{2\bar{3}}^{3^*2^*}$	$t_{3\bar{1}}^{1^*3^*}$	$t_{3\bar{2}}^{2^*3^*}$	$t_{3\bar{3}}^{3^*3^*}$
$t_{1\bar{1}}^{1^*1^*}$	0.142	-0.036	-0.036	-0.036	0.000	0.000	-0.036	0.000	0.000
$t_{1\bar{2}}^{2^*1^*}$	-0.036	0.142	-0.036	0.000	-0.036	0.000	0.000	-0.036	0.000
$t_{1\bar{3}}^{3^*1^*}$	-0.036	-0.036	0.142	0.000	0.000	-0.036	0.000	0.000	-0.036
$t_{2\bar{1}}^{1^*2^*}$	-0.036	0.000	0.000	0.142	-0.036	-0.036	-0.036	0.000	0.000
$t_{2\bar{2}}^{2^*2^*}$	0.000	-0.036	0.000	-0.036	0.142	-0.036	0.000	-0.036	0.000
$t_{2\bar{3}}^{3^*2^*}$	0.000	0.000	-0.036	-0.036	-0.036	0.142	0.000	0.000	-0.036
$t_{3\bar{1}}^{1^*3^*}$	-0.036	0.000	0.000	-0.036	0.000	0.000	0.142	-0.036	-0.036
$t_{3\bar{2}}^{2^*3^*}$	0.000	-0.036	0.000	0.000	-0.036	0.000	-0.036	0.142	-0.036
$t_{3\bar{3}}^{3^*3^*}$	0.000	0.000	-0.036	0.000	0.000	-0.036	-0.036	-0.036	0.142

Table A.2: Linear coupling matrix for the PP and IP exchange amplitudes for nitrogen (N_2) at a N-N bond length of 7.50 Å with unrestricted PP orbitals in the minimal active space in the 6-31G* basis.

In general, for a given PP amplitude there are three classes of possible OS exchange IP amplitudes: those which share no indices, those which excite from the same α orbital (we will call this one the fragment 1 corresponding IP amplitude) and those which excite from the same β orbital (fragment 2). The matrix elements of these combinations were examined above. If two IP amplitudes excite from a common index they will also have a nonzero matrix element b , and with these rules in hand one may construct \hat{H} . Consider a blocking of \hat{H}_{IJ} such that a PP amplitude I and its corresponding fragment 1 IP amplitudes (indexed by J) are grouped together in a block which is ordered by their beta indices. In conventional spin-orbital notation this ordering is written: $\{\hat{T}_{i\bar{1}}^{1^*i^*}, \hat{T}_{i\bar{2}}^{2^*i^*}, \hat{T}_{i\bar{i}}^{i^*i^*}, \dots, \hat{T}_{i\bar{n}}^{n^*i^*}\}$.

Symbolically one may construct the diagonal block (\underline{A}) for the general case and see that it has the shape below, and determinant $(a - b)^{n-1}(a + (n - 1)b)$. The off-diagonal blocks (\underline{B}) are themselves diagonal, with value b and determinant b^n . The complete matrix has the following block structure with this ordering, and the determinant of \hat{H} for n pairs ($n > 2$) is $(a - 2b)^{(n-1)^2}(a + (n - 2)b)^{2(n-1)}(a + 2(n - 1)b)$. The matrix will be singular when $b = -a/2$, or if $(a + (n - 2)b) = 0$ or $(a + 2(n - 1)b) = 0$. In the full space, correlations of spin-paired basis functions often lift this linear dependence by coupling to this block, explaining the robust strength of unrestricted coupled cluster demonstrated in the literature.

$$\underline{A} = \begin{bmatrix} a & b & \cdots & b \\ b & a & \cdots & b \\ \vdots & & \ddots & \vdots \\ b & b & \cdots & a \end{bmatrix} ; \underline{B} = \begin{bmatrix} b & 0 & \cdots & 0 \\ 0 & b & \cdots & 0 \\ \vdots & & \ddots & \vdots \\ 0 & 0 & \cdots & b \end{bmatrix} ; \hat{H} = \begin{bmatrix} \underline{A} & \underline{B} & \cdots & \underline{B} \\ \underline{B} & \underline{A} & \cdots & \underline{B} \\ \vdots & & \ddots & \vdots \\ \underline{B} & \underline{B} & \cdots & \underline{A} \end{bmatrix} \quad (\text{A.35})$$

A.3 Chapter 5: Orbitals that are unrestricted in active pairs for GVB-CC methods

A.3.1 Additional timings

The following tables present additional timings tables to compare UAP-PP to restricted PP and freely spin-unrestricted PP.

	Method	Initial Guess (s)	Time per Iter. (s)	Num. of Iter.
Methane	Restricted	2.98	2.22	11
Methane	Free Unrest.	8.71	4.00	12
Methane	UAP	4.74	2.46	12
Ethane	Restricted	112.53	22.99	12
Ethane	Free Unrest.	225.02	42.84	13
Ethane	UAP	115.12	24.97	12
Propane	Restricted	62.31	115.33	12
Propane	Free Unrest.	115.02	218.40	14
Propane	UAP	57.81	122.12	13
Butane	Restricted	177.84	386.91	13
Butane	Free Unrest.	464.58	742.57	14
Butane	UAP	186.36	404.17	13

Table A.3: A timing comparison against all the developed spin implementations of PP. All calculations done in the aug-cc-pVDZ basis.

	Multiplicity	Initial Guess (s)	Time per Iter. (s)	Num. of Iter.
O ₂	singlet	0.70	1.85	29
O ₂	triplet	0.67	1.84	41
O ₂ ⁻¹	doublet	0.67	1.81	55
O ₂ ⁺¹	doublet	0.71	1.89	33
N ₂	singlet	0.67	1.70	18
N ₂	triplet	0.65	1.70	24
N ₂ ⁻¹	doublet	0.67	1.78	28
N ₂ ⁺¹	doublet	0.63	1.67	80
F ₂	singlet	0.73	1.97	50
F ₂	triplet	0.70	1.88	87
F ₂ ⁻¹	doublet	0.69	1.92	79
F ₂ ⁺¹	doublet	0.71	1.97	35

Table A.4: A timing comparison for different spin/charge states of diatomic molecules in UAP-PP. All calculations done in the aug-cc-pVDZ basis.

A.3.2 The need for amplitude regularization in multi-pair cases

The illustrative plot demonstrating large unphysical amplitudes for the 1-pair case is Figure 5.1. The large unphysical amplitude is manifest in the multi-pair problem as well. Figures A.4 and A.5 show the PP two angle spin-unrestriction surfaces for ethene in the

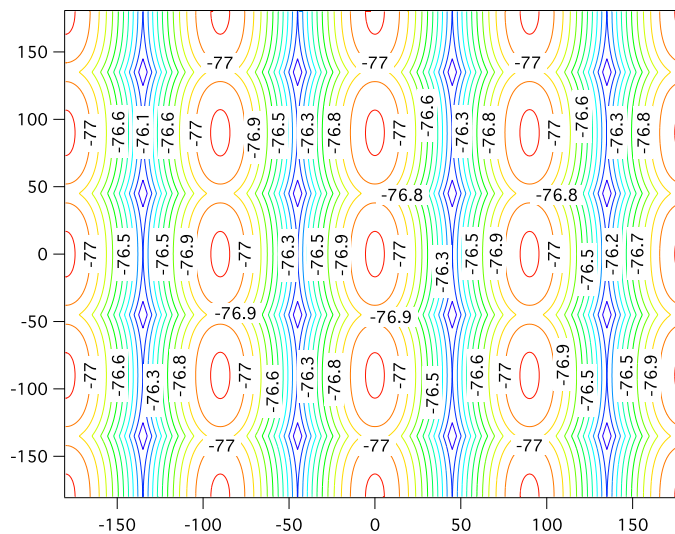


Figure A.4: The unrestriction angle PES for (4,4) ethene at 1.33 Å C-C separation in ethene using PP (choosing the most energy lowering amplitudes) with the STO-3G basis.

STO-3G basis at equilibrium and dissociation, respectively. The correlation energy overcompensation for an inverted reference leads to discontinuous cusps on the surface, and incorrect energies for dissociation channels. The solution at $(+45^\circ, +45^\circ)$ represents the appropriate triplet methylene fragments whereas the $(-45^\circ, +45^\circ)$ solution represents dissociation into open-shell singlets. The need for amplitude regularization was demonstrated in Chapter 4 and this data reinforces the conclusions made there.

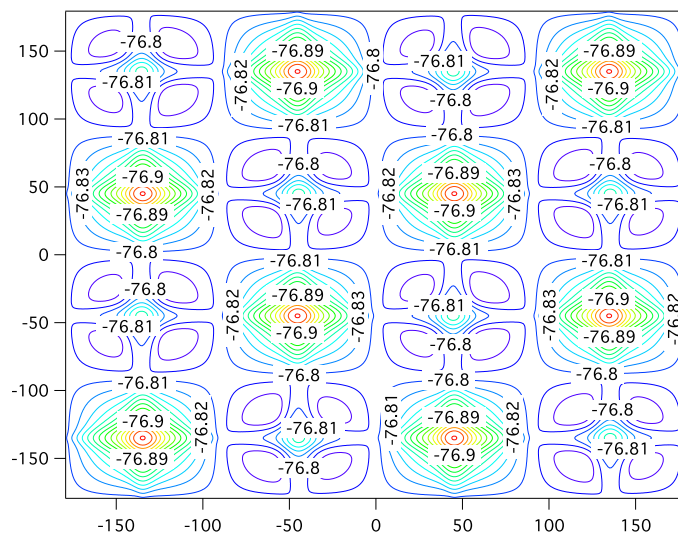


Figure A.5: The unrestricted angle PES for (4,4) ethene at 5.00 Å C-C separation in ethene using PP (choosing the most energy lowering amplitudes) with the STO-3G basis.

Appendix B

Basis Sets for Doing Electron Correlation with 3d Block Metals

These are all-electron basis sets built for doing treating 3d block metals originally created by Wachters [209,210]. The basis sets were expanded by adding higher order polarization functions of f and g angular momentum. To create the f functions' exponents, the arithmetic mean of d functions' exponents was taken. For the g functions, the arithmetic mean of the created f functions' exponents was taken. To expand and make a hexuple-zeta basis set, the contracted functions in Wachters' original basis were de-contracted and the same prescription as above was taken to fill in the missing higher angular momentum functions. Only the f and g functions are presented here, as the rest of the functions are published and available online at: <https://bse.pnl.gov/bse/portal>. The elements included here go from Sc to Zn. These basis sets ignore the f functions created by Bauschlicher et al [211] and rely only on Wachters' original basis sets.

B.1 Wachters-pQZ Basis

```

SC 0
F 1 1.00
2.000000000 1.000000000
F 1 1.00
0.600000000 1.000000000
F 1 1.00
0.180000000 1.000000000
G 1 1.00
1.095445115 1.000000000
G 1 1.00
0.328633535 1.000000000

```

TI 0

F 1 1.00

2.300000000 1.00000000

F 1 1.00

0.690000000 1.00000000

F 1 1.00

0.207000000 1.00000000

G 1 1.00

1.259761882 1.00000000

G 1 1.00

0.377928565 1.00000000

V 0

F 1 1.00

2.600000000 1.00000000

F 1 1.00

0.780000000 1.00000000

F 1 1.00

0.234000000 1.00000000

G 1 1.00

1.424078650 1.00000000

G 1 1.00

0.427223595 1.00000000

CR 0

F 1 1.00

2.900000000 1.00000000

F 1 1.00

0.870000000 1.00000000

F 1 1.00

0.261000000 1.00000000

G 1 1.00

1.588395417 1.00000000

G 1 1.00

0.476518625 1.00000000

MN 0

F 1 1.00

3.200000000 1.00000000

F 1 1.00

0.960000000 1.00000000
F 1 1.00
0.288000000 1.00000000
G 1 1.00
1.752712184 1.00000000
G 1 1.00
0.525813655 1.00000000

FE 0
F 1 1.00
3.500000000 1.00000000
F 1 1.00
1.050000000 1.00000000
F 1 1.00
0.315000000 1.00000000
G 1 1.00
1.917028951 1.00000000
G 1 1.00
0.575108685 1.00000000

CO 0
F 1 1.00
3.900000000 1.00000000
F 1 1.00
1.170000000 1.00000000
F 1 1.00
0.351000000 1.00000000
G 1 1.00
2.136117974 1.00000000
G 1 1.00
0.640835392 1.00000000

NI 0
F 1 1.00
4.300000000 1.00000000
F 1 1.00
1.290000000 1.00000000
F 1 1.00
0.387000000 1.00000000
G 1 1.00
2.355206997 1.00000000


```
G 1 1.00
0.706562099 1.00000000
****
CU 0
F 1 1.00
4.800000000 1.00000000
F 1 1.00
1.440000000 1.00000000
F 1 1.00
0.432000000 1.00000000
G 1 1.00
2.629068276 1.00000000
G 1 1.00
0.788720483 1.00000000
****
ZN 0
F 1 1.00
5.400000000 1.00000000
F 1 1.00
1.620000000 1.00000000
F 1 1.00
0.486000000 1.00000000
G 1 1.00
2.957701811 1.00000000
G 1 1.00
0.887310543 1.00000000
****
```

B.2 Wachers-p6Z Basis

```
SC 0
F 1 1.00
22.22222222 1.00000000
F 1 1.00
6.666666667 1.00000000
F 1 1.00
2.000000000 1.00000000
F 1 1.00
0.600000000 1.00000000
F 1 1.00
```

0.180000000 1.00000000
G 1 1.00
12.17161239 1.00000000
G 1 1.00
3.651483717 1.00000000
G 1 1.00
1.095445115 1.00000000
G 1 1.00
0.328633535 1.00000000

TI 0
F 1 1.00
25.55555556 1.00000000
F 1 1.00
7.666666667 1.00000000
F 1 1.00
2.300000000 1.00000000
F 1 1.00
0.690000000 1.00000000
F 1 1.00
0.207000000 1.00000000
G 1 1.00
13.99735425 1.00000000
G 1 1.00
4.199206274 1.00000000
G 1 1.00
1.259761882 1.00000000
G 1 1.00
0.377928565 1.00000000

V 0
F 1 1.00
28.88888889 1.00000000
F 1 1.00
8.666666667 1.00000000
F 1 1.00
2.600000000 1.00000000
F 1 1.00
0.780000000 1.00000000
F 1 1.00
0.234000000 1.00000000

G 1 1.00
15.82309611 1.00000000
G 1 1.00
4.746928832 1.00000000
G 1 1.00
1.424078650 1.00000000
G 1 1.00
0.427223595 1.00000000

CR 0
F 1 1.00
32.22222222 1.00000000
F 1 1.00
9.666666667 1.00000000
F 1 1.00
2.900000000 1.00000000
F 1 1.00
0.870000000 1.00000000
F 1 1.00
0.261000000 1.00000000
G 1 1.00
17.64883796 1.00000000
G 1 1.00
5.294651389 1.00000000
G 1 1.00
1.588395417 1.00000000
G 1 1.00
0.476518625 1.00000000

MN 0
F 1 1.00
35.55555556 1.00000000
F 1 1.00
10.66666667 1.00000000
F 1 1.00
3.200000000 1.00000000
F 1 1.00
0.960000000 1.00000000
F 1 1.00
0.288000000 1.00000000
G 1 1.00

19.47457982 1.00000000
G 1 1.00
5.8423739467 1.00000000
G 1 1.00
1.752712184 1.00000000
G 1 1.00
0.525813655 1.00000000

FE 0
F 1 1.00
38.88888889 1.00000000
F 1 1.00
11.66666667 1.00000000
F 1 1.00
3.500000000 1.00000000
F 1 1.00
1.050000000 1.00000000
F 1 1.00
0.315000000 1.00000000
G 1 1.00
21.30032168 1.00000000
G 1 1.00
6.390096504 1.00000000
G 1 1.00
1.917028951 1.00000000
G 1 1.00
0.575108685 1.00000000

CO 0
F 1 1.00
43.33333333 1.00000000
F 1 1.00
13.00000000 1.00000000
F 1 1.00
3.900000000 1.00000000
F 1 1.00
1.170000000 1.00000000
F 1 1.00
0.351000000 1.00000000
G 1 1.00
23.73464416 1.00000000

G 1 1.00
7.120393248 1.00000000
G 1 1.00
2.136117974 1.00000000
G 1 1.00
0.640835392 1.00000000

NI 0
F 1 1.00
47.77777778 1.00000000
F 1 1.00
14.33333333 1.00000000
F 1 1.00
4.30000000 1.00000000
F 1 1.00
1.29000000 1.00000000
F 1 1.00
0.38700000 1.00000000
G 1 1.00
26.16896664 1.00000000
G 1 1.00
7.85068999 1.00000000
G 1 1.00
2.35520699 1.00000000
G 1 1.00
0.70656209 1.00000000

CU 0
F 1 1.00
53.33333333 1.00000000
F 1 1.00
16.00000000 1.00000000
F 1 1.00
4.80000000 1.00000000
F 1 1.00
1.44000000 1.00000000
F 1 1.00
0.43200000 1.00000000
G 1 1.00
29.21186973 1.00000000
G 1 1.00

8.763560920 1.00000000
G 1 1.00
2.629068276 1.00000000
G 1 1.00
0.788720483 1.00000000

ZN 0
F 1 1.00
60.00000000 1.00000000
F 1 1.00
18.00000000 1.00000000
F 1 1.00
5.400000000 1.00000000
F 1 1.00
1.620000000 1.00000000
F 1 1.00
0.486000000 1.00000000
G 1 1.00
32.86335345 1.00000000
G 1 1.00
9.859006035 1.00000000
G 1 1.00
2.957701811 1.00000000
G 1 1.00
0.887310543 1.00000000

Bibliography

- [1] E. Schrödinger, Annalen Der Physik **77**, 43 (1925).
- [2] E. Schrödinger, Annalen Der Physik **79**, 361 (1926).
- [3] E. Schrödinger, Annalen Der Physik **79**, 489 (1926).
- [4] E. Schrödinger, Annalen Der Physik **79**, 734 (1926).
- [5] E. Schrödinger and F. V, Zeitschrift Fur Physik , 808 (1931).
- [6] A. Kramers and W. Heisenberg, Zeitschrift Fur Physik **31**, 681 (1925).
- [7] W. Heisenberg, Zeitschrift Fur Physik **31**, 617 (1925).
- [8] W. Heisenberg, Zeitschrift Fur Physik **35**, 557 (1926).
- [9] W. Heisenberg, Zeitschrift Fur Physik , 587 (1933).
- [10] P. Dirac, Proc. Royal Soc. London , 621 (1927).
- [11] M. Planck, Archives Neerlandaises des Sciences Exactes et Naturelles , 164 (1900).
- [12] M. Planck, Archives Neerlandaises des Sciences Exactes et Naturelles , 55 (1901).
- [13] M. Planck, Annalen Der Physik **6**, 818 (1906).
- [14] A. Einstein, Annalen Der Physik **1**, 180 (1906).

-
- [15] L. De Broglie, *Research on Quantum Theory*, 1924.
- [16] M. Born and R. Oppenheimer, *Annalen Der Physik* **84**, 457 (1927).
- [17] W. Pauli, *Zeitschrift Fur Physik* **31**, 765 (1925).
- [18] J. Slater, *Phys. Rev.* **32**, 339 (1928).
- [19] J. Slater, *Phys. Rev.* **35**, 210 (1928).
- [20] D. Hartree, *Proc. Cambridge Phil. Soc.* **24**, 89 (1928).
- [21] D. Hartree, *Proc. Cambridge Phil. Soc.* **24**, 111 (1928).
- [22] D. Hartree, *Proc. Cambridge Phil. Soc.* **24**, 426 (1928).
- [23] V. Fock, *Comp. Rend. de l'Ac. Sci. de l'URSS* **8**, 295 (1935).
- [24] A. Szabo and N. S. Ostlund, *Modern Quantum Chemistry: Introduction to Advanced Electronic Structure Theory*, Dover Publications, Inc., 1996.
- [25] I. Levine, *Quantum Chemistry, Fifth Edition*, Prentice Hall, 2000.
- [26] C. Roothaan, *Rev. Mod. Phys.* **23**, 69 (1951).
- [27] J. Pople and R. Nesbet, *J. Chem. Phys.* **22**, 571 (1954).
- [28] M. Head-Gordon and J. A. Pople, *J. Phys. Chem.* **92**, 3063 (1988).
- [29] W. Press, S. Teukolsky, and W. Vetterling, *Numerical Recipes: The Art of Scientific Computing, Third Edition*, Cambridge University Press, 2007.
- [30] T. Van Voorhis and M. Head-Gordon, *Mol. Phys.* **100**, 1713 (2002).
- [31] O. Kysel, S. Budzák, M. Medved, and P. Mach, *Int. J. Quantum Chem.* **108**, 1533 (2008).

- [32] K. Pei and H. Li, THEOCHEM **676**, 105 (2004).
- [33] R. Lin, C. Wu, S. Jang, and F. Li, J. Mol. Model. (2009).
- [34] K. Houk, P. Lee, and M. Nendel, J. Org. Chem. **66**, 5517 (2001).
- [35] Z. Qu, D. Zhang, C. Liu, and Y. Jiang, J. Phys. Chem. A **113**, 7909 (2009).
- [36] C. Møller and M. S. Plesset, Phys. Rev. **46**, 618 (1934).
- [37] K. Nakayama, H. Nakana, and K. Hirao, Int. J. Quantum Chem. **66**, 157 (1998).
- [38] P. Löwdin, Adv.Chem. Phys. **2**, 207 (1959).
- [39] B. Roos and P. Siegbahn, *Methods of Electronic Structure Theory, 3rd Ed.*, Plenum, New York, 1977.
- [40] C. Bauschlicher and P. Taylor, J. Chem. Phys. **85**, 2779 (1986).
- [41] P. Knowles and N. Handy, Chem. Phys. Lett. **111**, 315 (1984).
- [42] T. Helgaker, P. Jørgensen, and J. Olsen, *Molecular Electronic Structure Theory*, John Wiley & Sons, Ltd., New York, 2002.
- [43] Y. Hatano and K. Hirao, Chem. Phys. Lett. **100**, 519 (1983).
- [44] R. Harrison and N. Handy, Chem. Phys. Lett. **95**, 386 (1983).
- [45] P. Knowles and N. Handy, Chem. Phys. Lett. **111**, 315 (1984).
- [46] C. Bauschlicher and P. Taylor, Theo. Chem. Act. **71**, 263 (1987).
- [47] P. Knowles and N. Handy, Comp. Phys. Commun. **54**, 75 (1989).
- [48] A. Povill and J. Rubio, Int. J. Quantum Chem. **61**, 35 (1998).
- [49] T. D. Crawford and H. F. Shaefer, Rev. Comp. Chem. **14**, 33 (2000).

- [50] P. E. M. Siegbahn, J. Almlöf, A. Heiberg, and B. O. Roos, *J. Chem. Phys.* **74**, 2384 (1981).
- [51] P. A. Malmqvist, A. Rendell, and B. O. Roos, *J. Phys. Chem.* **94**, 5477 (1982).
- [52] B. O. Roos, *Adv. Chem. Phys.* **69**, 399 (1987).
- [53] K. Ruedenberg, M. W. Schmidt, M. M. Gilbert, and S. T. Elbert, *Chem. Phys.* **71**, 41 (1982).
- [54] R. Shepard, *Ab Initio Methods in Quantum Chemistry II*, ed. K. P. Lawley, volume 69, John Wiley and Sons, Ltd., Chichester, 1987.
- [55] R. Shepard, *Adv. Chem. Phys.* **69**, 64 (1987).
- [56] W. A. Goddard and L. B. Harding, *Annu. Rev. Phys. Chem.* **29**, 363 (1978).
- [57] J. M. Langlois et al., *J. Chem. Phys.* **92**, 7488 (1990).
- [58] S. F. Boys, *Rev. Mod. Phys.* **32**, 296 (1960).
- [59] C. Edmiston and K. Ruedenberg, *Rev. Mod. Phys.* **35**, 457 (1963).
- [60] C. Edmiston and K. Ruedenberg, *J. Chem. Phys.* **43**, S97 (1965).
- [61] J. W. Mintmire and B. I. Dunlap, *Phys. Rev. A* **25**, 88 (1982).
- [62] M. Feyereisen, G. Fitzgerald, and A. Komornicki, *Chem. Phys. Lett.* **208**, 359 (1993).
- [63] B. I. Dunlap, *Phys. Chem. Chem. Phys.* **2**, 2113 (2000).
- [64] J. Subotnik, Y. Shao, W. Liang, and M. Head-Gordon, *J. Chem. Phys.* **121**, 9220 (2004).
- [65] A. Thom, E. Sundstrom, and M. Head-Gordon, *Phys. Chem. Chem. Phys.* (2009).

- [66] J. Pipek and P. G. Mezey, *J. Chem. Phys.* **90**, 4916 (1989).
- [67] J. Boughton and P. Pulay, *J. Comput. Chem.* **14**, 736 (1993).
- [68] T. Sano, *J. of Mol. Strut.-TheoChem* **528**, 177 (2000).
- [69] J. Čížek, *J. Chem. Phys.* **45**, 4256 (1966).
- [70] J. Čížek, *Adv. Chem. Phys.* **14**, 35 (1969).
- [71] J. Čížek and J. Paldus, *Int. J. Quantum Chem.* **5**, 359 (1971).
- [72] A. C. Hurley, *Electron Correlation in Small Molecules*, Academic Press, London, 1976.
- [73] H. J. Monkhorst, *Int. J. Quantum Chem. Symp.* **11**, 421 (1977).
- [74] J. A. Pople, R. Krishnan, H. B. Schlegel, and J. S. Binkley, *Int. J. Quantum Chem. Symp.* **14**, 545 (1978).
- [75] R. J. Bartlett and G. D. Purvis, *Int. J. Quantum Chem.* **14**, 561 (1978).
- [76] G. D. Purvis and R. J. Bartlett, *J. Chem. Phys.* **76**, 1910 (1982).
- [77] J. F. Stanton, J. Gauss, J. D. Watts, and R. J. Bartlett, *J. Chem. Phys.* **94**, 4334 (1991).
- [78] J. Cullen, *Chem. Phys.* **202**, 217 (1996).
- [79] T. Van Voorhis and M. Head-Gordon, *J. Chem. Phys.* **115**, 7814 (2001).
- [80] C. D. Sherrill, A. I. Krylov, E. F. C. Byrd, and M. Head-Gordon, *J. Chem. Phys.* **109**, 4171 (1998).
- [81] A. I. Krylov, C. D. Sherrill, E. F. C. Byrd, and M. Head-Gordon, *J. Chem. Phys.* **109**, 10669 (1998).

- [82] T. Van Voorhis and M. Head-Gordon, *J. Chem. Phys.* **117**, 9190 (2002).
- [83] T. Van Voorhis and M. Head-Gordon, *Chem. Phys. Lett.* **317**, 575 (2000).
- [84] G. J. O. Beran and M. Head-Gordon, *Mol. Phys.* **104**, 575 (2006).
- [85] J. A. Parkhill, K. V. Lawler, and M. Head-Gordon, *J. Chem. Phys.* **130**, 084101 (2009).
- [86] G. J. O. Beran, B. Austin, A. Sodt, and M. Head-Gordon, *J. Phys. Chem. A* **109**, 9183 (2005).
- [87] G. J. O. Beran and M. Head-Gordon, *J. Phys. Chem. A* **110**, 9915 (2006).
- [88] B. O. Roos, P. Linse, P. E. M. Siegbahn, and M. R. A. Bloomberg, *Chem. Phys.* **66**, 197 (1981).
- [89] K. Wolinski, H. L. Sellers, and P. Pulay, *Chem. Phys. Lett.* **140**, 225 (1987).
- [90] K. Wolinski and P. Pulay, *J. Chem. Phys.* **90**, 3647 (1989).
- [91] J. J. W. McDouall, K. Peasley, and M. A. Robb, *Chem. Phys. Lett.* **148**, 183 (1988).
- [92] K. Andersson, P. A. Malmqvist, B. O. Roos, A. J. Sadlej, and K. Wolinski, *J. Phys. Chem.* **94**, 5483 (1990).
- [93] K. Andersson, P. A. Malmqvist, and B. O. Roos, *J. Chem. Phys.* **96**, 1218 (1992).
- [94] K. Wolinski, *Theor. Chim. Acta* **82**, 459 (1992).
- [95] Z. Konkoli, Z. He, and D. Cremer, *Theor. Chem. Acct.* **96**, 71 (1997).
- [96] B. D. Dunietz, R. B. Murphy, and R. A. Friesner, *J. Chem. Phys.* **4**, 1921 (1999).
- [97] M. Sejpál and R. P. Messmer, *J. Chem. Phys.* **114**, 4796 (2001).

- [98] B. D. Dunietz and R. A. Friesner, *J. Chem. Phys.* **115**, 11052 (2001).
- [99] S. R. Gwaltney and M. Head-Gordon, *Chem. Phys. Lett.* **323**, 21 (2000).
- [100] S. R. Gwaltney, C. D. Sherrill, M. Head-Gordon, and A. I. Krylov, *J. Chem. Phys.* **113**, 3548 (2000).
- [101] S. R. Gwaltney and M. Head-Gordon, *J. Chem. Phys.* **115**, 2014 (2001).
- [102] S. R. Gwaltney, E. F. C. Byrd, T. Van Voorhis, and M. Head-Gordon, *Chem. Phys. Lett.* **353**, 359 (2002).
- [103] G. J. O. Beran, M. Head-Gordon, and S. R. Gwaltney, *J. Chem. Phys.* **124**, 114107 (2006).
- [104] E. Kraka, *Chem. Phys.* **161**, 149 (1992).
- [105] T. Leininger, H. Stoll, H. J. Werner, and A. Savin, *Chem. Phys. Lett.* **275**, 151 (1997).
- [106] B. Miehlich, H. Stoll, and A. Savin, *Mol. Phys.* **91**, 527 (1997).
- [107] N. O. J. Malcolm and J. J. W. McDouall, *Chem. Phys. Lett.* **282**, 121 (1998).
- [108] S. Grimme and M. Waletzke, *J. Chem. Phys.* **111**, 5645 (1999).
- [109] K. Kusakabe, *J. Phys. Soc. Jpn.* **70**, 2038 (2001).
- [110] R. Takeda, S. Yamanake, and K. Yamaguchi, *Chem. Phys. Lett.* **366**, 321 (2002).
- [111] R. Pollet, A. Savin, T. Leininger, and H. Stoll, *J. Chem. Phys.* **116**, 1250 (2002).
- [112] J. J. W. McDouall, *Mol. Phys.* **101**, 361 (2003).
- [113] T. Ukai, K. Nakata, S. Yamanake, T. Takada, and K. Yamaguchi, *Mol. Phys.* **105**, 2667 (2007).

-
- [114] R. P. Muller and M. P. Desjarlais, *J. Chem. Phys.* **125**, 054101 (2006).
- [115] M. Weimer, F. Della Salla, and A. Gorling, *J. Chem. Phys.* **128**, 144109 (2008).
- [116] A. J. Pérez-Jiménez and J. M. Pérez-Jordá, *J. Chem. Phys.* **120**, 18 (2004).
- [117] A. J. Pérez-Jiménez and J. M. Pérez-Jordá, *Phys. Rev. A* **75**, 012503 (2007).
- [118] K. V. Lawler, G. J. O. Beran, and M. Head-Gordon, *J. Chem. Phys.* **128**, 024107 (2008).
- [119] K. V. Lawler, J. A. Parkhill, and M. Head-Gordon, *Mol. Phys.* **106**, 2309 (2008).
- [120] K. V. Lawler, J. A. Parkhill, and M. Head-Gordon, *J. Chem. Phys.* **130**, 184113 (2009).
- [121] P. Hohenberg and W. Kohn, *Phys. Rev. B* **136**, B864 (1964).
- [122] C. T. Lee, W. T. Yang, and W. G. Parr, *Phys. Rev. B* **37**, 785 (1988).
- [123] Y. Kurzweil, K. V. Lawler, and M. Head-Gordon, *Mol. Phys.* **107**, 2103 (2009).
- [124] W. Kohn, A. D. Becke, and R. G. Parr, *J. Phys. Chem.* **100**, 12974 (1996).
- [125] W. Koch and M. Holthausen, *A Chemist's Guide to Density Functional Theory*, Wiley-VCH, 2001.
- [126] M. Head-Gordon, *J. Phys. Chem.* **100**, 13213 (1996).
- [127] D. W. Small et al., *J. Am. Chem. Soc.* **126**, 13850 (2004).
- [128] G. K. L. Chan and M. Head-Gordon, *J. Chem. Phys.* **116**, 4462 (2002).
- [129] J. Hachmann, W. G. Cardoen, and G. K. L. Chan, *J. Chem. Phys.* **125**, 144101 (2006).

- [130] F. Faglioni and W. A. Goddard, *Int. J. Quantum Chem.* **73**, 1 (1999).
- [131] A. Sodt, G. J. O. Beran, Y. S. Jung, B. Austin, and M. Head-Gordon, *J. Chem. Theory Comput.* **2**, 300 (2006).
- [132] Y. S. Jung and M. Head-Gordon, *ChemPhysChem* **4**, 522 (2003).
- [133] Y. S. Jung and M. Head-Gordon, *J. Phys. Chem. A* **107**, 7475 (2003).
- [134] Y. S. Jung and M. Head-Gordon, *Phys. Chem. Chem. Phys.* **6**, 2008 (2004).
- [135] Y. S. Jung, M. Brynda, P. P. Power, and M. Head-Gordon, *J. Am. Chem. Soc.* **128**, 7185 (2006).
- [136] B. D. Dunietz, R. B. Murphy, and R. A. Friesner, *J. Chem. Phys.* **110**, 1921 (1999).
- [137] A. F. Voter and W. A. Goddard, *J. Chem. Phys.* **75**, 3638 (1981).
- [138] P. C. Hiberty, S. Humbel, C. P. Byrman, and J. H. Vanlenthe, *J. Chem. Phys.* **101**, 5969 (1994).
- [139] S. Saebo and P. Pulay, *Annu. Rev. Phys. Chem.* **44**, 213 (1993).
- [140] R. A. Friesner et al., *J. Phys. Chem. A* **103**, 1913 (1999).
- [141] T. Van Voorhis and M. Head-Gordon, *J. Chem. Phys.* **112**, 5633 (2000).
- [142] Y. Shao et al., *Phys. Chem. Chem. Phys.* **8**, 3172 (2006).
- [143] T. Helgaker, P. Jorgensen, and N. C. Handy, *Theor. Chim. Acta* **76**, 227 (1989).
- [144] E. Kapuy, Z. Csepes, and C. Kozmutza, *Int. J. Quantum Chem.* **23**, 981 (1983).
- [145] E. Kapuy, F. Bartha, F. Bogar, Z. Csepes, and C. Kozmutza, *Int. J. Quantum Chem.* **38**, 139 (1990).

- [146] J. Pipek and F. Bogar, *Top. Curr. Chem.* **203**, 43 (1999).
- [147] J. E. Subotnik and M. Head-Gordon, *J. Chem. Phys.* **122**, 034109 (2005).
- [148] J. E. Subotnik, A. Sodt, and M. Head-Gordon, *J. Chem. Phys.* **125**, 074116 (2006).
- [149] S. Grimme, *J. Chem. Phys.* **118**, 9095 (2003).
- [150] Y. S. Jung, R. C. Lochan, A. D. Dutoi, and M. Head-Gordon, *J. Chem. Phys.* **125**, 9793 (2004).
- [151] R. A. DiStasio, R. P. Steele, Y. M. Rhee, Y. H. Shao, and M. Head-Gordon, *J. Comput. Chem.* **28**, 839 (2007).
- [152] Y. Wang and R. A. Poirier, *J. Molec. Struct.* **340**, 1 (1995).
- [153] Y. S. Jung, T. Heine, P. v. R. Schleyer, and M. Head-Gordon, *J. Am. Chem. Soc.* **126**, 3132 (2004).
- [154] A. Sekiguchi, T. Matsuo, and M. Tanaka, *Organometallics* **21**, 1072 (2002).
- [155] C. M. Mikulski et al., *J. Am. Chem. Soc.* **97**, 6358 (1975).
- [156] H. C. Allen and E. K. Plyler, *J. Am. Chem. Soc.* **80**, 2673 (1958).
- [157] G. Herzberg, *Electron Spectra of Polyatomic Molecules*, Van Nostrand, Princeton, NJ **1**, 1 (1966).
- [158] W. Haugen and M. Traetteberg, *Acta. Chem. Scand.* **20**, 1726 (1966).
- [159] R. H. Baughmann, B. E. Kohler, I. J. Levy, and C. Spangler, *J. Phys. Chem.* **97**, 9360 (1993).
- [160] J. A. Pople and R. K. Nesbet, *J. Chem. Phys.* **22**, 571 (1954).
- [161] R. J. Bartlett and M. Musial, *Rev. Mod. Phys.* **79**, 291 (2007).

- [162] T. Živković and H. Monkhorst, *J. Math Phys.* **19**, 1007 (1978).
- [163] K. Jankowski and J. Paldus, *Int. J. Quantum Chem.* **18**, 1243 (1980).
- [164] P. Piecuch, S. Zarrabian, J. Paldus, and J. Čížek, *Phys. Rev. B* **42**, 3351 (1990).
- [165] J. Paldus, P. Piecuch, L. Pylypov, and B. Jeziorski, *Phys. Rev. A* **47**, 2738 (1993).
- [166] K. Kowalski and K. Jankowski, *Phys. Rev. Lett.* **81**, 1195 (1998).
- [167] K. Jankowski and K. Kowalski, *J. Chem. Phys.* **111**, 2940 (1999).
- [168] K. Jankowski and K. Kowalski, *J. Chem. Phys.* **111**, 2952 (1999).
- [169] K. Kowalski and P. Piecuch, *Phys. Rev. A* **61**, 052506 (2000).
- [170] P. Szakács and P. R. Surján, *Int. J. Quantum Chem.* **108**, 2043 (2008).
- [171] T. P. Hamilton and P. Pulay, *J. Chem. Phys.* **84**, 5728 (1986).
- [172] T. Korona and H.-J. Werner, *J. Chem. Phys.* **118**, 3006 (2003).
- [173] J. D. Watts and R. J. Bartlett, *J. Chem. Phys.* **101**, 3073 (1994).
- [174] H. K. O. Christiansen and P. Jorgensen, *Chem. Phys. Lett.* **243**, 409 (1995).
- [175] M. Kallay and J. Gauss, *J. Chem. Phys.* **121**, 9257 (2004).
- [176] S. Hirata, *J. Chem. Phys.* **121**, 51 (2004).
- [177] M. M. Hurley, L. F. Pacios, P. A. Christiansen, R. B. Ross, and W. C. Ermler, *J. Chem. Phys.* **84**, 6840 (1986).
- [178] K. Kowalski and P.-D. Fan, *J. Chem. Phys.* **130**, 084112 (2009).
- [179] A. G. Taube and R. J. Bartlett, *J. Chem. Phys.* **130**, 144112 (2009).

- [180] A. P. Morgan, A. J. Sommesse, and C. W. Wampler, *Numer. Math.* **58**, 669 (1991).
- [181] L. A. Curtiss, K. Raghavachari, G. W. Trucks, and J. A. Pople, *J. Chem. Phys.* **94**, 7221 (1991).
- [182] L. A. Curtiss, K. Raghavachari, P. C. Redfern, V. Rassolov, and J. A. Pople, *J. Chem. Phys.* **109**, 7764 (1998).
- [183] X. Li and J. Paldus, *J. Chem. Phys.* **130**, 084110 (2009).
- [184] D. W. Small and M. Head-Gordon, *J. Chem. Phys.* **130**, 084103 (2009).
- [185] A. T. Amos and G. G. Hall, *Proc. Royal Soc. London* , 483 (1961).
- [186] J. Hutter, M. Parrinello, and S. Vogel, *J. Chem. Phys.* **101**, 3862 (1994).
- [187] W. Kurlancheek and M. Head-Gordon, *Mol. Phys.* **107**, 1223 (2009).
- [188] T. Bally, D. A. Hrovat, and B. W. T, *Phys. Chem. Chem. Phys.* **2**, 3363 (2000).
- [189] W. Kohn and L. J. Sham, *Phys. Rev.* **140**, 1133 (1965).
- [190] R. M. Dreizler and E. K. U. Gross, *Density Functional Theory: An approach to the quantum many-body problem*, Springer, Berlin, 1990.
- [191] M. Gruning, O. V. Gritsenko, and E. J. Baerends, *J. Chem. Phys.* **118**, 7183 (2003).
- [192] S. Kummel, L. Kronik, and J. P. Perdew, *Phys. Rev. Lett.* **93**, 213002 (2004).
- [193] B. Braida, P. C. Hiberty, and A. Savin, *J. Phys. Chem. A* **102**, 7872 (1998).
- [194] R. Takeda, S. Yamanake, and K. Yamaguchi, *Int. J. Quantum Chem.* **93**, 317 (2003).
- [195] B. G. Johnson, C. A. Gonzales, P. M. W. Gill, and J. A. Pople, *Chem. Phys. Lett.* **221**, 100 (1994).

- [196] S. Kummel and J. P. Perdew, *Mol. Phys.* **101**, 1363 (2003).
- [197] J. Baker, A. Scheiner, and A. J., *Chem. Phys. Lett.* **216**, 380 (1993).
- [198] V. I. Anisimov and O. Gunnarsson, *Phys. Rev. B* **43**, 7570 (1991).
- [199] V. I. Anisimov, J. Zaanen, and O. K. Andersen, *Phys. Rev. B* **44**, 943 (1991).
- [200] T. Korzdorfer, S. Kummel, and M. Mundt, *J. Chem. Phys.* **129**, 014110 (2008).
- [201] J. D. Chai and M. Head-Gordon, *J. Chem. Phys.* **128**, 084106 (2008).
- [202] S. Kummel and L. Kronik, *Rev. Mod. Phys.* **80**, 3 (2008).
- [203] K. Takatsuka, T. Fueno, and K. Yamaguchi, *Theor. Chim. Acta* **48**, 175 (1978).
- [204] M. Head-Gordon, *Chem. Phys. Lett.* **372**, 508 (2003).
- [205] R. Colle and O. Salvetti, *Theor. Chim. Acta* **53**, 55 (1979).
- [206] S. Yamanake et al., *Chem. Lett.* **35**, 242 (2006).
- [207] J. Gerratt, D. L. Cooper, P. B. Karadakov, and M. Raimondi, *Chem. Soc. Rev.* **26**, 87 (1997).
- [208] I. Mayer, *Int. J. Quantum Chem.* **63**, 31 (1997).
- [209] A. J. H. Wachters, *IBM Tech. Rept.* **5J584** (1969).
- [210] A. J. H. Wachters, *J. Chem. Phys.* **52**, 1033 (1970).
- [211] C. W. Bauschlicher, S. R. Langhoff, and L. A. Barnes, *J. Chem. Phys.* **91**, 2399 (1989).